INVESTIGATIONS OF AIR-WATER MULTIPHASE FLOW IN TUBES: COMPUTATIONAL FLUID DYNAMICS

GOO WEI HONG

FACULTY OF ENGINEERING
UNIVERSITY OF MALAYA
KUALA LUMPUR

2020

INVESTIGATIONS OF AIR-WATER MULTIPHASE FLOW IN TUBES: COMPUTATIONAL FLUID DYNAMICS

GOO WEI HONG

RESEARCH REPORT SUBMITTED IN FULFILMENT OF THE REQUIREMENTS FOR THE DEGREE OF MASTER OF MECHANICAL ENGINEERING

FACULTY OF ENGINEERING
UNIVERSITY OF MALAYA
KUALA LUMPUR

2020

UNIVERSITY OF MALAYA
ORIGINAL LITERARY WORK DECLARATION

Name of Candidate: Goo Wei Hong

Matric No: 17202391/1

Name of Degree: Master of Mechanical Engineering

Title of Research Report: Investigations of Air-Water Multiphase Flow in Tubes:

Computational Fluid Dynamics

Field of Study: Computational Fluid Dynamics, Fluid Mechanics and Multiphase Flow

I do solemnly and sincerely declare that:

(1) I am the sole author/writer of this Work;
(2) This Work is original;
(3) Any use of any work in which copyright exists was done by way of fair dealing and for permitted purposes and any excerpt or extract from, or reference to or reproduction of any copyright work has been disclosed expressly and sufficiently and the title of the Work and its authorship have been acknowledged in this Work;
(4) I do not have any actual knowledge nor do I ought reasonably to know that the making of this work constitutes an infringement of any copyright work;
(5) I hereby assign all and every rights in the copyright to this Work to the University of Malaya ("UM"), who henceforth shall be owner of the copyright in this Work and that any reproduction or use in any form or by any means whatsoever is prohibited without the written consent of UM having been first had and obtained;
(6) I am fully aware that if in the course of making this Work I have infringed any copyright whether intentionally or otherwise, I may be subject to legal action or any other action as may be determined by UM.

    Candidate's Signature   Date:

Subscribed and solemnly declared before,

    Witness's Signature   Date:

Name:

Designation:

[INVESTIGATIONS OF AIR-WATER MULTIPHASE FLOW IN TUBES:

COMPUTATIONAL FLUID DYNAMICS]

ABSTRACT

Mixing is a very crucial process in many industries, such as food processing industry, minerals processing industry, petrochemicals and refining industry, pulp and paper industry, polymer industry, pharmaceuticals industry and many more. There are different types of mixing, such as liquid-gas mixing, liquid-liquid mixing, solid-liquid mixing and many more. The definition of multiphase flow is the simultaneous flow of materials with multiple thermodynamic phases. A lot of process industries require multiphase flows during operation. Bubbly flow is defined as the flow of liquids that contains dispersed gas bubbles. One of the main applications of multiphases flows and bubbly flows is static mixer. The experimental and simulation studies on multiphase flows, especially bubbly flows are not widely performed due to due to several constraints. Therefore, the focus of this research project is on investigating bubbly flow using Computational Fluid Dynamics (CFD) software. The three most common multiphase models in FLUENT are Volume of Fluid (VOF) model, Mixture model and Eulerian model. The two most common models under Eulerian multiphase model in simulating bubbly flow are Population Balance Model (PBM) and Interfacial Area Concentration (IAC) model. The PBM and IAC model are compared with an available case study from ANSYS in simulating bubbly flow in a 2D vertical bubble column reactor. It is found that the simulation results obtained using PBM compared to IAC model, such as air volume fraction contours, water velocity vectors, air bin 0 fraction contours, graphs of air bin 3 fraction versus X direction at the centre of the 2D vertical bubble column reactor, discrete size 3 fraction of air contours, Sauter mean diameter of air contours and Sauter mean diameter distribution of air histograms have higher similarity with the results from the case study, but there exist some differences between the results. Not only that, the bubbly

iii

flow in 2D horizontal pipe is studied by manipulating the ratio of air velocity to water velocity (AV/WV) using PBM. It is found that the air volume fraction in the 2D horizontal pipe decreases when the AV/WV ratio decreases from 1. It is found that the air bubbles migrate towards the top wall of the 2D horizontal pipe almost instantly when the ratio of AV/WV is higher than 1 due to the larger buoyancy force whereas the air bubbles tend to travel the furthest at the centre of the 2D horizontal pipe before migrating to the top wall when the ratio of AV/WV is 1. However, the distance the air bubbles travel at the centre of the 2D horizontal pipe reduces if the AV/WV ratio decreases from 1. Lastly, CFD simulation of air-water multiphase flow in 3D Kenics static mixer is performed using VOF multiphase model by manipulating the volume fraction of air at the inlet. It is found that the mixing characteristics of the 3D Kenics static mixer are almost similar for the different volume fractions of air at the air inlet. However, reversed flow of water occurs due to the pressure-outlet boundary conditions at the outlets.

Keywords: **Mixing; Multiphase flow; Bubbly flow; Static Mixer; Computational Fluid Dynamics**

[INVESTIGASI ALIRAN MULTIFASA UDARA-AIR DALAM TIUB:

PENGIRAAN DINAMIK CECAIR]

ABSTRAK

Pencampuran merupakan proses yang amat penting dalam banyak industri, seperti industri pemprosesan makanan, industri pemprosesan mineral, industri petrokimia dan penapisan, industri pulpa dan kertas, industri polimer, industry farmaseutikal dan selain-lainnya. Terdapat pelbagai jenis pencampuran, seperti pencampuran cecair-gas, pencampuran cecair-cecair, pencampuran pepejal-air dan selain-lainnya. Definisi aliran multifasa ialah aliran serentak bahan-bahan yang mempunyai pelbagai fasa-fasa termodinamik yang berbeza. Banyak industri proses memerlukan aliran multifasa semasa beroperasi. Definisi aliran berbuih ialah aliran cecair yang menpunyai buih-buih gas yang tersebar. Salah satu daripada aplikasi-aplikasi utama aliran multifasa dan aliran berbuih ialah pengadun statik. Kajian eksperimen dan simulasi dalan aliran multifasa, terutamanya aliran berbuih tidak dilakukan secara meluas kerana disebabkan oleh beberapa kekangan. Oleh itu, fokus projek penyelidikan ini adalah menyiasat aliran berbuih dengan menggunakan perisian Pengiraan Dinamik Cecair (PDC). Tiga model multifasa yang paling umum dalam FLUENT ialah model Isipadu Cacair (IC), model Campuran dan model Eulerian. Dua model yang paling umum bawah model multifasa Eulerian dalam mensimulasikan aliran berbuih ialah Model Keseimbangan Populasi (MKP) dan model Kepekatan Kawasan Antara Muka (KKAM). MKP dan model KKAM dibandingkan dengan kajian kes yang tersedia dari ANSYS dalam mensimulasikan aliran berbuih dalam reaktor lajur menegak 2D. Hasil simulasi yang diperoleh dengan menggunakan MKP berbanding dengan model KKAM, seperti kontur pecahan isipadu udara, vektor halaju air, kontur pecahan tong udara 0, graf pecahan bin udara 3 berbanding dengan arah X di tengah reaktor lajur menegak 2D, kontur pecahan ukuran 3 diskrit, kontur diameter min Sauter udara dan histogram pengedaran diameter min Sauter udara

didapati mempunyai similariti yang lebih tinggi dengan hasil daripada kajian kes tersebut, tetapi terdapat beberapa perbezaan antara hasil-hasil tersebut. Selain itu, aliran berbuih dalam paip mendatar 2D juga dikaji dengan memanipulasi nisbah halaju udara kepada halaju air (HU/HA) dengan menggunakan MKP. Pecahan isipadu air dalam paip mendatar 2D didapati menurun apabila nisbah HU/HA menurun daripada 1. Buih-buih udara didapati bermigrasi ke dinding atas paip mendatar hampir sekelip mata apabila nisbah HU/HA lebih tinggi daripada 1 disebabkan oleh daya apung yang lebih besar manakala buih-buih udara bergerak paling jauh di tengah paip mendatar 2D sebelum bermigrasi ke dinding atas apabila nisbah HU/HA adalah 1. Walau bagaimanapun, jarak buih-buih udara bergerak di tengah paip mendatar 2D berkurang apabila nisbah HU/HA menurun daripada 1. Akhirnya, simulasi PDC aliran multifasa udara-air dalam pengadun statik Kenics 3D dilakukan dengan menggunakan model multifasa (IC) dengan manipulasi pecahan isipadu udara di saluran masuk. Ciri-ciri pencampuran pengadun statik Kenics 3D didapati hampir serupa untuk pecahan isipadu udara yang berbeza di saluran masuk udara. Walau bagaimanapun, aliran air terbalik berlaku disebabkan oleh keadaan-keadaan sempadan di saluran-saluran keluar ialah saluran keluar-tekanan.

Kata-Kata Kunci: **Pencampuran; Aliran multifasa; Aliran berbuih; Pengadun statik; Pengiraan Dinamik Cecair**

ACKNOWLEDGEMENTS

Firstly, I would love to convey my deepest gratitude to University of Malaya for providing me a once in a blue moon chance to obtain new knowledge and experience through this research project. Countless people have assisted and guided me in completing this research project. The completion of this project is impossible without their assistance and guidance along the way.

I would love to thank my hardworking and humble supervisor, Associate Prof. Dr. Poo Balan A/L Ganesan for providing me with an interesting project title in the field of CFD, fluid mechanics and multiphase flow. I am grateful that Dr. Poo Balan was able to guide and assist me very thoroughly in this project. Not only that, Dr. Poo Balan also assisted me in using the computer fluid dynamics software, ANSYS FLUENT 2019 R2. Dr. Poo Balan helped and taught me the correct methods to use the various settings in the software in order to obtain credible results.

Besides, I would love to convey my sincerest gratitude to my parents for providing physical and emotional supports during the journey of completing this research project and throughout my entire life. Finally, I would also love to express my deepest thanks to all my beloved university friends for assisting me in making this research project a success.

Once again, I would love to offer my thanks to everyone for their contribution in the completion of this project. Their guidance and assistance surely made the journey to complete this research project much simpler for me.

TABLE OF CONTENTS

LIST OF FIGURES

LIST OF TABLES

LIST OF SYMBOLS AND ABBREVIATIONS

CFD	:	Computational Fluid Dynamics
VOF	:	Volume of fluid
PBM	:	Population balance model
IAC	:	Interfacial area concentration
AV/WV	:	Air velocity to water velocity
EB-RSM	:	Elliptic blending Reynold stress model
H_d	:	Spacing between upper and lower impeller
RTD	:	Residence time distribution
H_d	:	Spacing between upper and lower impeller
Re	:	Reynolds number
HPAM	:	Partially hydrolyzed polyacrylamide
LB	:	Lattice Boltzmann
We	:	Weber
SAR	:	Split-and-recombine
HEV	:	High-efficiency vortex
LPD	:	Low-pressure drop
LLPD	:	Low-low-pressure drop
CFL	:	Courant number

LIST OF APPENDICES

CHAPTER 1: INTRODUCTION

1.1 General Introduction

Multiphase flows are very common in many process industries. Multiphase flow is defined as simultaneous flow of materials with several thermodynamic phases (Wikipedia, 2020). Bubbly flow is a type of multiphase flow and it is defined as a liquid continuum that contains dispersed gas bubbles (Kataoka, Isao, Serizawa, & Akimi, 2010). Multiphase flows and bubbly flows can be investigated by conducting experiments or running simulations using CFD software such as FLUENT. One of the main applications of multiphases flows and bubbly flows is static mixer. Static mixers are found to be able to improve the mixing performance of different kinds of multiphase flows.

Nowadays, methods to improve heat transfer performance in fluid channels are very important because heat exchangers are very widely used. Structures are usually integrated within channels or pipes in order to improve heat transfer by inducing mixing and swirling (Kwon, Liebenberg, Jacobi, & King, 2019). A lot of challenges are faced in enabling various industrial processes to produce fluid products that are quite complex. Particulate solids of large amount are usually found in a lot of multiphase products. Particle jamming may cause shear conditions which will lead to viscous rheology. This causes blending operations in industry to usually occur under laminar flow conditions which provide difficulties for product homogeneity to be achieved (Ramsay, Simmons, Ingram, & Stitt, 2016). Therefore, a mixing device such as static mixer is required to perform mixing of viscoelastic fluids.

The study of mixing is very important for the environment because it controls byproduct effluents and efficiency of process (Ghanem, Lemenand, Valle, & Peerhossaini, 2013). Static mixers can be incorporated in order to enhance the efficiency of mixing for the processes. In many industrial operations, such as chemical reactions, food processing, polymer blending, wastewater treatment, cosmetics and pharmaceutics, static mixers are broadly used in the process of homogenization (Meijer, Singh, & Anderson, 2011). One of the main operations in many process industries is the liquid bulks dispersed by various gaseous phases. Static mixers can be integrated to perform mixing in feed lines to increase the interfacial area density, thus greatly enhancing mass transfer and chemical reaction (Rabha, Schubert, Grugel, Banowski, & Hampel, 2014).

1.2   Problem Statement

Mixing is a very crucial process in heat exchangers and process industries. Mixing involves multiphase flow. Multiphase flow is a very common phenomenon in static mixers. Static mixers can enhance mixing efficiency compared to empty channels, tubes or pipes. Besides, the advantages of static mixers compared to dynamic mixers such as rotators, impellers and agitators are narrower residence time distribution, enhanced mixing, lower installation cost, low space requirement, near plug flow behavior, lower operating and maintenance cost, lesser erosion and generation of higher interfacial behavior (Soman & Madhuranthakam, 2017). However, multiphase flows, especially bubbly flows have not been widely studied and characterized yet. The lack of information about the mixing characteristics and fluid flow in various multiphase flows is because of the difficulty to conduct experimental investigations due to nature of the flows. It is even more difficult to perform experiments to investigate multiphase flows when the flow is turbulent due to the formation of unsteady vortices of different sizes. Not only that, the

20

investigation of multiphase flows, especially bubbly flows using CFD is not widely conducted too.

There are three main problem statements in this research project, this first problem statement is the accuracy of PBM and IAC model in simulating air-water multiphase flows, especially bubbly flows in tubes is not clearly reported due to the lack of experimental and simulation investigations. The second problem statement is the flow characteristics of bubbly flow, such as the flow physics of air bubbles in horizontal tube are not widely investigated and studied yet. The third problem statement is the flow characteristics of air-water multiphase flow in tube with complex geometry such as extended fins, also known as static mixer are also not widely characterized and studied yet.

Therefore, this research project is intended to perform investigation and analysis of multiphase flows using numerical method. The numerical method is going to be carried out using CFD whereas the software that is going to be used is ANSYS FLUENT 2019 R2 student version software. CFD simulation of bubbly flow in 2D vertical bubble column reactor will be done using PBM and IAC model. The results will then be compared and validated by benchmarking against an available case study. Not only that, the flow physics of air bubbles in 2D horizontal pipe will be investigated. Besides, CFD simulation of air-water multiphase flow in a static mixer using VOF model will also be conducted. Lastly, the relevant contours and graphs will be displayed and plotted. The differences between PBM and IAC model in simulating bubbly flows can be identified and the knowledge on the fluid flow characteristics of air-water multiphase flow, especially bubbly flow can be increased through conducting this research project.

Furthermore, the knowledge on the fluid flow characteristics of air-water multiphase flow in 3D Kenics static mixer can also be increased through conducting this research project.

1.3   Objectives of the Study

The objectives of the research project are as below:

1. To investigate and compare CFD model of bubbly flow in a 2D vertical bubble column reactor based on Population Balance Model and Interfacial Area Concentration model.

2. To investigate bubbly flow in a 2D horizontal pipe by manipulating the ratio of air velocity to water velocity using Population Balance Model.

3. To investigate air-water multiphase flow in a static mixer using Volume of Fluid multiphase model for different inlet air volume fractions.

1.4   Scope and Limitations of the Study

The entirety of this research project is to be conducted using CFD, which is using ANSYS FLUENT 2019 R2 student version software. Firstly, bubbly flow in a 2D vertical bubble column reactor simulated using PBM and IAC model will be investigated, compared and benchmarked against an available case study from ANSYS. Then, the flow physics of bubble flow in 2D horizontal pipe will be investigated by manipulating the ratio of AV/WV. PBM is going to be used for the second objective. Not only that, the effects of different inlet volume fractions of air on air-water multiphase flow in a static mixer, which is a 3D Kenics static mixer will be studied. The multiphase model that is going to be used is VOF model. Lastly, the relevant contours and graphs for the three main objectives will be displayed, plotted, analyzed and discussed.

There is one major limitation in this research project. The major limitation is the low number of nodes during meshing. The first reason is due to the low computing power of the computer used to perform CFD simulations. Not only that, the CFD software used only allows 512000 nodes as the maximum number of nodes during meshing. The size of the mesh must be very small in order to obtain accurate simulation results. However, this requires the time step size to be very small in order to prevent divergence of solution. Small time step size will greatly increase the computational cost in terms of computational power and simulation time. Mesh dependency test is not able to be done in order to ensure that simulation results obtained are accurate and consistent due to the low computing power of the computer. Therefore, the mesh size used in this research project is small enough in order to obtain simulation results with reasonable accuracy and to prevent the simulation time from becoming too long.

CHAPTER 2: LITERATURE REVIEW

2.1   Multiphase Flow

2.1.1   Bubbly Flow

Flow regime map for horizontal flow and vertical flow of a gas-liquid mixture are shown in Figure 2.1 and Figure 2.2 respectively whereas the different flow types of gas-liquid mixture for horizontal flow and vertical flow are shown in Figure 2.3 and Figure 2.4 respectively. There are bubble flow, slug flow, plug flow, annular flow, stratified flow, disperse flow and wavy flow for horizontal flow of gas-liquid mixture whereas there are only bubbly flow, slug flow, churn flow, annular flow and disperse flow for vertical flow of gas-liquid mixture. Bubbly flow and bubble flow are the only focus here. Bubbly flow and bubble flow can be defined as distribution of gas phase as deformable bubbles with different sizes in the continuous liquid phase. For a horizontal flow, bubble flow has flow regime of high mass flux of water but low mass flux of air with the ratio of mass flux of air to mass flux of water around 1×10^{-5}. For a vertical flow, bubbly flow has flow regime of high volumetric flux of water but low volumetric flux of gas with the ratio of volumetric flux of water to volumetric flux of gas around 0.1 (Fetoui, 2017).
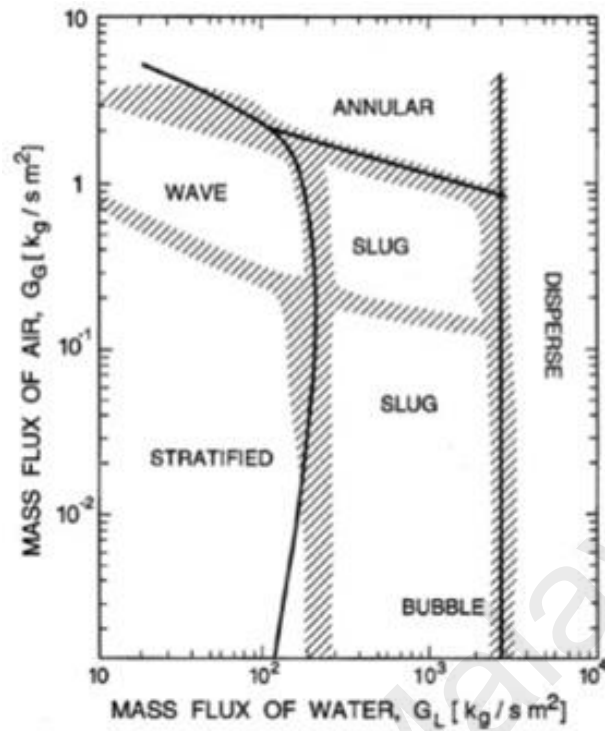
Figure 2.1 Map of Flow Regime for Horizontal Flow of a Gas-Liquid Mixture
(Fetoui, 2017)
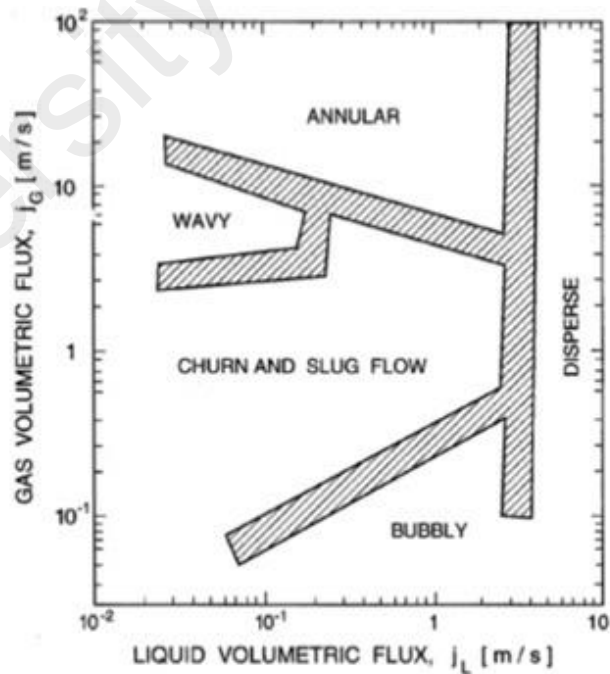
Figure 2.2 Map of Flow Regime for Vertical Flow of a Gas-Liquid Mixture
(Fetoui, 2017)
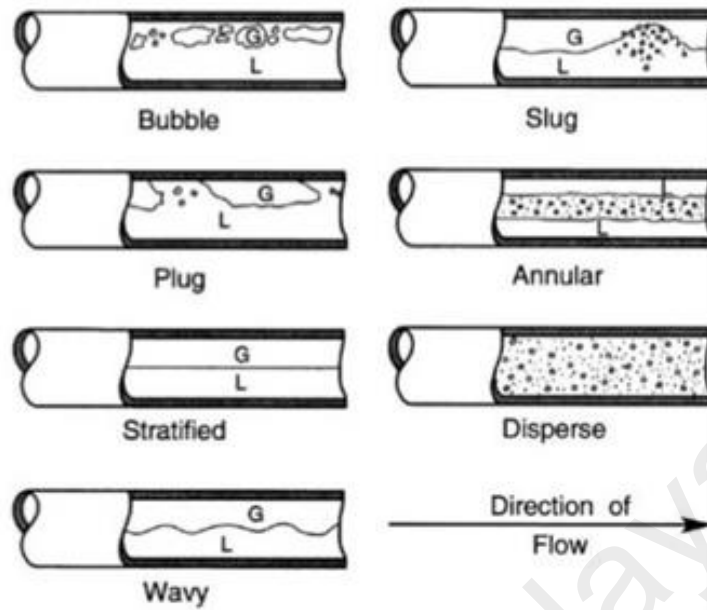
Figure 2.3 Types of Flow for Horizontal Flow of A Gas-Liquid Mixture (Fetoui, 2017)
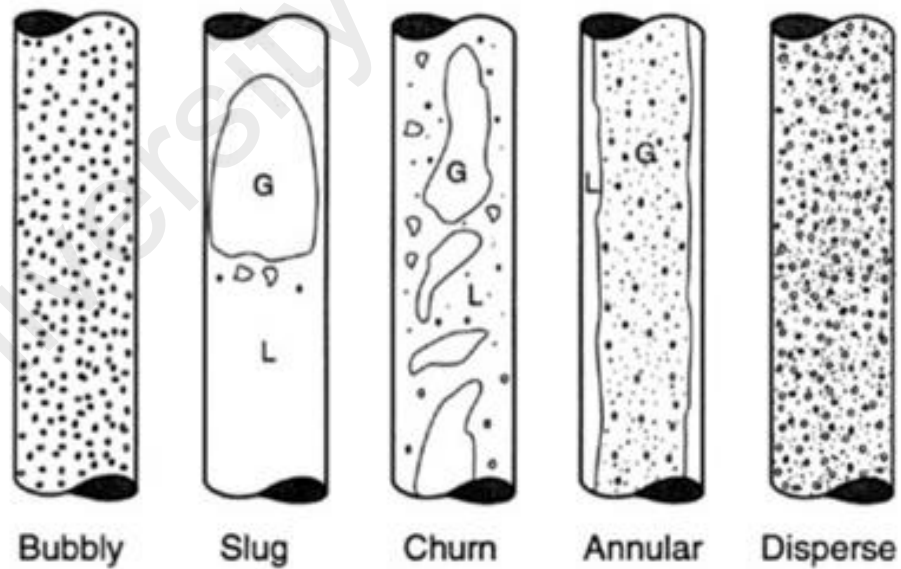
Figure 2.4 Types of Flow for Vertical Flow of A Gas-Liquid Mixture (Fetoui, 2017)

A study has been conducted by Kashinsky and Randin to investigate downward bubbly gas-liquid flow in a vertical pipe. It is found that for the same velocity, wall shear stress of higher value is generated by downward bubbly flow than single-phase flow. Wall shear stress ratio increases if the mean bubble size increases. It is also found that velocity distribution near the wall of the pipe can be accurately described by the parameter of the actual two-phase wall shear stress. Not only that, wall shear stress and fluctuations of liquid velocity display phenomena of turbulence suppression in downward bubbly flow. However, fluctuations of liquid velocity for downward bubbly flow are reduced more compared to single-phase flow when scaling parameter of friction velocity is applied (Kashinsky & Randin, 1998).

Dynamics of bubble plumes have been predicted by Fraga, Stoesser, Lai and Socolofsky using a refined numerical methodology of large-eddy simulations with Eulerian-Lagrangian approach. The accuracy of the method has been validated. The numerical framework, advantages and disadvantages of the method are discussed in the journal (Fraga, Stoesser, Lai, & Socolofsky, 2015). Bubbly flows have been predicted by Colombo and Fairweather using Eulerian-Eulerian approach with High Re, k-ε and elliptic blending Reynold stress model (EB-RSM) turbulence models. It is found that the continuous phase turbulence in bubbly flows can be predicted by EB-RSM turbulence model. All the turbulence models can generate the main characteristics of the flow and the distribution of void fraction. Overall, the results obtained from CFD simulations using all the turbulence models are about the same as the experimental results. However, the turbulence models can be further improved by considering the turbulence action properly, modelling the near wall region properly and improving the lift model (Colombo & Fairweather, 2018).

Simulations using OpenFOAM software and ANSYS-CFX software on multiphase flow in a bubbly pipe flow are conducted by Rzehak and Kriebitzsch. It is found to be about similar but with some differences in the simulation results obtained using the different software. The main reason of the differences is due to the near-wall turbulence modeling. Cell-centered discretization and vertex-based scheme are used by OpenFOAM software and ANSYS-CFX software respectively. It is found that the turbulent frequency near the wall of the pipe is higher when computed using OpenFOAM software compared to ANSYS-CFX software (Rzehak & Kriebitzsch, 2014). Lastly, a review about the present status of closures for interfacial forces have been done by Khan, Wang, Zhang, Tian, Su and Qiu (Khan, et al., 2020).

2.1.2 Two Phase Flow

CFD simulation and particle image velocimetry measurement have been carried out by Zou, Ye, Wang and Fei to study liquid-liquid two-phase flow in pump-mix mixer. It is found that the velocity of the continuous phase around impeller is higher than that in the upper region due to the low location of impeller. The velocity around impeller decreases as the impeller speed and the flow ratio increases due to more droplets at higher impeller speed and flow rate. At high velocity region, continuous phase local velocity decreases due to the higher viscosity of the dispersed phase droplet. It is found that a lot of droplets are formed at the top of mixer which will decrease mass transfer whereas a lesser homogenous holdup through the entire mixer is shown when the flow rate is higher. Lower average level and lesser homogenous distribution of holdup are caused by larger drop size. Not only that, it is found that the fluid discharged by the turbine flows to the bottom and then rises up along the wall without any mixing process by the upper impeller in velocity profile of dual-impeller with spacing between upper and lower impeller (H_d) = 60 mm. In the upper region, an improvement in the velocity profile is shown by dual-

impeller with H_d = 100 mm with a flow field of double loop. It is also found that improvement is shown by both dual-impellers with more homogeneous holdup. Kerosene is not found to be accumulated at the top of the mixer. Lastly, it is found that dual-impeller with H_d = 100 mm shows the greatest performance in fluid agitating by dissipating 48 % more power and discharging 193 % more fluid than the single impeller (Zou , Ye, Wang, & Fei, 2015).

2.1.3   T Junction

CFD modelling has been carried out by Athulya and Miji to study multiphase flow through T junction. The geometry of pipe is shown in Figure 2.5. It is found that the branch arm shows greater phase separation due to a larger amount of air pockets formed at branch arm's lower part whereas the run arm shows negligible phase separation due to gravitational effect. At the outlet, the phase separation is observed to be more than at the junction. Phase separation is also observed to be more at the outlet and near the junction when using one way coupling analysis whereas about the same amount of air and water is observed after a distance of 0.125 m from the junction although junction has the maximum volume fraction of air when using two way coupling analysis. Not only that, it is observed that higher concentration of stress at the upper part of the pipe's junction causes deformation of the pipe at that region. Lastly, it is observed that the concentration of stress, which is higher at the upper part compared to the lower part of run arm, causes more deformation at the upper part than the lower part of run arm (Athulya & Miji, 2015).

Figure 2.5 Geometry of Pipe (Athulya & Miji, 2015)

2.1.4   Principles of Mixing

2.1.4.1   Macromixing

Macromixing can be defined as mixing on the scale of the whole vessel which determines the concentrations of environment by convecting the fluid particles in the flow domain. The process of mixing is dependent on the transfer efficiency of the mean flow at different scales. Macromixing consists in the dispersive capacity of the flow at the reactor or heat exchanger scale and is usually characterized by the residence time distribution (RTD) method as a signature of velocity field uniformity. RTD is related to the global motion of the flow because it represents the time the fluid particles require to migrate from the inlet to the outlet of device. Macromixing is the large-scale convective transfer where the fluid particles are driven by the motion due to mean flow velocity to move between high and low momentum regions in the reactor/heat exchanger volume. Macromixing can be improved by generating a radial convective transfer such as longitudinal vortices or baffles so that the fluid path can be perturbed (Ghanem, Lemenand, Valle, & Peerhossaini, 2013).

2.1.4.2   Mesomixing

The exchange of course scale turbulent between the fresh feed and its surroundings governed by the turbulent fluctuations at the intermediate scale is defined as mesomixing. Mesomixing is also related to the inertial-convective disintegration of large eddies. Mixing by this process does not affect the molecular mixing. Process of inertial-convective mixing is dependent on the length scale of turbulent fluctuations, turbulent kinetic energy and their combinations in the turbulent diffusivity. This process is highly dependent on operating conditions such as diameter of pipe, ratio of feed stream velocity to mean velocity of flow surrounding the feed point and eventual back-mixing into the feed pipe. Mesomixing is governed by the turbulent fluctuations and the random path of

31

the fluid particles except the mean flow which is related to the velocity fluctuations magnitude of eddies and the length scale of these fluctuations (Ghanem, Lemenand, Valle, & Peerhossaini, 2013).

2.1.4.3 Micromixing

Micromixing consists of viscous-convective deformation of fluid elements that accelerates the size reduction of aggregate up to the diffusion scale. Micromixing affects the selectivity of chemical reactions. The deformation and engulfment of Kolmogorov micro-scale eddies is required by this mechanism. Micromixing is also the limiting process of local concentration gradients reduction. The mechanism can be distinguished by a micromixing time that is correlated to the turbulence energy dissipation rate. An increase in the turbulence kinetic energy which characterize the drop breakup in multiphase flows will improve the micromixing process, thus reducing the maximum drop size in multiphase flows and enhancing the selectivity of fast chemical reactions (Ghanem, Lemenand, Valle, & Peerhossaini, 2013). Recent study proves that the use of Kenics static mixer will improve the efficiency of micromixing in both the laminar and turbulent flow regimes compared to an empty tube on the basis of a unique parallel competing reaction scheme proposed by Villermaux et al. (Fang & Lee, 2001).

2.1.5   Multiphase Flow Models

There are various multiphase models in FLUENT that can be utilized to simulate multiphase flows, such as VOF model, Mixture model and Eulerian model. Two or more immiscible fluids can be modeled by the VOF model by solving a single set of momentum equations and tracking the volume fraction of each of the fluids in the domain. The Mixture model is a simplified multiphase model that can be utilized to model multiphase flows where the phases move at different velocities but assume local equilibrium over short spatial length scales. The Mixture model can model n phases, whether it is particulate or fluid by solving the continuity, momentum and energy equations for the mixture, the volume fraction equations for the secondary phases and algebraic expressions for the relative velocities. The Eulerian model can model multiple separating and interacting phases. Each phase is treated by a Eulerian treatment whereas each phase is treated by Eulerian-Lagrange in the discrete phase model. Stability or convergence issues may be encountered when solving a multiphase system because it is very difficult to solve a multiphase system (Fluent Inc., 2001). The suitability of the multiphase models is highly dependent on the type and nature of the problem.

Bubbly flow, a two-phase flow is formed when dispersion and suspension of small bubbles occur in a liquid continuum (Kataoka, Isao, Serizawa, & Akimi, 2010). Bubbly flow is a very common phenomenon in static mixers. Under the Eulerian multiphase model, there are two different algorithms to simulate the mixture of air bubbles and liquid, which are PBM and IAC model. PBM can track the size distribution of the dispersed phases and accounting for the coalescence and breakage effects in bubbly flows (Ekambara, Sean Sanders, Nandakumar, & Masliyah, 2012). Population balance is a balance equation utilized to describe the changes in the population of particle, as well as momentum, mass and energy balances. A number density function is introduced to

account for the population of particle (ANSYS, Inc., 2009). The most common method in PBM is the Discrete method. In this method, the particle population is discretized into a finite number of size intervals and has the benefit of computing the particle size distribution directly. However, this method has high computational cost if many intervals are needed and several transport equations are required to be solved (ANSYS, Inc., 2009). The definition of IAC is the interfacial area between two phases per unit volume of mixture. It is a crucial parameter to predict transfers of mass, momentum and energy through the interface between the phases. A transport equation for every secondary phase is utilized by IAC model. However, IAC model currently can only be used to simulate bubbly flows in liquid. IAC model is less computationally expensive than PBM. The most common models under IAC model are the Hibiki-Ishii model and Ishii-Kim model (ANSYS, Inc., 2009).

2.2   Static Mixer

2.2.1   Introduction to Static Mixer

Static mixer is a mixing equipment which the mixing elements are arranged alternately to each other perpendicularly (Soman & Madhuranthakam, 2017). In other words, static mixer comprises of multiple inserts that are motionless installed in tubes or pipes of which the purpose is to divide and redistribute the fluid streams sequentially until good mixing is obtained (Rauline, Le Blévec, Bousquet, & Tanguy, 2000). Pressure drives the fluid through the static mixer and provides the energy required to achieve mixing (Kumar, Shirke, & Nigam, 2007). Static mixers only contain stationary parts unlike conventional agitator. Motionless mixer is the alternative name of static mixer. Static mixers show a lot of advantages compared to conventional agitators, such as a more scalable and controlled rate of dilution is able to be provided by static mixers in fed batch system and feed streams can be homogenized by static mixers with a minimal residence time with

lesser consumption of energy (Zhang, et al., 2014). The advantages of a static mixer compared to a conventional agitator are tabulated in Table 2.1. There are two concepts of static mixer. The first concept of static mixer is a hollow tube with specific geometry that influences the fluid flow in a way to promote secondary transverse flow that improves heat transfer in the cross-section whereas the second concept of static mixer is a series of stationary and identical inserts installed in tubes. The main motive of the inserts is to redistribute the fluids in the radial and tangential directions. The inserts are also known as elements (Ghanem, Lemenand, Valle, & Peerhossaini, 2013).

Static mixers have many geometries and parameters that can be adjusted, such as number of elements in series and aspect ratio (ratio of length to an element diameter) for specific applications (Thakur, Vial, Nigam, Nauman, & Djelveh, 2003). The two most common types of static mixer are Kenics static mixer (Chemineer, Inc.) as shown in Figure 2.6 and SMX static mixer (Sulzer, Inc.) as shown in Figure 2.7. The Kenics static mixer is constructed with right and left-handed twisted plates. The elements are orientated and alternated to ensure that leading edge of the element is at 90 ° with respect to the trailing edge of the next element. The elements in a SMX static mixer are made of stacked lamella. An intricate network of flow channels are formed where each element is a rotation of 90 ° of the previous element (Rauline, Le Blévec, Bousquet, & Tanguy, 2000)

Table 2.1 Advantages of a Static Mixer Compared to a Conventional Agitator (Thakur, Vial, Nigam, Nauman, & Djelveh, 2003)

Static Mixer	Conventional Agitator
Cost of equipment is low	Cost of equipment is high
Space requirement is small	Space requirement is large
No power consumption except for pumping	Power consumption is high
Seal requires small flanges	Seal requires small flanges and a large flange
Residence time is short	Residence time is long
Parts are stationary except pump	Have moving parts such as seals and agitator drive
Excellent mixing performance at low shear rate	Sensitive materials can be damaged by high shear rate produced during mixing
Mixing approaches plug flow	Residence time shows exponential distribution
Mixing elements are interchangeable or disposable and static mixer can perform self-cleaning	Large vessels are required to be cleaned manually
Product grade change is fast	Waste could be generated during product grade change

Figure 2.6 Kenics Static Mixer (Thakur, Vial, Nigam, Nauman, & Djelveh, 2003)
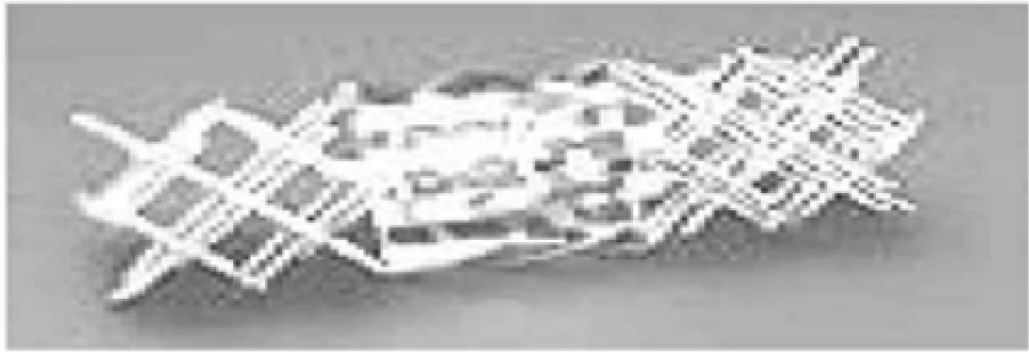
Figure 2.7 SMX Static Mixer (Thakur, Vial, Nigam, Nauman, & Djelveh, 2003)

2.2.2 Fundamentals of Static Mixer

2.2.2.1 Mixing of Miscible Fluids (Distributive Mixing)

Turbulent flow in high viscosity fluids has certain pressure limitations (Thakur, Vial, Nigam, Nauman, & Djelveh, 2003). Therefore, mixing of high viscosity fluids usually occurs in laminar flow. However, mixing of low levels in laminar flow has the effect of giving spatial inhomogeneities in composition. Static mixers are used in order to redistribute the fluid in the tangential and radial directions (spatial mixing) in order to homogenize the fluid. The redistribution of fluid also provides temporal mixing which homogenize the temporal inhomogeneities in undisturbed laminar flow (Thakur, Vial, Nigam, Nauman, & Djelveh, 2003).

2.2.2.2 Interface Generation (Dispersive Mixing)

One of the common operations in the process industries is a continuous phase dispersed by a secondary phase. Static mixers can be utilized as interface generators in multiphase flows because locally high shear rates can be produced by static mixers. The purpose of static mixers is to increase the mass transfer in unit operations such as formation of polymer dispersion, liquid-liquid extraction or gas-liquid absorption.

However, the performance of the static mixer is dependent on the physico-chemical properties of the phases, such as density ratio, volumetric flow rate ratio and viscosity ratio. Static mixers are also utilized to create emulsions, dispersions and emulsions that are partially stabilized by surfactants. Static mixers are utilized in multiphase systems in order to increase interfacial mass transfer and to reduce drop sizes of dispersed phase. The breakup of elongated fluid structures due to surface tension in laminar flow relates to the Rayleigh-Taylor instability. Elongated structures are metastable and will disintegrate into drops of a characteristic size and smaller satellite drops. SMX elements are found to be more effective in generating bubble or drop compared to Kenics elements. Static mixers are also able to disperse a solid phase into a liquid phase. The viscosity, probability of collision between particles, hydrodynamic forces intensity and flocculation rate that are responsible for breakage will increase if the concentration of solid increases. Static mixers are found to be difficult to perform mixing in dilute suspensions (Thakur, Vial, Nigam, Nauman, & Djelveh, 2003).

2.2.3 Performance of Static Mixers

2.2.3.1 Experimental

A study has been conducted by Fang and Lee to investigate the micromixing efficiency in Kenics static mixer. It is found that Kenics static mixer compared to an empty tube may initiate early transition to turbulence. The segregation index decreases as the Reynolds number (Re) increases. However, it is found that the hydrodynamic transition regime does not show any sudden change of Re. The segregation index can reach lesser than 0.1 when Re is above 200. The micromixed environment is improved by the Kenics static mixer whereby the first two elements are better than the subsequent elements of the Kenics static mixer. Not only that, it is found that the micromixing time decreases as the power consumption rate increases and reaches 0.001 s in the regime of turbulent flow.

This proves that the Kenics static mixer is more efficient compared to the continuous stirred tank reactor in micromixed environment due to shorter micromixing time (Fang & Lee, 2001).

A study has been carried out by Ramsay, Simmons, Ingram and Stitt to investigate the mixing performance of viscoelastic fluids in a Kenics KM in-line static mixer. It is found that the fluids performance at the outlet of a 6-element Kenics KM static mixer is greatly affected by the viscoelasticity of fluids by manifesting as the striation pattern changes from a typical lamellar structure related to the helical twist element design of Kenics static mixer towards a more amorphous and segregated structure. Re, Weissenberg number, elasticity number and generalised Re have been proven to significantly affect the Kenics KM mixer's performance of mixing in term of mixing fraction of two different fluids (Ramsay, Simmons, Ingram, & Stitt, 2016). A study conducted by Rafiee, Simmons, Ingram and Stitt using positron emission particle tracking has found that cores of high velocity travel from the centre of the Kenics static mixer to the corner of the geometry towards the end of the Kenics static mixer. The non-Newtonian fluid displays wider cores of high velocity compared to Newtonian fluid. It is also proven that Newtonian fluid has longer entrance length than non-Newtonian fluid (Rafiee, Simmons, Ingram, & Stitt, 2013).

A study has been conducted by Kwon, Liebenberg, Jacobi and King to investigate the heat transfer enhancement of internal laminar flows using additively manufactured static mixers. The static mixers that are being investigated are twisted tape static mixers and chevron static mixers. The fabricated devices are shown in Figure 2.8. It is found that both twisted tape static mixers and chevron static mixers have been proven to improve the convective heat transfer coefficient by nearly 2 times when the Re is below 1000

compared to the plain channel device. The static mixers not only can enhance heat transfer and mass transport in additively manufactured-fabricated heat exchangers, but also can reduce the mass and volume of the heat exchangers (Kwon, Liebenberg, Jacobi, & King, 2019).
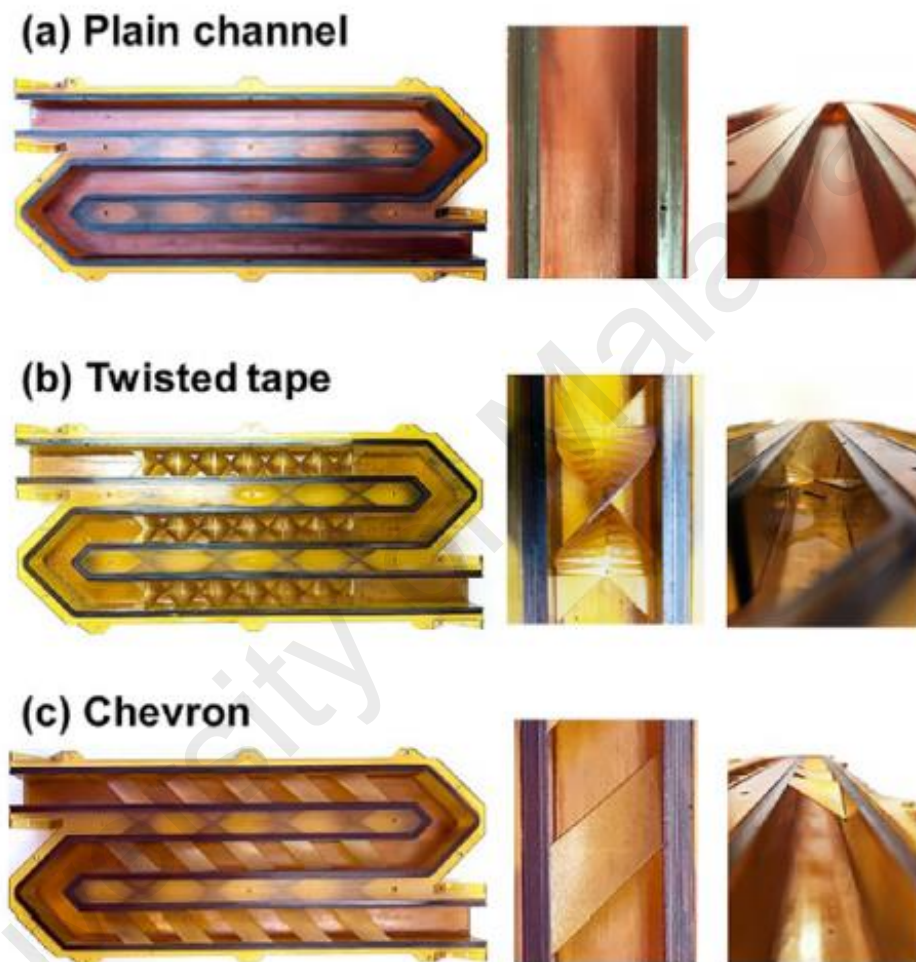
Figure 2.8 Images of Fabricated Devices: (a) Plain Channel (b) Rectangular Channel with Twisted Tape Static Mixers (c) Rectangular Channel with Chevron Static Mixers (Kwon, Liebenberg, Jacobi, & King, 2019)

A study has been carried out by Zhang, Dong, Jiang, Sun, Zhang and Hao to investigate the mixing performance of ultra-high molecular weight partially hydrolyzed polyacrylamide (HPAM) using combination of Kenics static mixer and SMX static mixer. It is found that shearing effect of the static mixers will cause viscosity of the HPAM solution to degrade. The viscosity degradation rate of the solution rises to the maximum at 7.31 % when the flow rate, concentration and relative molecular mass of the HPAM are 0.5 m^3/h, 7000 mg/L and 35 million respectively. The pressure drops across the combination of static mixers are lesser than 6.5 kPa. The non-uniformity degree of mixture through the static mixers increases when the flow rate increases. For HPAM solution with the same relative molecular mass, the non-uniformity degree of HPAM solution increases as the concentration of HPAM solution increases. It is found that the viscosity degradation rate of the HPAM solution rises to the maximum at the value of 4.91 % when flow rate of HPAM solution, flow rate of deionized water, concentration of HPAM solution and the relative molecular mass of HPAM solution are 0.5 m^3/h, 0.5 m^3/h, 7000 mg/L and 35 million respectively. The SMX static mixer has higher pressure drop and degradation rate compared to the Kenics static mixer. It is proven that the combination of Kenics static mixer and SMX static mixer achieve superior performance of mixing with acceptable viscosity degradation rate of liquid. Therefore, the mixing process of polymer solution and water from oilfield can be enhanced by using this combination of static mixers (Zhang, et al., 2014).

A study has been conducted by Soman and Madhuranthakam to investigate the overall mixing capacity of different static mixer geometries. Z factor of a static mixer is the ratio of pressure drop of static mixer to pressure drop of empty tube. Z factor of a static mixer increases when energy cost of the static mixer increases due to increase of mixing elements in the static mixer. It is found that Z factor almost does not depends on the

41

variations of Re until Re reaches 10. Z factor then increases non-linearly when the Re is increased from 10 to 100. It is also found that the pressure drop in static mixer increases continuously when Re is more than 10 because of an increase in the shear force, inertial effects and frictional losses. The internal geometry modifications of static mixers are shown in Figure 2.9. The pressure drop decreases when increasing the number of holes of D/20. However, this will reduce the flow area for the fluid to pass through the static mixer elements, thus causing an increase in the pressure drop when the size of holes are reduced from D/20 to D/40. Static mixer with circular serrations and static mixer with triangular serrations have the least pressure drop among all modified static mixer geometries whereas static mixer with square serrations has the same pressure drop as the standard SMX geometry, which makes it an inferior choice compared to the static mixers with circular serrations and static mixer with triangular serrations (Soman & Madhuranthakam, 2017).
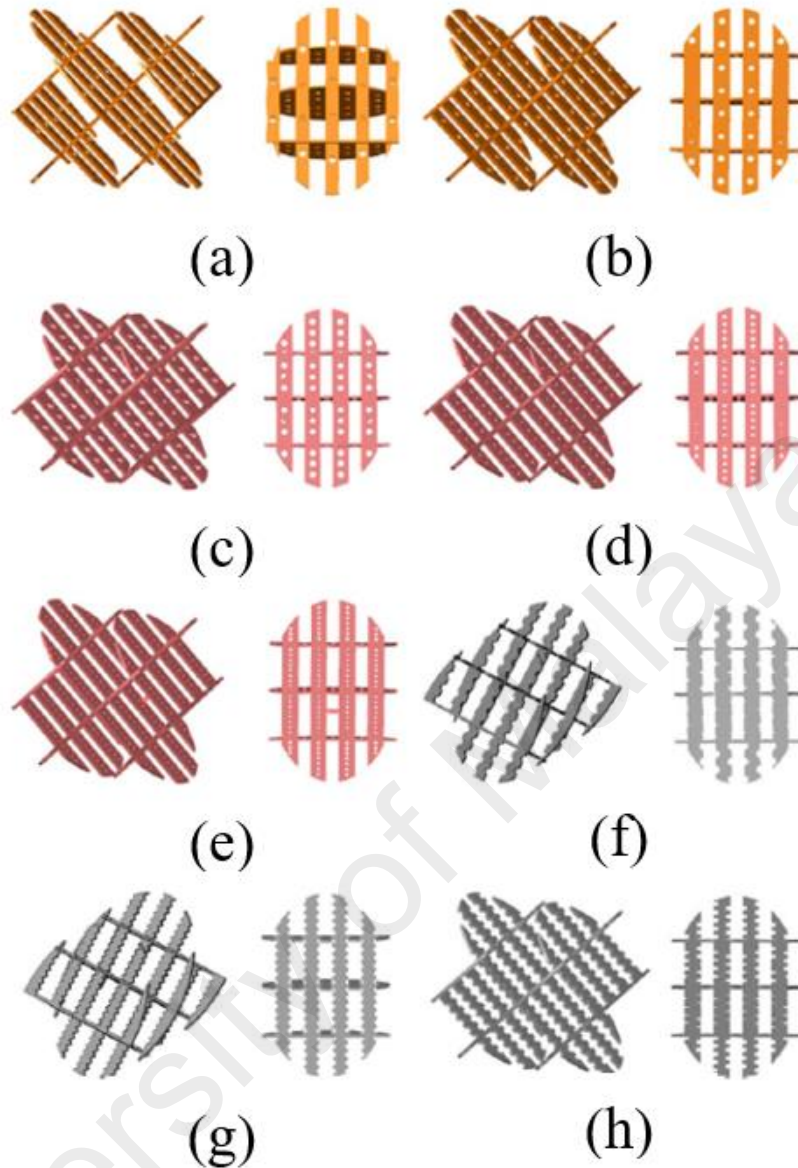
Figure 2.9 Front View and Side View of (a) Perforated SMX (b) Perforated SMX 4 Holes (c) Perforated SMX Maximum Number of D/20 Holes (d) Perforated SMX Maximum Number of D/30 Holes (e) Perforated SMX Maximum Number of D/40 Holes (f) SMX with Circular Serrations (g) SMX with Triangular Serrations (h) SMX with Square Serrations (Soman & Madhuranthakam, 2017)

It is found that the pressure decreases when the axial distance increases for all static mixers. SMX with circular serrations, SMX with triangular serrations and D/20 perforated SMX have higher pressure at the end of eighth mixer element. SMX with circular serrations has the lowest pressure drop. It is also found that SMX with circular serrations eases minimum volume average velocity. The volume average velocity provided by SMX with triangular serrations and D/20 perforated SMX are slightly higher than SMX with circular serrations but it is lower than the standard SMX. Highest volume average velocity is displayed by SMX with square serrations. SMX with circular serrations shows more uniform velocity distribution while SMX with triangular serrations and perforated D/20 SMX show relatively more variations in transverse velocity (Soman & Madhuranthakam, 2017).

Besides, it is found that that the standard SMX has the highest mean shear rate whereas SMX with circular serrations and SMX with triangular serrations have lower shear rate and show identical mean shear rate when Re is increased. SMX with square serrations shows similar results as standard SMX. Mean shear rate of perforated D/20 SMX is slightly lower than standard SMX but is higher than SMX with circular serrations and SMX with triangular serrations. SMX with circular serrations has the minimum mean shear rate due to the lowest pressure drop. It is also found that the elongational flow inside the static mixers and extensional efficiency decrease due to increasing inertial effects when the Re increases. SMX with circular serrations displays a good transition of flow across the cross-blades and more elongational flows are generated within the flow domain. Elongational flow is significantly affected by the geometry of the static mixers. The standard SMX has the lowest extensional efficiency. The ability to generate elongational flows is the highest for SMX with circular serrations. Higher extensional

efficiency is shown by perforated D/20 SMX than SMX with triangular serrations (Soman & Madhuranthakam, 2017).

Not only that, it is observed that the distribution of particles improves with each mixing element for all the static mixers. However, the distribution of particles of a standard SMX at the last element is not effective. D/30 perforated SMX and D/20 perforated SMX show almost similar pattern of distribution of particles but better distribution of particles than the standard SMX. Distributive mixing capabilities displayed by SMXs with serrations are lower than the D/20 perforated SMX and D/30 perforated SMX but higher than the standard SMX. Enhanced distribution of particle is shown by SMX with circular serrations and SMX with triangular serrations with a standard deviation value of 24 % and 27 % respectively whereas D/30 perforated SMX and D/20 perforated SMX display standard deviation values of 16 % and 21 % respectively. Lastly, it is observed that SMX with square serrations has poor dispersive mixing capability but better distributive mixing capability than the standard SMX (Soman & Madhuranthakam, 2017).

2.2.3.2 CFD Simulation

A study has been conducted by Vimal Kumar, Vaibhav Shirke and Nigam to investigate the performance of Kenics static mixer over a wide range of Re. An increase in the pressure drop per unit element in Kenics static mixer is observed when the Re increases. The gradient of pressure drop in Kenics static mixer is high when the Re is more than 12000. It is found that the flow in Kenics static mixer is affected in the transition region of element-to-element up to 30% of the element length. However, the flow is found to be well developed in the element's other region. Formation of forced vortex and free vortex are found in central part and near the wall of the tube respectively (Kumar, Shirke, & Nigam, 2007).

A study has been conducted by van Wageningen, Kandhai, Mudde and van den Akker to investigate dynamic flow in a Kenics static mixer using various CFD methods such as lattice Boltzmann (LB) solver and FLUENT solver. It is found that the efficiency of FLUENT solver is higher than LB solver at low Re where the flow is steady. FLUENT solver is about twice as fast as LB solver when Re is 200 because FLUENT solver is able to use the steady-state solver and a courser grid at the same time. For complex geometries, LB solver requires dense grid to resolve the flow accurately because the wall boundaries in LB solver are staircased. It is found that FLUENT solver is about five times as slow as LB solver at high Re using transient solver because oscillations of vortices in the flow can only be captured by FLUENT solver using small time step, which leads to a long computational and simulation time. LB solver is shows excellent performance in investigating the dynamic behavior in transitional flows because the time step is small and the spatial resolution is high at low computational cost. It is also observed that the flow in Kenics static mixer is chaotic due to formation of vortices at low Re and the turbulent flow is achieved when Re is at around 1000 (van Wageningen, Kandhai, Mudde, & van den Akker, 2004).

A CFD study has been performed by Lisboa, Fernandes, Simões, Mota and Saatdjian on a Kenics static mixer as a heat exchanger for a supercritical carbon dioxide. K-ε, RNG k-ε and k-ω turbulence models are applied to model the heat transfer and turbulent flow under high pressure conditions and with large differences in physical properties. It is found that the most accurate results are obtained by the RNG k–ε turbulence model when compared with the data from experiments, especially when the pressures are 8 MPa and 9 MPa. However, the average heat transfer coefficient at higher pressures is slightly overestimated by the RNG k–ε turbulence model. It is found that the

thermal efficiency of Kenics static mixer is about three times as high as an empty pipe with the same area of heat transfer (Lisboa, Fernandes, Pedro, Mota, & Saatdjian, 2010).

CFD modelling has been performed by Haddadi, Hosseini, Rashtchian and Ahmadi on immiscible liquids turbulent dispersion in Kenics static mixer which focuses on droplet behavior using Eulerian-Eulerian and Eulerian-Lagrangian approaches. The Sauter mean diameter and the distribution of droplet size are predicted using PBM that includes the droplet breakage and coalescence models in the Eulerian-Eulerian approach. It is found that the mean relative error for the Fanning fraction factor is 5.5 % whereas the mean relative errors for the Sauter mean diameter through the Kenics static mixer with three, six and ten mixing elements are 8 %, 5 % and 7 % respectively. It is also found that the Sauter mean diameter decreases as the Weber (We) number and number of mixing elements decreases. The RTD of droplets is predicted using the one-way coupling of the discrete phase model in the Eulerian-Lagrangian approach. It is found that the RTD decreases when the We number increases or the number of mixing elements decreases. In the discrete phase model, random walk model links the turbulent dispersion of the droplets to the continuous phase turbulence. The SST k-ε turbulence model is used and the Schiller-Naumann model is used for the drag coefficient in both Eulerian-Eulerian and Eulerian-Lagrangian approaches (Haddadi, Hosseini, Rashtchian, & Ahmadi, CFD Modeling of Immiscible Liquids Turbulent Dispersion in Kenics Static Mixers: Focusing on Droplet Behavior, 2019). A correlation of pressure drop in a Kenics static mixer developed by Song and Han using CFD can be applied for all range of Re from laminar to turbulent flow (Song & Han, 2005).

A study has been conducted by Rabha, Schubert, Grugel, Banowski and Hampel to perform the visualization and quantitative analysis of dispersive mixing by a helical mixer in upward co-current gas-liquid flow. It is found that at lower slip ratio, the number of static mixer elements greatly affects the bubble breakup. The specific interfacial area and gas holdup are dependent on the number of static mixer elements and the slip ratio. The effect to increase the specific interfacial area and gas holdup by increasing the number of static mixer elements is the most significant at higher velocities of liquid. Not only that, the most common correlations for dimensionless diameters of bubbles in the helical static mixers, such as Kenics static mixers unable to provide enough predictions in the gas-liquid vertical up-flow systems. The pressure drop rather than the velocity of gas in helical static mixer is more greatly affected by the velocity of fluid flow and number of static mixer elements. Lastly, the power dissipation per unit mass of the liquid will increase when the number of static mixer elements is increased. Fluid flow velocity is found to have more effect on the power dissipation per unit mass of the liquid compared to the gas superficial velocity and the number of static mixer elements (Rabha, Schubert, Grugel, Banowski, & Hampel, 2014).

A CFD simulation has been carried out by Zidouni, Krepper, Rzehak, Rabha, Schubert and Hampel on bubbly gas-liquid flow in a helical static mixer using Eulerian-Eulerian approach. It is found that the mixer zone has higher pressure drop due to flow resistance. It is also observed in the flow direction, the front side of the mixing element that recedes from the gas is accumulated by the gas. The bubble size influence is noticeable when applying simplified treatment using a mono-disperse approximation with prescribed bubble size. However, a more comprehensive modelling and accurate spatially resolved data is required in order to improve the accuracy of result (Zidouni, et al., 2015).

A study has been conducted by Habchi, Ghanem, Lemenand, Valle and Peerhossaini to investigate the mixing performance in Split-And-Recombine (SAR) milli-static mixers. The split and recombine mechanism produces chaotic structures. Mixing by molecular diffusion is promoted because the interfacial area between the layers of fluid is being increased by the mechanism. The flow that contributes to repeated folding and stretching of the viscous fluid are passively imposed by a few rotations and changes in the flow direction between the phases of split and recombination. Eulerian approach and finite volume method are used to solve the governing momentum and passive scalar conservation equations whereas SIMPLE algorithm is used for pressure-velocity coupling. The different flow configurations are shown in Figure 2.10. It is found that SAR 2 mixer shows better mixing performance compared to the other configurations. Not only that, it is found that SAR mixers produce lower pressure drops compared to 3D-Flow and the plain channel. The reason is the head losses in the SAR mixers decrease due to the fluid in SAR mixers flows with only 50 % of the velocity at the inlet due to splitting. It is also found that the maximum efficiency for 3D Flow, SAR 1 and SAR 2 are 22 %, 83 % and 83 % respectively. Excellent characteristics such as the fastest mixing rates, moderate pressure drops and dissipating gradients of concentration with minimal residence time are displayed by the SAR 2 mixer (Habchi, Ghanem, Lemenand, Valle, & Peerhossaini, 2018).
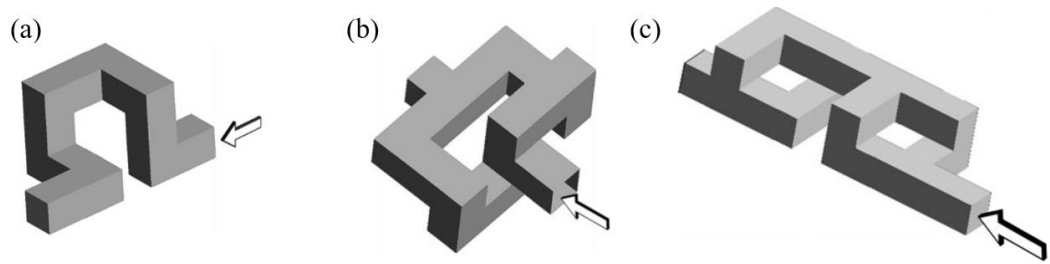
Figure 2.10 Isometric View of An Element from Each Flow Configuration (a) 3D-Flow (b) SAR 1 (c) SAR 2 (Habchi, Ghanem, Lemenand, Valle, & Peerhossaini, 2018)

A comparative analysis has been conducted by Haddadi, Hosseini, Rashtchian and Olazar on the performance of various static mixers using CFD technique. The static mixers that are used in this study are Kenics static mixer, SMX static mixer, Komax static mixer and a new static mixer. The new static mixer is shown in Figure 2.11. It is found that the Z factor of the new static mixer is approximately 45 % lower than the SMX static mixer under the same condition for all Re. The new static mixer is found to have the highest mixing efficiency by producing higher extensional efficiency and lower coefficient of variation compared to the other static mixers. Not only that, static mixers that have equal dispersive mixing capability may have different distributive mixing capability. Lastly, it is also proven that the efficiency of deforming fluid of the new static mixer is the highest compared to the other static mixers because the new static mixer generates high extensional efficiency (Haddadi, Hosseini, Rashtchian, & Olazar, Comparative Analysis of Different Static Mixers Performance by CFD Technique: An Innovative Mixer, 2019).
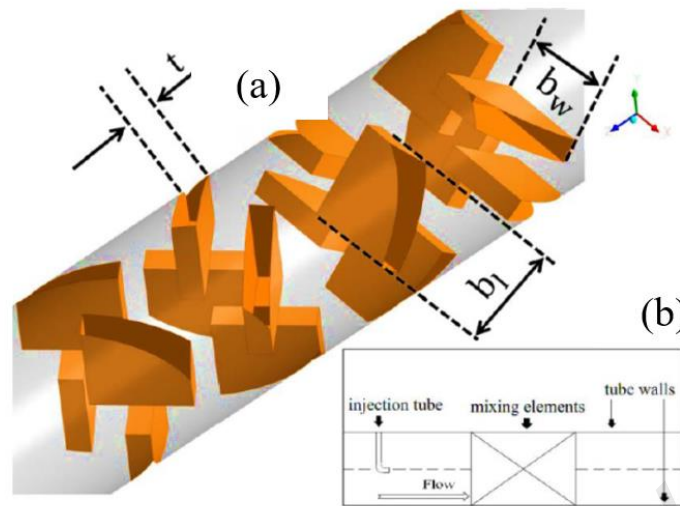
Figure 2.11 (a) Geometry of the Blades in the New Static Mixer (b) Sketch of the Pipeline Equipped with Mixing Elements (Haddadi, Hosseini, Rashtchian, & Olazar, Comparative Analysis of Different Static Mixers Performance by CFD Technique: An Innovative Mixer, 2019)

Turbulent liquid-liquid dispersion in high-efficiency vortex (HEV) static mixer has been studied by Vikhansky using CFD simulation. It is observed that breakup of droplets mostly occurs near the wall of the HEV static mixer due to maximum rate of turbulent dissipation. The baffles generate vortices that transport the droplets to and from the wall of the HEV static mixer. It is found that the friction velocity and radial transport of the dispersed phase greatly affects the efficiency of the HEV static mixer. The mixing performance of the HEV static mixer could be improved by applying more intensive mixing to the fluids (Vikhansky, 2020).

CFD simulation has been performed by Göbel, Golshan, Norouzi, Zarghami and Mostoufi to study granular mixing in a static mixer using the discrete element method. Blending elements such as Kenics and Low-Pressure Drop (LPD) are utilized in the static mixers. The constant decrease of average flow rate of solids from 101.8 g/s to 54.2 g/s is

observed for static mixers with 2 to 5 blending elements whereas the efficiency of mixing improves when the number of blending elements is increased from 2 to 4 at a fixed number of passes. No significant differences are found between 4 and 5 blending elements. It is found that Kenics elements with twist angle of 150 ° and 180 ° and LPD elements with angle of slope of 60 ° can provide maximum efficiency of mixing while maintaining high flow rates of particles. Not only that, performance of static mixers can be improved by increasing the diameter of tube. Lastly, it is found that Kenics static mixer with four blending elements at twist angle of 180 ° and LPD static mixer with three blending elements at slope angle of 60 ° have the best performance in terms of flow rate and mixing quality (Göbel, Golshan, Norouzi, Zarghami, & Mostoufi, 2019).

A study to compare the performance of Kenics static mixer and SMX static mixer is conducted by Rauline, Blévec, Bousquest and Tanguy. It is found about 3 SMX elements and about 7-8 Kenics elements are required for SMX static mixer and Kenics static mixer respectively in order to achieve the limit for intensity of segregation. The mean shear rate for SMX static mixer and Kenics static mixer are 21 s^{-1} and 10 s^{-1} respectively at the same flow rate and diameter. The Lyapunov exponent, which is a signature of chaos in fluid for SMX static mixer and Kenics static mixer are about 1.9 and 0.5 respectively. This shows that the mixing efficiency of SMX static mixer is higher than the Kenics static mixer as the system in SMX static mixer is more chaos than Kenics static mixer. The pressure drop in SMX static mixer is found to be higher than the Kenics static mixer if the diameter and number of elements are the same. The mixer length depends on the diameter and number of the static mixer elements. Lastly, it is concluded that Kenics static mixer is more efficient for easy mixing tasks due to lower cost whereas SMX static mixer is more efficient for difficult mixing tasks as the mixing efficiency of SMX static mixer is higher than Kenics static mixer (Rauline, Le Blévec, Bousquet, & Tanguy, 2000).

A study has been conducted by Meijer, Singh and Anderson to study the performance of static mixers using quantitative approach. The static mixers that are being studied are Kenics RL 180 °, Standard SMX (2,3,8), LPD RL 90 °, Low-Low-Pressure Drop (LLPD) RL 120 °, SMX (3,5,9) circular, SMX (4,7,12), SMX (1,1,3) circular, SMX (1,1,4) 135 ° and Kenics RL 140 °. It is found that the LPD RL 120 ° uses the longest length in mixing, followed by Kenics RL 180 ° and LPD RL 90 °. Kenics RL 140 ° uses 20 % less length compared to the standard Kenics RL 180 ° for the same mixing quality and about the same as Standard SMX (2,3,8). Not only that, it is also found that the SMX series: (n, N_p, N_x) = (n, 2n-1, 3n) has the highest compactness. SMX (3,5,9) is at least twice as good as the standard SMX (2,3,8) whereas SMX (4,7,12) has even higher compactness while achieving the same high mixing performance (Meijer, Singh, & Anderson, 2011).

The ORCA CFD software has been validated by Szalai and Muzzio using SMX and Kenics static mixers. It is found that the ORCA CFD package shows almost similar results with the experimental results obtained for both SMX and Kenics static mixers in terms of pressure drop, stretching field and mixing performance. The capability in solving more complicated problems is feasible if the time required to calculate the solution is reduced due to higher computational power. This simplifies the process of designing complex systems of static mixers while accounting for the optimization of pressure drop, blend time and residence time of the system (Szalai & Muzzio, 2002).

2.3   Industrial Applications of Static Mixers

In industry, static mixers are most commonly used in mixing of miscible fluids. Concentration gradients are reduced or eliminated by blending two or more fluids or a reaching mixture. Static mixers can also be applied for solid blending and blending of particulate solids. Not only that, static mixers can also be used for gas mixing, gas/liquid dispersion and spray evaporation. Static mixers are also used in processing glues whereas one of the household applications of disposable static mixers is the blending of two-part epoxy resins using disposable static mixers (Ghanem, Lemenand, Valle, & Peerhossaini, 2013). A gear pump and static mixer are used to blend additives such as stabilizers, internal lubricants, plasticizers, fillers, flame retardants and colorants into polymer melts. Static mixers can homogenize concentration and temperature in blending of nearly immiscible polymers. In the food industry, static mixers are applied to mix juices, acids, beverages, oils, chocolate, sauces or milk drinks in food formulation. Lastly, static mixers are also used in sludge treatment and water clarification. Low concentrations of suspended solid particles cause turbidity in drinking water. Flocculating agent such as alginate is dispersed by static mixers as the first step in clarification. Static mixers are also used for dechlorination in water treatment. Static mixers are reported to be able to reduce requirements of additive during sludge conditioning in water treatment. Besides, static mixers are also used for pre-reactor feed blending in order to improve reaction yields. Static mixers can reduce emission of nitric oxide in combustor effectively. Lastly, static mixers are incorporated in nuclear industry in order to enhance sampling and analysis of contaminants in an air flow (Thakur, Vial, Nigam, Nauman, & Djelveh, 2003).

2.4   Research Gap

Multiphase flows, especially bubbly flows have not been widely studied using experimental investigations and CFD simulations. There are several outcomes for this research project. The first outcome is a deeper understanding on the differences of PBM and IAC model in simulating bubbly flows can be obtained. The simulation of bubbly flow in a 2D vertical bubble column reactor using PBM and IAC model can be studied and verified by benchmarking against an available case study. The differences in the results obtained in simulating 2D vertical bubble column reactor using PBM and IAC model can be compared too. Not only that, the second outcome is the knowledge on the flow characteristics of bubbly flow, such as the flow physics of bubbly flow in 2D horizontal pipe by manipulating the ratio of AV/WV using PBM can be increased. Lastly, the third outcome is the effects of varying the inlet air volume fraction on the mixing characteristics of 3D Kenics static mixer can be better understood too. All the results can be utilized to improve the knowledge on the methods to enhance the mixing performance and fluid flow of multiphase flows, especially bubbly flows in the industries.

The mesh size is constructed to be not too small due to the low computational power of the computer used to perform the CFD simulations. This will certainly affect the accuracy of the CFD simulation results as smaller mesh size generally will generate CFD simulation results that have higher accuracy. Mesh dependency test is also not conducted due to the low computational power of the computer used to perform the CFD simulations. As such, validation of the accuracy of the CFD simulation results cannot be done. Air and water are assumed to be incompressible in order to prevent solution divergence.

CHAPTER 3: METHODOLOGY

3.1   Introduction

This chapter discusses about the various procedures required to obtain the simulation results in order to achieve all the objectives. Firstly, the governing equations that are solved in FLUENT such as the continuity equation, conservation of momentum equation and the equations related to PBM and IAC model are stated. Then, important steps such as the geometry, meshing and numerical method for each of the objectives are mentioned and discussed. Lastly, the settings used for each of the steps are discussed and justified in detail too.

3.2   Governing Equations

The important equations solved in FLUENT are stated here. The continuity equation and the conservation of momentum equation are used for multiphase flows whereas the population balance equation and the interfacial area concentration model equation are used when there are air bubbles in a multiphase flow.

3.2.1   Continuity

Continuity Equation (ANSYS, Inc., 2009):

$$\frac{\partial}{\partial t}\left(\alpha_q \rho_q\right) + \nabla \cdot \left(\alpha_q \rho_q \vec{v}_q\right) = \sum_{p=1}^{n}\left(\dot{m}_{pq} - \dot{m}_{qp}\right) + S_q \tag{3.1}$$

The notations and their definitions for the continuity equation are tabulated in Table 3.1

3.2.2   Conservation of Momentum

Conservation of Momentum Equation (ANSYS, Inc., 2009):

$$\frac{\partial}{\partial t}\left(\alpha_q \rho_q \vec{v}_q\right) + \nabla \cdot \left(\alpha_q \rho_q \vec{v}_q \vec{v}_q\right) = -\alpha_q \nabla p + \nabla \cdot \bar{\bar{\tau}}_q + \alpha_q \rho_q \vec{g} + \sum_{p=1}^{n}\left(\vec{R}_{pq} + \right.$$

$$\left. \dot{m}_{pq}\vec{v}_{pq} - \dot{m}_{qp}\vec{v}_{qp}\right) + \left(\vec{F}_q + \vec{F}_{lift,q} + \vec{F}_{vm,q}\right) \tag{3.2}$$

The notations and their definitions for the conservation of momentum equation are also tabulated in Table 3.1.

Table 3.1 Notations and Their Definitions for Continuity Equation and Conservation of Momentum Equation (ANSYS, Inc., 2009)

Notation	Definition
p	Phase p
q	Phase q
α	Volume Fraction
ρ	Density
$\dot{m}$	Mass Flow Rate
$\vec{v}$	Velocity Vector
S	Source Term
$\bar{\bar{\tau}}$	Stress-Strain Tensor
$\vec{g}$	Gravity Vector
$\vec{R}$	Interaction Force
$\vec{F}$	External Force Vector
$\vec{F}_{lift}$	Lift Force Vector
$\vec{F}_{vm}$	Virtual Mass Force Vector

3.2.3   Population Balance Model

Population Balance Equation (ANSYS, Inc., 2009):

$$\frac{\partial}{\partial t}[n(V,t)] + \nabla \cdot [\vec{u}n(V,t)] + \nabla_v \cdot [G_v n(V,t)] = \frac{1}{2}\int_0^V a(V-V',V')n(V-$$

$$V',t)n(V',t)dV' - \int_0^\infty a(V,V')n(V,t)n(V',t)dV' + \int_{\Omega_v} pg(V')\beta(V|V')n(V',t)dV' -$$

$$g(V)n(V,t) \tag{3.3}$$

The boundary and initial conditions (ANSYS, Inc., 2009):

$$n(V, t = 0) = n_v \tag{3.4}$$

$$n(V = 0, t)G_v = \dot{n}_0 \tag{3.5}$$

The important notations and their definitions are tabulated in Table 3.2. The third term on the left-hand side of the population balance equation is the growth term whereas the first term, second term, third term and fourth term on the right-hand side of the population balance equation are the birth due to aggregation term, death due to aggregation term, birth due to breakage term and death due to breakage term respectively (ANSYS, Inc., 2009).

Table 3.2 Important Notations and Their Definitions for Population Balance Equation (ANSYS, Inc., 2009), (ANSYS, Inc., 2009), (ANSYS, Inc., 2009)

Notation	Definition
G_v	Growth Rate Based on Particle Volume (m^3/s)
$g(V')$	Frequency of Breakage ($m^{-3}s^{-1}$)
p	Number of Child Particles
$\beta(V\|V')$	Distribution Function of Particle Fragmentation
$\dot{n}_0$	Nucleation Rate (Particles/$m^3 \cdot s$)

3.2.4   Interfacial Area Concentration Model

IAC Model Transport Equation (ANSYS, Inc., 2009):

$$\frac{\partial(\rho_g \chi_p)}{\partial t} + \nabla \cdot \left(\rho_g \vec{u}_g \chi_p\right) = \frac{1D\rho_g}{3Dt}\chi_p + \frac{2\dot{m}_g}{3\alpha_g}\chi_p + \rho_g(S_{RC} + S_{WE} + S_{TI}) \tag{3.6}$$

The notations and their definitions are tabulated in Table 3.3. The first term and second term on the left hand side of the IAC transport equation are expansion of gas bubble due to compressibility and expansion of gas bubble due to mass transfer respectively (ANSYS, Inc., 2009).

58

Table 3.3 Notations and Their Definitions for IAC Transport Equation
(ANSYS, Inc., 2009)

Notation	Definition
ρ	Density
χ	Interfacial Area Concentration (m^2/ m^3)
$\vec{u}$	Velocity Vector
α	Volume Fraction
$\dot{m}$	Mass Transfer Rate
S_{RC}	Coalescence Sink Term Due to Random Collision
S_{WE}	Coalescence Sink Term Due to Wake Entrainment
S_{TI}	Breakage Source Term Due to Turbulent Impact

3.3 CFD Simulation of 2D Vertical Bubble Column Reactor

3.3.1 2D Geometry of Vertical Bubble Column Reactor

The 2D model of the vertical bubble column reactor is shown in Figure 3.1 whereas the parameters and dimensions of the 2D model are tabulated in Table 3.4. The 2D model of the vertical bubble column reactor is obtained from the mesh file that is provided by the case study from ANSYS (ANSYS, Inc., n.d.). Air bubbles enter from the inlet, which is located at the bottom of the 2D vertical bubble column reactor and represented by the blue line and then travels to the outlet, which is located at the top of the 2D vertical bubble column. There is a region in the 2D vertical bubble column reactor that initially contains air bubbles and is represented by the region of red colour. The location of the region is from 1.8 m to 2.0 m in the +X direction and from 0 m to 0.145 m in the +Y direction. The domain is the 2D model of the fluid inside the vertical bubble column as shown in Figure 3.1.
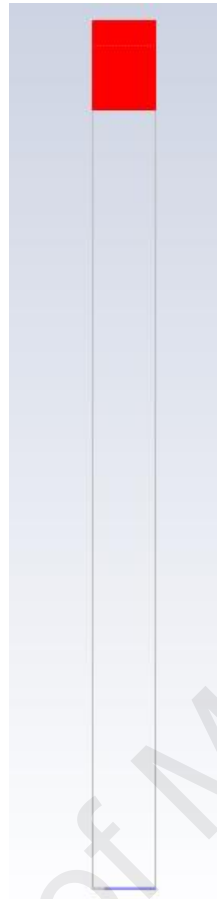
Figure 3.1 2D Model of the Vertical Bubble Column Reactor

Table 3.4 Parameters and Dimensions of the 2D Vertical Bubble Column Reactor

Parameter	Dimension
Height (m)	2
Diameter (m)	0.145
Diameter of the Inlet (m)	0.115
Diameter of the Outlet (m)	0.145
Area of Region That Initially Contains Air Bubbles (m^2)	0.029

3.3.2   Meshing of 2D Vertical Bubble Column Reactor

Meshing of the domain is already completed in the mesh file and is shown in Figure 3.2. The grids used are the same as the case study in order to ensure that almost similar simulation results are produced. In many cases, different quality of mesh used for the same simulation will produce different results.
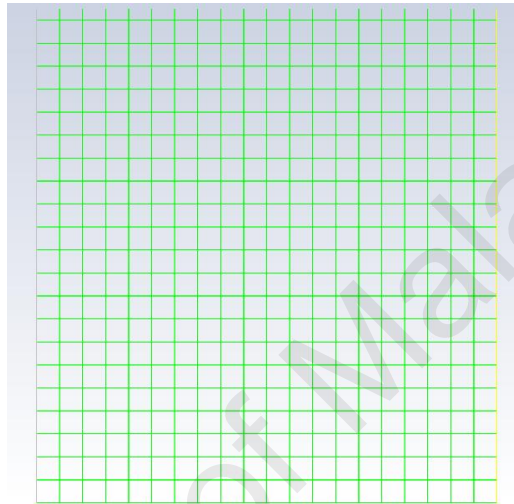
Figure 3.2 Meshing of the Domain of the 2D Vertical Bubble Column Reactor

3.3.3   Numerical Method for Objective 1 (PBM)

The title of the case study from ANSYS is "Tutorial: Modeling Bubble Breakup and Coalescence in a Bubble Column Reactor" (ANSYS, Inc., 2012). The settings used are referred to the guideline provided by the case study. "Double Precision" function is enabled. Only one core is used to calculate the solution. Gravity with magnitude 9.81 m/s² is included in the -X direction. Viscous model of k-ε turbulence model is used. Eulerian multiphase model is used and solved with implicit formulation. Surface tension coefficient between water and air is set at 0.07 N/m (nanoScience Instruments, n.d.). Schiller-Naumann model is used for the drag coefficient. PBM is enabled. The parameters

and settings of PBM are tabulated in Table 3.5 whereas the parameters and settings of the

bins are tabulated in Table 3.6. The bins and their respectively diameters are tabulated in

Table 3.7.

Table 3.5 Parameters and Settings of PBM for 2D Vertical Bubble Column Reactor

Parameter	Characteristic
Method	Discrete
Particle Volume Coefficient, Kv	0.5235988
Definition	Geometric Ratio
Aggregation Kernel (m^3/s)	Luo-Model
Breakage Kernel: Frequency (1/s)	Luo-Model
Formulation	Hagesather

Table 3.6 Parameters and Settings of Bin in PBM for 2D Vertical Bubble Column Reactor

Parameter	Setting
Phases	Air
Number of Bins	6
Ratio Exponent	2
Min Diameter (m)	0.001191
Max Diameter (m)	01200453

Table 3.7 Bins and Their Respective Diameters for 2D Vertical Bubble Column Reactor

Bin	Diameter (m)
0	0.01200453
1	0.0075623797
2	0.0047640005
3	0.0030011322
4	0.0018905947
5	0.001191

The boundary conditions and their settings are tabulated in Table 3.8. The materials

and their thermophysical properties such as density (p) and dynamic viscosity (μ) are

tabulated in Table 3.9. The thermophysical properties are taken from Fluent database.

Table 3.8 Boundary Conditions and Their Settings for 2D Vertical Bubble Column Reactor

Boundary Condition	Setting
Velocity-Inlet	Air Velocity of 0.1 m/s at X Direction
	Water Velocity of 0 m/s
	Air Volume Fraction of 1
	Bin 3 Fraction of 1
	Hydraulic Diameter of 0.145 m
Pressure-Outlet	0 Pa (Gauge Pressure)
	Air Backflow Volume Fraction of 1
	Bin 3 Backflow Volume Fraction of 1
	Backflow Hydraulic Diameter of 0.145 m
Axis	-
Wall of Fluids	Stationary
	No Slip
Operating Density (kg/m^3)	1.225

Table 3.9 Materials and Their Thermophysical Properties

Material	Thermophysical Property	
	ρ (kg/m^3)	μ (Pa•s)
Air	1.225	1.7894 x 10^{-5}
Water	998.2	1.003 x 10^{-3}

The solution methods and their settings are tabulated in Table 3.10. SIMPLE scheme is used for pressure-velocity coupling because the computational time can be reduced due to high rate of convergence. Least squares cell based gradient for spatial discretization is chosen because the accuracy of least square cell based gradient is relatively high for poor quality meshes. Not only that, the computational cost of least square cell based gradient is relatively low (ANSYS, Inc., 2009). The momentum, turbulent kinetic energy, turbulent dissipation rate and air bin equations are solved in second order. However, the pressure volume fraction equation is solved in first order following the guideline of the case study. The parameters of the calculation methods and their settings are tabulated in Table 3.11. The total flow time at the end of the simulation is 50 s.

Table 3.10 Solution Methods and Their Settings for 2D Vertical Bubble Column Reactor

Solution Method	Setting
Pressure-Velocity Coupling	
Scheme of Pressure-Velocity Coupling	Phase Coupled SIMPLE
Spatial Discretization	
Gradient	Least Squares Cell Based
Pressure	PRESTO!
Momentum	Second Order Upwind
Volume Fraction	First Order Upwind
Turbulent Kinetic Energy	Second Order Upwind
Turbulent Dissipation Rate	Second Order Upwind
Air Bin	Second Order Upwind
Transient Formulation	Second Order Implicit

Table 3.11 Parameters of the Calculation Methods and Their Settings of PBM for 2D Vertical Bubble Column Reactor

Parameter	Setting
Solver	
Type	Pressure-Based
Velocity Formulation	Absolute
Time	Transient
2D Space	Axisymmetric
Calculation of Solution	
Time Stepping Method	Fixed
Time Step Size (s)	0.001
Number of Time Steps	50000
Max Iterations / Time Step	5000
Reporting Interval	1
Profile Update Interval	1

3.3.4 Numerical Method for Objective 1 (IAC Model)

The settings in this section are almost similar section 3.3.3. IAC model instead of PBM is enabled. The parameters and settings of IAC model are tabulated in Table 3.12. IAC of 0.00001 m^{-1} is set for the velocity-inlet boundary condition whereas backflow IAC of 0.00001 m^{-1} is also set for the pressure-outlet boundary condition. There is an additional equation to be solved in solution method, which is the IAC equation. IAC equation is solved using second order upwind. The parameters of the calculation methods and their settings for IAC model are tabulated in Table 3.13.

Table 3.12 Parameters and Settings of IAC Model for 2D Vertical Bubble Column Reactor

Parameter	Setting
Diameter (m)	0.003
Surface Tension (N/m)	0.07
Coalescence Kernel	Hibiki-Ishii
Breakage Kernel	Hibiki-Ishii
Nucleation Rate	None
Dissipation Function (m^2/s^3)	Wu-Ishii-Kim
Hydraulic Diameter (m)	0.145
Min Diameter (m)	0.001
Max Diameter (m)	0.012

Table 3.13 Parameters of the Calculation Methods and Their Settings of IAC Model for 2D Vertical Bubble Column Reactor

Parameter	Setting
Solver	
Type	Pressure-Based
Velocity Formulation	Absolute
Time	Transient
2D Space	Axisymmetric
Calculation of Solution	
Time Stepping Method	Fixed
Time Step Size (s)	0.01
Number of Time Steps	5000
Max Iterations / Time Step	500
Reporting Interval	1
Profile Update Interval	1

3.3.5   Simulation and Analysis for Objective 1

The simulation results obtained are benchmarked against the case study from ANSYS. The flux reports of net mass flow rate for both PBM and IAC model will be tabulated. The differences in simulation results obtained using PBM and IAC model with the simulation results from the case study will be compared, analyzed and discussed. Contours such as air volume fraction contours, air bin 0 fraction contours, discrete size 3 fraction contours and Sauter mean diameter of air contours for the three cases will be displayed, compared and discussed. Water velocity vectors for the three cases will be displayed, compared and discussed too. Not only that, graphs of bin 3 fraction against X direction at the centre of the 2D vertical bubble column reactor for PBM and the case study will be plotted, analyzed and discussed as well. Lastly, Sauter mean diameter of air distribution histograms for the three cases will be plotted, analyzed and discussed too.

3.4   CFD Simulation of Bubbly Flow in 2D Horizontal Pipe

3.4.1   2D Geometry of Horizontal Pipe

The 2D model of the horizontal pipe is drawn using DesignModeler and is shown in Figure 3.3 whereas the parameters and dimensions of the 2D model are tabulated in Table 3.14. The inlet height of air is only 10 % of the total height of the pipe and is represented by B in Figure 3.3, which is in the middle of the inlet of the 2D horizontal pipe whereas the remaining height of the inlet is water inlet. This indicates that there is an air inlet and two water inlets for the 2D horizontal pipe. Air and water flow from the air inlet and water inlets respectively to the outlet of the 2D horizontal pipe. The domain is the fluids in the 2D horizontal pipe as shown in Figure 3.3. This is because we are only interested in the flow characteristics of the bubbly flow in the 2D horizontal pipe.
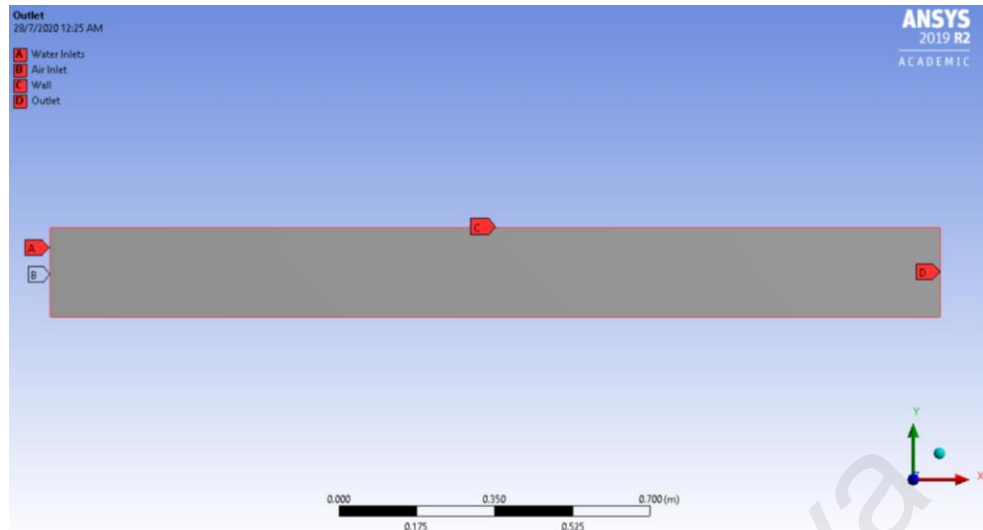
Figure 3.3 2D Model of the Horizontal Pipe

Table 3.14 Parameters and Dimensions of the 2D Horizontal Pipe

Parameter	Dimension
Total Height (m)	0.2
Inlet Height of Air (m)	0.02
Number of Water Inlet	2
Inlet Height of Water (m)	0.09
Total Length (m)	2

3.4.2   Meshing of 2D Horizontal Pipe

The meshing of the domain is shown in Figure 3.4 whereas the parameters and characteristics of the mesh are tabulated in Table 3.15. The function of grids is to divide a region in space into smaller regions (Encyclopedia.com, 2020). Grid is very crucial because the discrete geometry in many fluid flow or heat transfer applications is represented by the grid. Not only that, designation of the cells or elements based on the type of flow is also done by the grid. The convergence rate, solution accuracy and computational cost are greatly affected by the quality of the grid. The two main types of grids are triangle (2D) or tetrahedron (3D) grid and quadrilateral (2D) or hexahedron (3D)

grid. Quadrilateral grid is used because the geometry of the 2D model is quite simple. The simulation results generated using quadrilateral grid are usually more accurate than using triangle grid for simple geometries.

Mesh metric of skewness, mesh metric of orthogonal quality, mesh metric criteria spectrum for skewness and mesh metric criteria spectrum for orthogonal quality are tabulated in Table 3.16, Table 3.17, Table 3.18 and Table 3.19 respectively. It can be concluded that good quality mesh is generated because the worst-case scenario for skewness of mesh falls under "Good" in the mesh metric criteria spectrum for skewness whereas the worst-case scenario for orthogonal quality of mesh falls under "Very Good" in the mesh metric criteria spectrum for orthogonal quality.
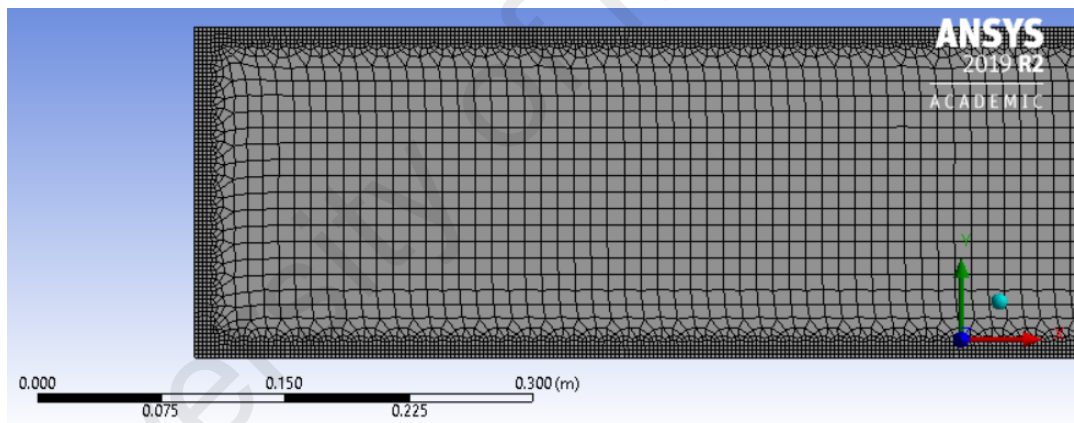
Figure 3.4 Meshing of the Domain of 2D Horizontal Pipe

Table 3.15 Parameters and Characteristics of the Mesh for 2D Horizontal Pipe

Parameter	Characteristic
Curvature Normal Angle	18 °
Smoothing	High
Method	Quadrilateral
Number of Nodes	14669
Number of Elements	13788

Table 3.16 Mesh Metric of Skewness for 2D Horizontal Pipe

Parameter	Number of Elements
Minimum	1.3057×10^{-10}
Maximum	0.51974
Average	0.10754
Standard Deviation	0.14225

Table 3.17 Mesh Metric of Orthogonal Quality for 2D Horizontal Pipe

Parameter	Number of Elements
Minimum	0.81934
Maximum	1
Average	0.98137
Standard Deviation	3.4263×10^{-2}

Table 3.18 Mesh Metric Criteria Spectrum for Skewness (Fatchurrohman & Chia, 2017)

Excellent	Very Good	Good	Acceptable	Bad	Very Bad
0-0.25	0.25-0.50	0.50-0.80	0.80-0.94	0.95-0.97	0.98-1.00

Table 3.19 Mesh Metric Criteria Spectrum for Orthogonal Quality (Fatchurrohman & Chia, 2017)

Very Bad	Bad	Acceptable	Good	Very Good	Excellent
0-0.001	0.001-0.14	0.15-0.20	0.21-0.69	0.70-0.95	0.95-1.00

3.4.3   Numerical Method for Objective 2

"Double Precision" function is enabled. Four cores are used to calculate the solution. Gravity with magnitude 9.81 m/s^2 is included in the -Y direction. Viscous model of k-ε turbulence model is used. Eulerian multiphase model is used and solved with explicit formulation. Surface tension coefficient between water and air is set at 0.07 N/m (nanoScience Instruments, n.d.). Schiller-Naumann model is used for the drag coefficient. PBM is enabled. PBM is used because it is found that the simulation results using PBM rather than IAC model have higher similarity with the results from the case study from

FLUENT. The parameters and settings of PBM are tabulated in Table 3.20. Only 1 air bin is used, which is air bin 0 and the diameter of the air bin is set at 0.0003 m. Aggregation kernel and breakage kernel are not activated. The smallest size of the grid is ensured to be bigger than the bubble size in order to avoid solution divergence issue.

Table 3.20 Parameters and Settings of PBM for 2D Horizontal Pipe

Parameter	Characteristic
Method	Discrete
Particle Volume Coefficient, Kv	0.5235988
Definition	Geometric Ratio

The boundary conditions and their settings are tabulated in Table 3.21. The materials and their properties are the same as in Table 3.9. The manipulated variable and its values are tabulated in Table 3.22. The solution methods and their settings are tabulated in Table 3.23. Lastly, the parameters of the calculation methods and their settings are tabulated in Table 3.24. The total flow time at the end of the simulation is 30 s.

Table 3.21 Boundary Conditions and Their Settings for 2D Horizontal Pipe

Boundary Condition	Setting
Velocity-Inlet (Air)	Air Velocity of 0.1 m/s at X Direction
	Water Velocity of 0 m/s
	Air Volume Fraction of 1
	Bin 0 Fraction of 1
Velocity-Inlet (Water)	Water Velocity of 0.1 m/s at X Direction
	Air Velocity of 0 m/s
Outflow	Flow Rate Weighting of 1
Wall of Fluids	Stationary
	No Slip
Operating Density (kg/m^3)	1.225

Table 3.22 Manipulated Variable and its Values for 2D Horizontal Pipe

Manipulated Variable	Value		
	Air Velocity (m/s)	Water Velocity (m/s)	AV/WV Ratio
Ratio of AV/WV	0.001	0.1	0.01
	0.005	0.1	0.05
	0.01	0.1	0.1
	0.1	0.1	1
	0.1	0.01	10
	0.1	0.001	100
	0.1	0.0001	1000

Table 3.23 Solution Methods and Their Settings for 2D Horizontal Pipe

Solution Method	Setting
Pressure-Velocity Coupling	
Scheme of Pressure-Velocity Coupling	Phase Coupled SIMPLE
Spatial Discretization	
Gradient	Least Squares Cell Based
Pressure	Second Order
Momentum	Second Order Upwind
Volume Fraction	QUICK
Turbulent Kinetic Energy	Second Order Upwind
Turbulent Dissipation Rate	Second Order Upwind
Air Bin	Second Order Upwind
Transient Formulation	First Order Implicit

Table 3.24 Parameters of the Calculation Methods and Their Settings for 2D Horizontal Pipe

Parameter	Setting
Solver	
Type	Pressure-Based
Velocity Formulation	Absolute
Time	Transient
2D Space	Planar
Calculation of Solution	
Time Stepping Method	Fixed
Time Step Size (s)	0.01
Number of Time Steps	3000
Max Iterations / Time Step	30
Reporting Interval	1
Profile Update Interval	1

3.4.4   Simulation and Analysis for Objective 2

The flux reports of net mass flow rate for all the different AV/WV ratios will be tabulated. The contours of air volume fraction and air bin 0 for all the different ratios of AV/WV will be displayed, analyzed and discussed. Graphs of Y axis against air volume fraction and air bin 0 for all the different ratios of AW/WV at different X coordinates will be plotted, analyzed and discussed. The flow characteristics of bubbly flow, such as the flow physics of air bubbles in the 2D horizontal pipe for all the different AV/WV ratios will be analyzed and discussed in detail. Mesh dependency test is not conducted due to the limitations faced as discussed in section 1.4.

3.5   CFD Simulation of Water-Air Multiphase Flow in 3D Kenics Static Mixer

3.5.1   3D Geometry of Kenics Static Mixer

The 3D model of the Kenics static mixer is constructed using DesignModeler as shown in Figure 3.5 whereas the parameters and dimensions of the 3D model are tabulated in Table 3.25. There are 10 Kenics elements in the tube. The Kenics elements are orientated and alternated to ensure that each leading edge of the element is at 90 ° with respect to the trailing edge of the next element (Rauline, Le Blévec, Bousquet, & Tanguy, 2000). Every Kenics mixing element is twisted for 0.5 turns. Air and water enter from the air inlet whereas only water enters from the water inlet of the Kenics static mixer. The mixture of air and water flows to the two outlets of the Kenics static mixer. The domain is the fluids in the 3D Kenics static mixer as shown in Figure 3.5. This is because we are only interested in the flow characteristics of the fluids in the 3D Kenics static mixer.
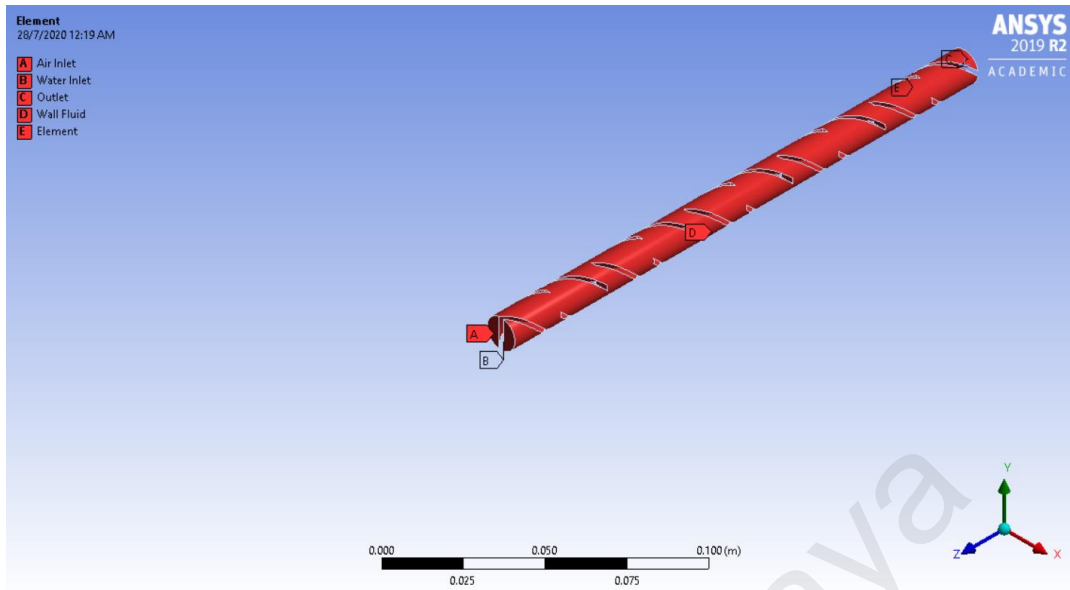
Figure 3.5 3D Model of the Kenics Static Mixer

Table 3.25 Parameters and Dimensions of the 3D Kenics Static Mixer

Parameter	Dimension
Length of Each Kenics Element (m)	0.02
Thickness of Each Kenics Element (m)	0.002
Number of Kenics Element	10
Number of Outlet	2
Length of Tube (m)	0.2
Diameter of Tube (m)	0.012

3.5.2   Meshing of 3D Kenics Static Mixer

The meshing of the domain is shown in Figure 3.6 whereas the parameters and characteristics of the mesh are tabulated in Table 3.26. Tetrahedron grids are chosen for the meshing of the domain because the geometry of the domain is quite complex. The advantage of tetrahedron grid is the time and efforts required for meshing will be significantly reduced. For complex geometries, hexahedron grid does not show any significant advantage in numerical calculation of solution compared to tetrahedron grid.

Mesh metric of skewness and mesh metric of orthogonal quality are tabulated in Table 3.27 and Table 3.28 respectively. It can be concluded that good quality mesh is generated because the worst-case scenario for both skewness and orthogonal quality of the mesh fall under "Good" criteria in the mesh metric criteria spectrum for skewness and orthogonal quality.
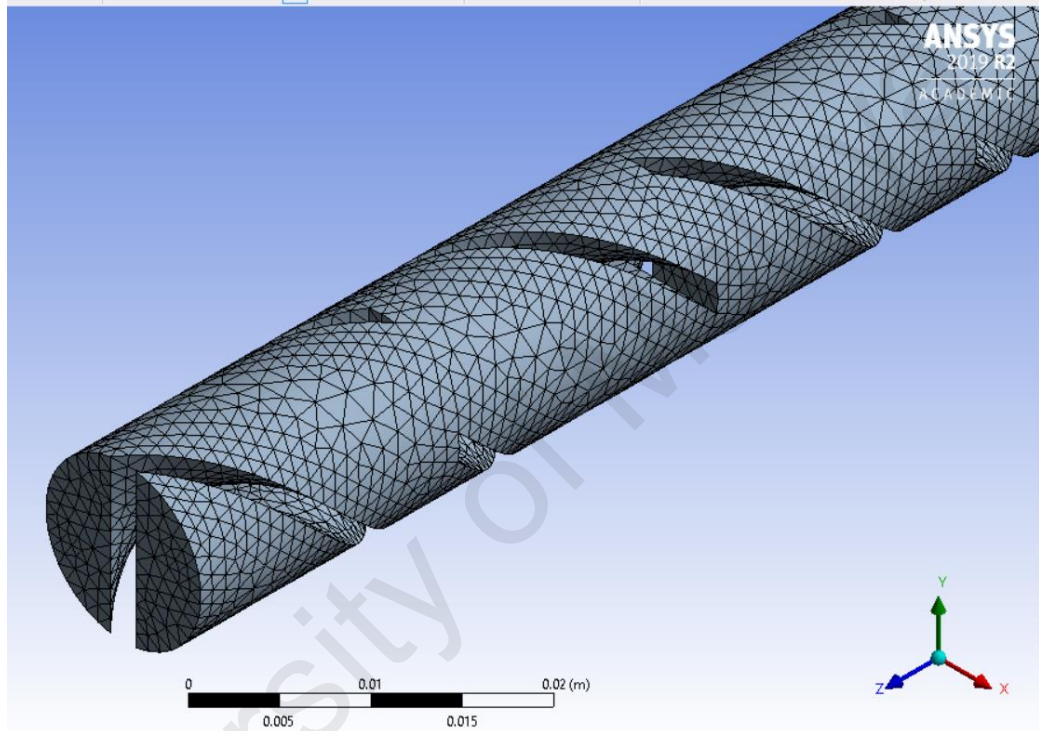
Figure 3.6 Meshing of the Domain of 3D Kenics Static Mixer

Table 3.26 Parameters and Characteristics of the Mesh for 3D Kenics Static Mixer

Parameter	Characteristic
Curvature Normal Angle	20 °
Smoothing	High
Method	Tetrahedron
Algorithm	Patch Conforming
Number of Nodes	24284
Number of Elements	107011

Table 3.27 Mesh Metric of Skewness for 3D Kenics Static Mixer

Parameter	Number of Elements
Minimum	5.3188×10^{-5}
Maximum	0.7809
Average	0.23289
Standard Deviation	0.11993

Table 3.28 Mesh Metric of Orthogonal Quality for 3D Kenics Static Mixer

Parameter	Number of Elements
Minimum	0.2191
Maximum	0.98928
Average	0.76555
Standard Deviation	0.11778

3.5.3 Numerical Method for Objective 3

"Double Precision" function is enabled in order to improve the accuracy of simulation results. However, memory usage and computational cost will be increased. Four cores are used for the calculation of solution. Gravity with magnitude 9.81 m/s^2 is included in the -Y direction. Viscous model of k-ε turbulence model is used. VOF multiphase model is enabled and explicit formulation is used to solve the VOF model. Surface tension coefficient between water and air is set at 0.07 N/m (nanoScience Instruments, n.d.). Schiller-Naumann model is used for the drag coefficient. The boundary conditions and their settings are tabulated in Table 3.29.

Table 3.29 Boundary Conditions and Their Settings for 3D Kenics Static Mixer

Boundary Condition	Setting
Velocity-Inlets	Air Velocity of 0.01 m/s at -Z Direction
	Water Velocity of 0.01 m/s at -Z Direction
Pressure-Outlets	0 Pa (Gauge Pressure)
	Air Backflow Volume Fraction of 0
Wall of Fluids	Stationary
	No Slip
Operating Density (kg/m^3)	1.225

The materials and their thermophysical properties are the same as in Table 3.9. The manipulated variable and its values are tabulated in Table 3.30 whereas the solution methods and their settings are tabulated in Table 3.31. The momentum, turbulent kinetic energy and turbulent dissipation rate equations are solved in second order whereas the volume fraction equation is solved in third order in order to improve the accuracy of results.

Table 3.30 Manipulated Variable and its Values for 3D Kenics Static Mixer

Manipulated Variable	Value
Air Volume Fraction at the Air Inlet of the Kenics Static Mixer	0.1
	0.2
	0.3

Table 3.31 Solution Methods and Their Settings for 3D Kenics Static Mixer

Solution Method	Setting
Pressure-Velocity Coupling	
Scheme of Pressure-Velocity Coupling	SIMPLE
Spatial Discretization	
Gradient	Least Squares Cell Based
Pressure	PRESTO!
Momentum	Second Order Upwind
Volume Fraction	QUICK
Turbulent Kinetic Energy	Second Order Upwind
Turbulent Dissipation Rate	Second Order Upwind
Transient Formulation	First Order Implicit

The parameters of the calculation methods and their settings are tabulated in Table 3.32. The total flow time at the end of the simulation is 30 s.

Table 3.32 Parameters of the Calculation Methods and Their Settings for 3D Kenics Static Mixer

Parameter	Setting
Solver	
Type	Pressure-Based
Velocity Formulation	Absolute
Time	Transient
2D Space	Planar
Calculation of Solution	
Time Stepping Method	Fixed
Time Step Size (s)	0.01
Number of Time Steps	3000
Max Iterations / Time Step	30
Reporting Interval	1
Profile Update Interval	1

3.5.4 Simulation and Analysis for Objective 3

The flux reports of net mass flow rate for various inlet air volume fractions will be tabulated. The contours of air volume fraction in isometric view for air volume fraction of 0.1, 0.2 and 0.3 will be displayed, analyzed and discussed. Not only that, the contours of air volume fraction at the face of every Kenics mixing element for the various inlet air volume fractions will be displayed, analyzed and discussed too. Lastly, the flow characteristics of air-water multiphase flow in the 3D Kenics static mixer will be studied, analyzed and discussed in detail too. Mesh dependency test is not conducted due to the limitations faced as discussed in section 1.4.

CHAPTER 4: RESULTS AND DISCUSSION

4.1   Introduction

This chapter presents the CFD simulation results obtained for all the three objectives. The relevant contours, graphs and histograms are displayed and plotted here. Not only that, this chapter also discusses about the simulation results obtained in achieving the objectives of this research project. The contours and plotted graphs will be analyzed, compared and discussed in detail.

4.2   Validation of PBM and IAC Model

4.2.1   Flux Reports for 2D Vertical Bubble Column Reactor

The flux reports of net mass flow rate of mixture, water and air in 2D vertical bubble column reactor for simulation using PBM and IAC model are tabulated in Table 4.1. From Table 4.1, it can be observed that the net mass flow rate of mixture, water and air in the 2D vertical bubble column reactor for simulation using PBM and IAC model are almost 0. This indicates that the mass of mixture, water and air in the 2D vertical bubble column reactor are conserved.

Table 4.1 Flux Reports for Simulation using PBM and IAC Model for 2D Vertical Bubble Column Reactor

Parameter	Mass Flow Rate (kg/s)		
	Mixture	Water	Air
PBM	-6.753756×10^{-5}	-6.762032×10^{-5}	8.276681×10^{-8}
IAC Model	-1.380255×10^{-8}	$-4.480912 \times 10^{-11}$	-1.375775×10^{-8}

4.2.2 Air Volume Fraction Contours for 2D Vertical Bubble Column Reactor

The air volume fraction contours simulated using PBM, simulated using IAC model and from the case study are displayed in Figure 4.1. From Figure 4.1, it can be observed that the air volume fraction contours simulated using PBM, simulated using IAC model and from the case study are almost similar but with some slight differences. For the three cases, the air volume fraction is higher near the inlet, then decreases from the inlet to the outlet of the 2D vertical bubble column reactor in the +X direction until X coordinate of 1.8 m. The air volume fraction at the top 0.2 m region of the 2D vertical bubble column reactor is 1 because the presence of air bubbles with size of air bin 3 is set as an initial condition at that region. The air volume fraction is the highest at the centre of the 2D vertical bubble column reactor, then gradually decreases in the +Y and -Y directions and eventually reaches zero near the vertical walls of the 2D vertical bubble column reactor until X coordinate of 1.8 m when simulated using PBM and from the case study. However, results simulated using IAC method show that the air volume fraction at the two vertical regions near the centre until X coordinate of 1.8 m is higher, which is around 0.075 compared to the other regions except the top 0.2 m region of the 2D vertical air bubble column reactor. The accuracy of IAC model is lower than PBM because IAC model only solves one transport equation per secondary phase whereas PBM solves several transport equations (ANSYS, Inc., 2009).
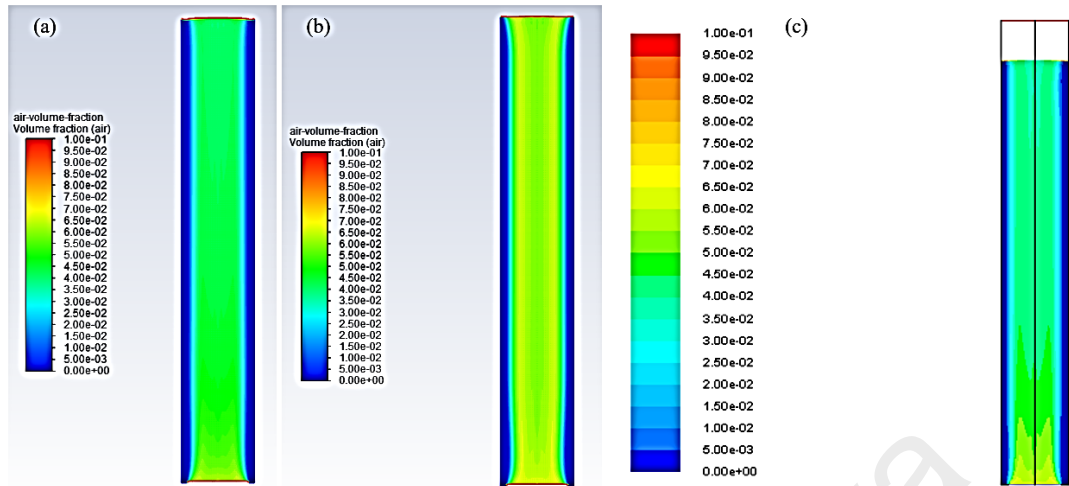
Figure 4.1 Air Volume Fraction Contour (a) Simulated using PBM (b) Simulated using IAC Model (c) From the Case Study (ANSYS, Inc., 2012)

4.2.3 Water Velocity Vectors for 2D Vertical Bubble Column Reactor

The water velocity vectors simulated using PBM, simulated using IAC model and from the case study are displayed in Figure 4.2. From Figure 4.2, it can be observed that the water velocity vectors simulated using PBM, simulated using IAC model and from the case study are about the same. The region with the highest magnitude of water velocity occurs at the inlet for the three cases. However, the region with the highest magnitude of water velocity simulated by PBM and IAC model is slightly larger than from the case study. The magnitude of water velocity decreases from the centre to the vertical walls of the 2D vertical bubble column reactor in the +Y and -Y directions until X coordinate of 1.8 m for all the cases. The water velocity magnitude is zero at the top 0.2 m region of the 2D vertical bubble column reactor due to the initial condition of air bubbles with size of air bin 3 present at that region. It can be observed that there are reversed flows of water at X coordinate of 1.8 m for the results simulated by PBM and IAC model.
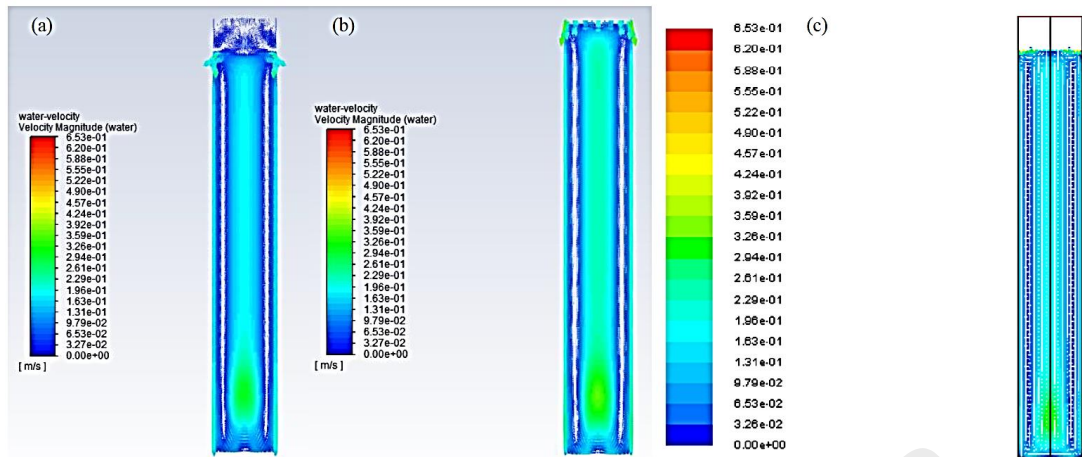
Figure 4.2 Water Velocity Vector (a) Simulated using PBM (b) Simulated using IAC Model (c) From the Case Study (ANSYS, Inc., 2012)

4.2.4 Air Bin 0 Fraction Contours for 2D Vertical Bubble Column Reactor

The air bin 0 fraction contours simulated using PBM and from the case study are displayed in Figure 4.3. From Figure 4.3, it can be observed that the air bin 0 fraction contours simulated using PBM and from the case study are almost similar, except for the top 0.2 m region of the 2D vertical bubble column reactor. IAC model does not have air bin 0 fraction contours because the settings of air bins are not included in the IAC model. The air bin 0 fraction near the vertical walls of the 2D vertical bubble column reactor until X coordinate of 1.8 m is 0 for the two cases. The air bin 0 fraction is zero near the inlet because only air bubbles with size of air bin 3 enter from the inlet. Not only that, the air bin 0 fraction is also zero near the vertical walls of the 2D vertical column reactor until X coordinate of 1.8 m. The air bin 0 fraction gradually increases from the inlet to X coordinate of 1.8 m in the +X direction due to the aggregation and breakage phenomena of the air bubbles. For the top 0.2 m region of the 2D vertical bubble column reactor, result simulated using PBM shows that the air bin 0 fraction at that entire region is around 0.8 whereas result from the case study shows that the air volume fraction is 0 at the centre

81

of that region. The case study also shows that the overall air volume fraction at that region is lower than the simulation results by PBM. The reason might be due to the differences in spatial discretization using PBM and from the case study. Most of the equations are solved in second order for the results simulated using PBM whereas the equations are solved in first order for the case study.
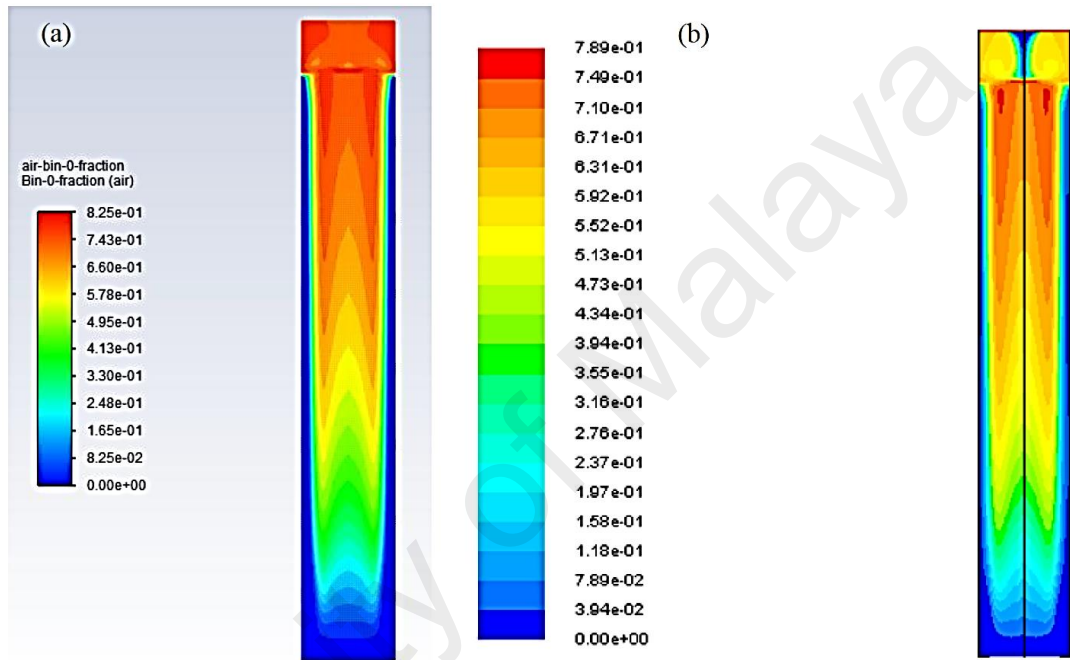
Figure 4.3 Air Bin 0 Fraction Contour (a) Simulated using PBM (b) From the Case Study (ANSYS, Inc., 2012)

4.2.5   Air Bin 3 Fraction Graphs for 2D Vertical Bubble Column Reactor

Graphs of air bin 3 fraction against +X direction at the centre of the 2D vertical bubble column reactor simulated using PBM and from the case study are displayed in Figure 4.4. From Figure 4.4, it can be observed that the air bin 3 fraction is inversely proportional to the +X direction at the centre of the 2D vertical bubble column reactor for both results simulated using PBM and from the case study. IAC model does not have this graph because the settings of air bins are not included in the IAC model. The air bin 3 fraction

82

decreases along the +X direction at the centre of the 2D vertical bubble column reactor due to the aggregation and breakage phenomena of the air bubbles, hence leading to the formation of smaller or bigger sizes of air bubbles as tabulated Table 3.7.
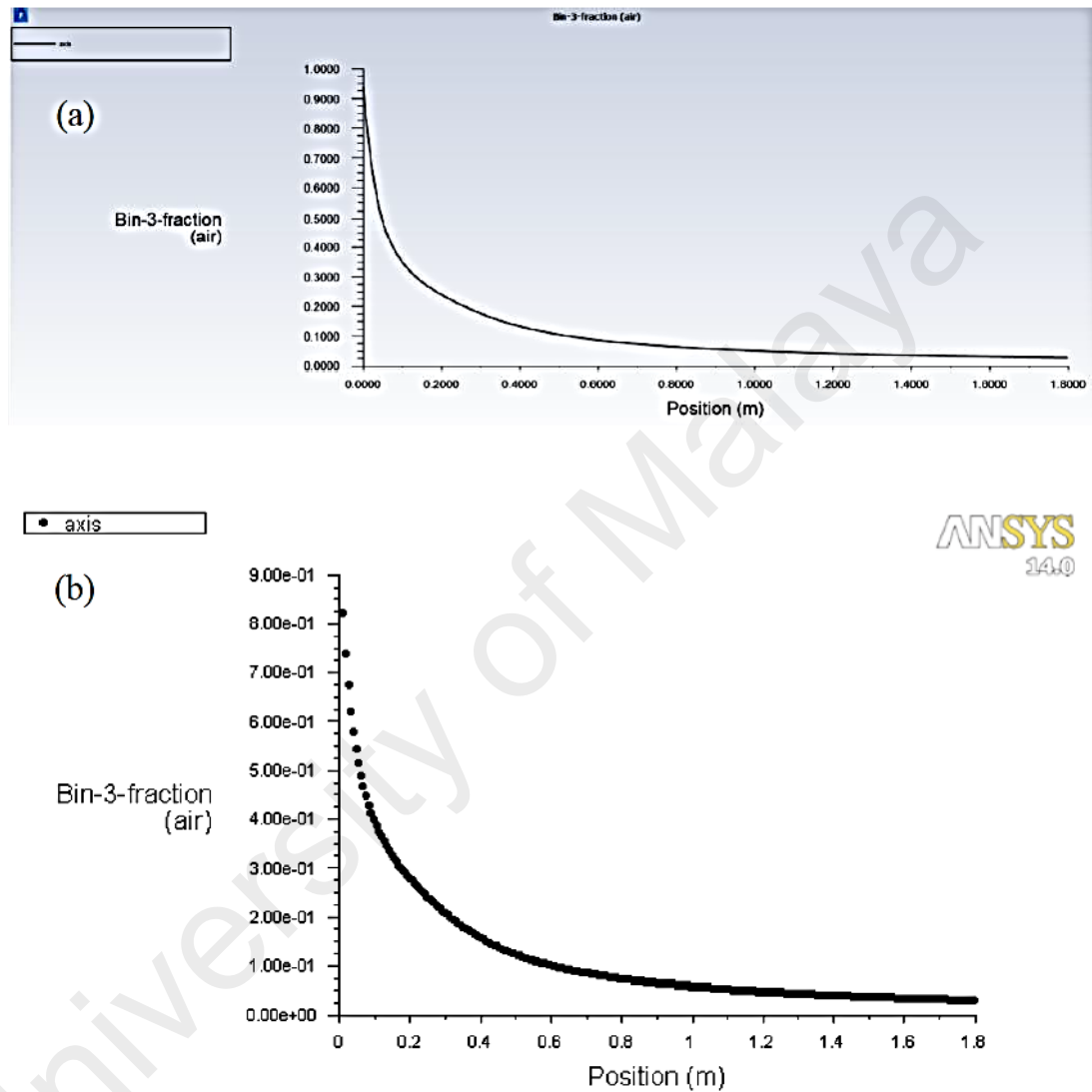
Figure 4.4 Graph of Air Bin 3 Fraction against +X Direction at the Centre of the 2D Vertical Bubble Column Reactor (a) Simulated using PBM (b) From the Case Study (ANSYS, Inc., 2012)

4.2.6   Discrete Size 3 Fraction of Air Contours for 2D Vertical Bubble Column Reactor

Discrete size 3 fraction of air contours simulated using PBM and from the case study are shown in Figure 4.5. From Figure 4.5, it can be observed that the discrete size 3 fraction of air contours simulated using PBM and from the case study are about the same, except for the top 0.2 m region of the 2D vertical bubble column reactor. The definition of discrete size 3 fraction of air is the air bin 3 fraction in the air volume fraction of the air-water mixture. IAC model does not have this graph because the settings of air bins are not included in the IAC model. The discrete size 3 fraction of air has the maximum value of 0.04 near the inlet of the 2D vertical bubble column reactor for both cases. The discrete size 3 fraction of air decreases and eventually reaches zero from the inlet to the X coordinate of 1.8 m in the +X direction due to the aggregation and breakage phenomena of the air bubbles. For the top 0.2 m region of the 2D vertical bubble column reactor, result simulated using PBM shows that the discrete size 3 fraction of air near the vertical walls at that region is around 0.032 to 0.04 whereas the discrete size 3 fraction of air at the remaining area of that region is 1. Result from the case study shows that the discrete size 3 fraction of air at the entire top 0.2 m region of the 2D vertical bubble column reactor is 1. This might be due to the differences in spatial discretization using PBM and from the case study which have already been explained in section 4.2.4.
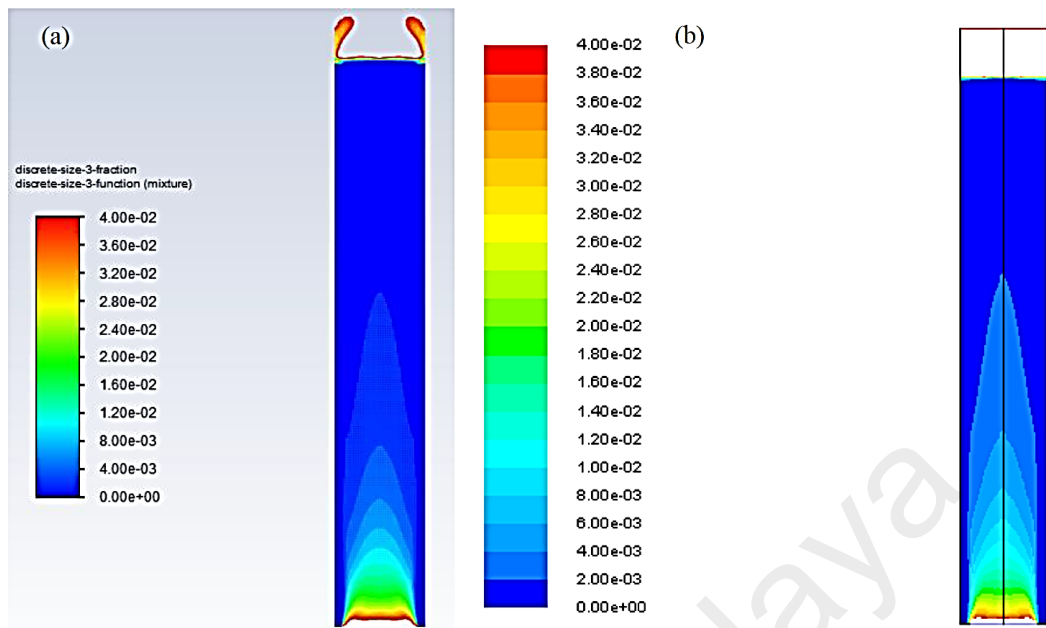
Figure 4.5 Discrete Size 3 Fraction of Air Contour (a) Simulated using PBM (b) From the Case Study (ANSYS, Inc., 2012)

4.2.7 Sauter Mean Diameter of Air Contours for 2D Vertical Bubble Column Reactor

The Sauter mean diameter of air contours simulated using PBM, simulated using IAC model and from the case study are displayed in Figure 4.6. From Figure 4.6, it can be observed that the Sauter mean diameter of air contours simulated using PBM, simulated using IAC model and from the case study are about the same, except for the top 0.2 m region of the 2D vertical bubble column reactor. The definition of Sauter mean diameter is the diameter of a sphere that has the same ratio of volume to surface area as a particle of interest (Wikipedia, 2015). The Sauter mean diameter of air in the entire 2D vertical bubble column reactor simulated using IAC model is 0.003 m because IAC model is unable to vary the air diameter since the inlet air diameter is set as 0.003 m. The results simulated using PBM and from the case study show that the smallest Sauter mean diameter of air occurs at around the inlet and near the vertical walls of the 2D vertical

85

bubble column reactor. The Sauter mean diameter of air decreases from the inlet to the X coordinate of 1.8 m in the +X direction due to aggregation and breakage phenomena of the air bubbles for both cases. For the top 0.2 m region of the 2D vertical bubble column reactor, result simulated using PBM shows that the Sauter mean diameter of air is lower at the centre of that region whereas the maximum Sauter mean diameter of air is located near the wall and the outlet. The result from the case study shows that the Sauter mean diameter of air at that region has the same characteristics as the results simulated using PBM but with lower values. The reason might be the differences in spatial discretization using PBM and from the case study which have already been explained in section 4.2.4.
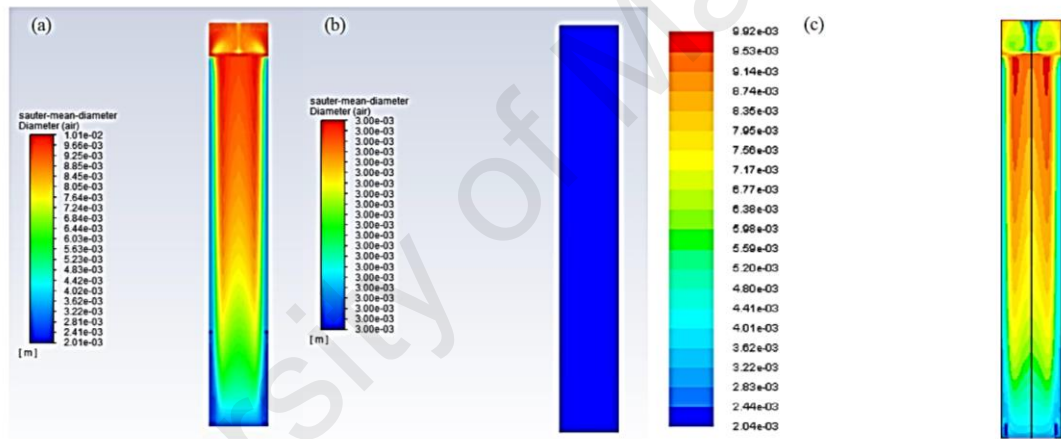
Figure 4.6 Sauter Mean Diameter of Air Contour (a) Simulated using PBM (b) Simulated using IAC Model (c) From the Case Study (ANSYS, Inc., 2012)

4.2.8 Sauter Mean Diameter Distribution of Air Histogram for 2D Vertical Bubble Column Reactor

Sauter mean diameter of air distribution histograms simulated using PBM, simulated using IAC model and from the case study are displayed in Figure 4.7. From Figure 4.7, it can be observed that Sauter mean diameter distribution of air histogram simulated using PBM, simulated using IAC model and from the case study are quite different. The Sauter mean diameter distribution of air histogram simulated using IAC model shows that the Sauter mean diameter of air in the entire 2D vertical bubble column reactor is 0.003 m. The reason for this has already been explained in section 4.2.7. The Sauter mean diameter distribution of air histogram simulated using PBM and from the case study has some differences in terms of the trend and values. For example, the number density of air with diameters between 0.00875 m and 0.0097 m simulated using PBM and from the case study are around 28 and 21 respectively. The reason might be the differences in spatial discretization using PBM and from the case study which have already been explained in section 4.2.4. The percentage differences of the number density from the smallest diameter of air group to the largest diameter of air group between simulation results obtained using PBM and from the case study are 0 %, 57.14 %, 101.54 %, 48.92 %, 7.88 %, 29.79 %, 22.07 %, 4.74 %, 33.33 % and 450.00 % respectively. The average percentage difference of the number density between simulation results obtained using PBM and from the case study is 75.54 %. It can be observed that the smallest and largest percentage differences are 0 % and 450.00 % respectively. The smallest percentage difference occurs at air with diameters between 0.0012 m and 0.002125 m whereas the largest percentage difference occurs at air with diameters between 0.0097 m and 0.01065 m. The reason for the large percentage differences might be the differences in special discretization which have already been explained in section 4.2.4.
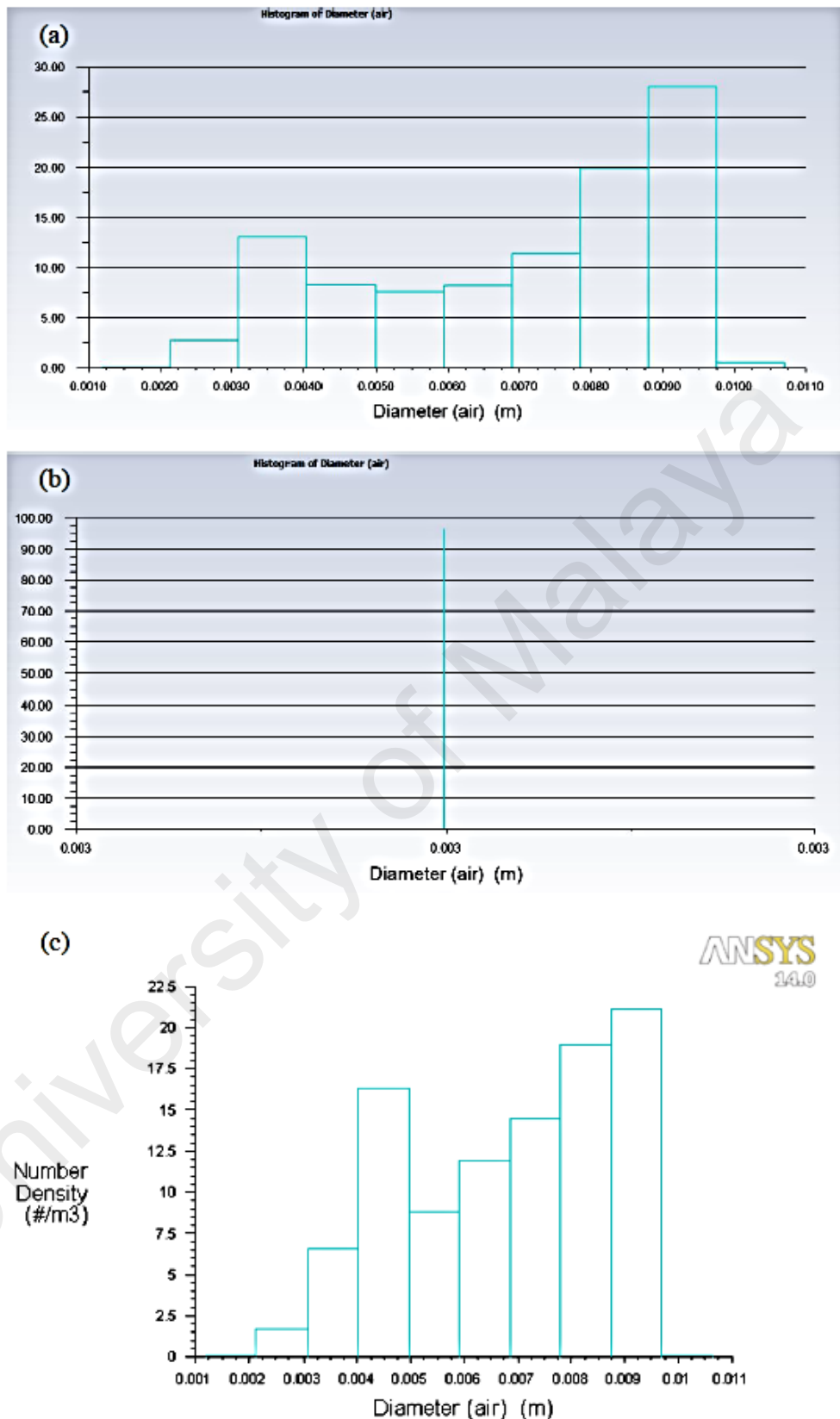
Figure 4.7 Sauter Mean Diameter of Air Distribution Histogram (a) Simulated using PBM (b) Simulated using IAC Model (c) From the Case Study (ANSYS, Inc., 2012)

4.3   CFD Simulation of Bubbly Flow in 2D Horizontal Pipe

4.3.1   Flux Reports for 2D Horizontal Pipe

The flux reports of net mass flow rate of mixture, water and air in 2D horizontal pipe for different ratios of AV/WV are tabulated in Table 4.2. From Table 4.2, it can be observed that the net mass flow rate of air in the 2D horizontal pipe for different ratios of AV/WV are almost 0. This indicates that the mass of air in the 2D horizontal pipe is conserved. However, the net mass flow rate of mixture and water are quite high compared to air. This is because cell size of the mesh used is larger than the air bubble size to prevent solution divergence. The area of the air bubbles will reduce the area of the water in the cell, causing the calculation performed on the water to be not sufficient. Therefore, the mass of mixture and water are not as conserved as air. This issue can be solved by designing the maximum cell size of the mesh to be smaller than the air bubble size, which is 0.0003 m. However, this will greatly increase the computational cost as smaller size of time step is required in order to prevent solution divergence.

Table 4.2 Flux Reports for Different Ratios of AV/WV for 2D Horizontal Pipe

AV/WV Ratio	Mass Flow Rate (kg/s)		
	Mixture	Water	Air
0.01	-3.928291×10^{-3}	-3.933118×10^{-3}	4.826758×10^{-6}
0.05	-9.53861×10^{-2}	-9.55033×10^{-2}	1.172025×10^{-4}
0.1	-4.429279×10^{-2}	-4.434722×10^{-2}	5.44233×10^{-5}
1	1.385999×10^{-2}	1.387702×10^{-2}	-1.703001×10^{-5}
10	-8.497332×10^{-2}	-8.507773×10^{-2}	1.044082×10^{-4}
100	-7.250969×10^{-2}	7.259878×10^{-2}	8.909388×10^{-5}
1000	-6.846134×10^{-2}	6.854546×10^{-2}	8.41196×10^{-5}

4.3.2 Air Volume Fraction Contours for 2D Horizontal Pipe

Air volume fraction contours for AV/WV ratios of 0.01, 0.05 and 0.1 are displayed in Figure 4.8 whereas air volume fraction contours for AV/WV ratios of 1, 10, 100, and 1000 are displayed in Figure 4.9. From Figure 4.8 and Figure 4.9, it can be observed that the air migrates to the top wall of the 2D horizontal pipe due to the buoyancy force and density difference between air and water when the air flows from the air inlet to the outlet in the +X direction. However, the distance it takes for the air to travel at the centre of the 2D horizontal pipe before migrating to the top wall varies with different ratios of AV/WV. It is found that the air travels the furthest at the centre before migrating to the top wall when the ratio of AV/WV is 1. The distance the air travels at the centre before migrating to the top wall decreases when the ratio of AV/WV decreases from 1. Not only that, it is also found that the air volume fraction is very much less or almost zero when the ratio of AV/WV is smaller than 1. This is because the air velocity is low compared to the water velocity which causes the air to be less stands out than the water. Besides, it is also observed that the air migrates to the top wall almost instantly when the ratio of AV/WV is larger than 1. Higher air velocity will increase the buoyancy force of the air according to Archimedes Principle. Therefore, AV/WV ratio of 1 will cause the air to travel the furthest before migrating to the top wall of the 2D horizontal pipe whereas reducing the AV/WV ratio will reduce the distance the air travels before migrating to the top wall and decrease the air volume fraction in the 2D horizontal pipe when the AV/WV is smaller than 1. Lastly, AV/WV ratio larger than 1 will cause the air to migrate to the top wall almost instantly due to larger buoyancy force.
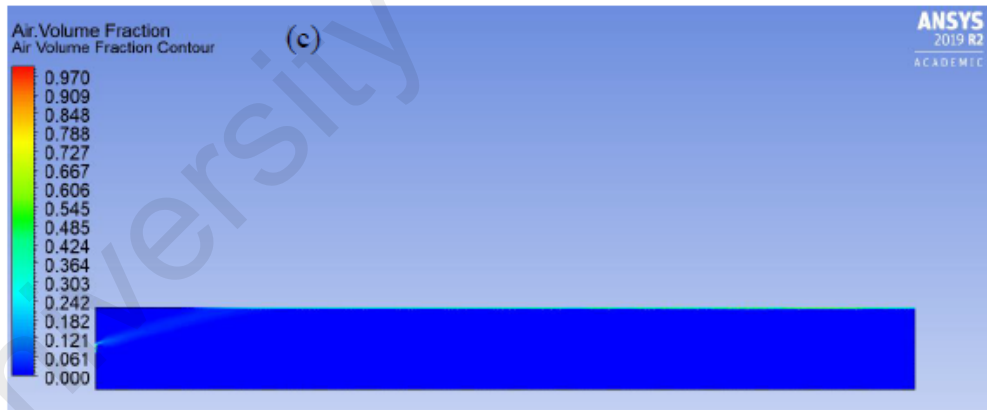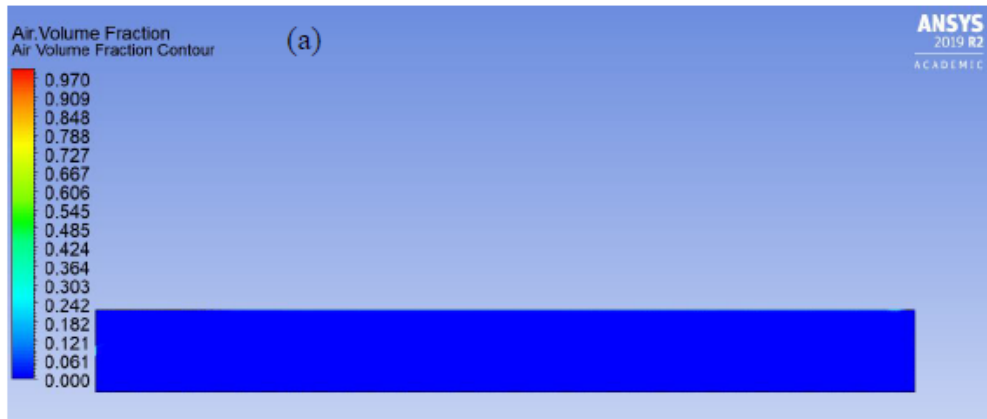
Figure 4.8 Air Volume Fraction Contour for AV/WV Ratio of (a) 0.01 (b) 0.05 (c) 0.1
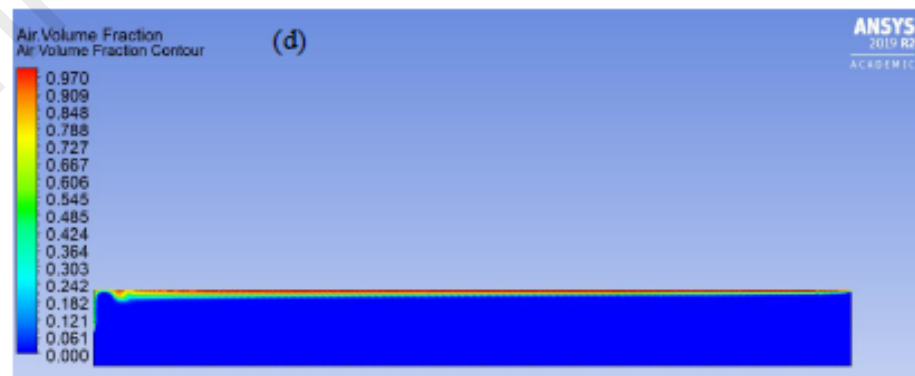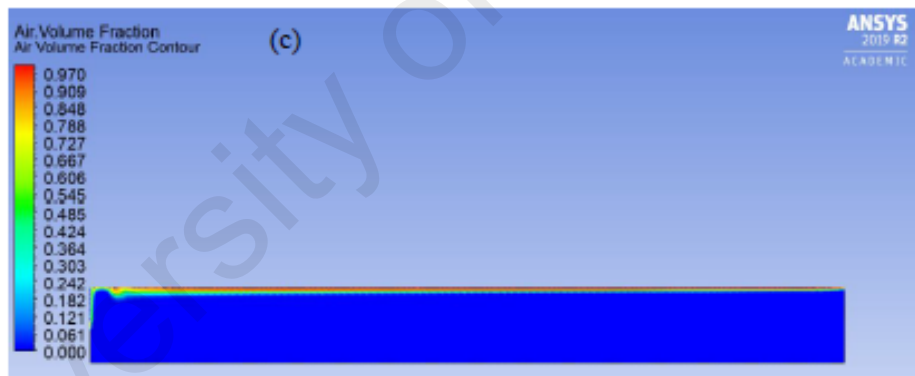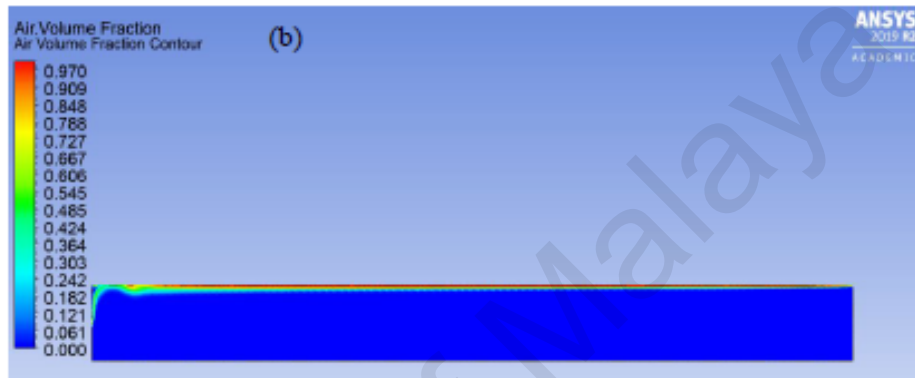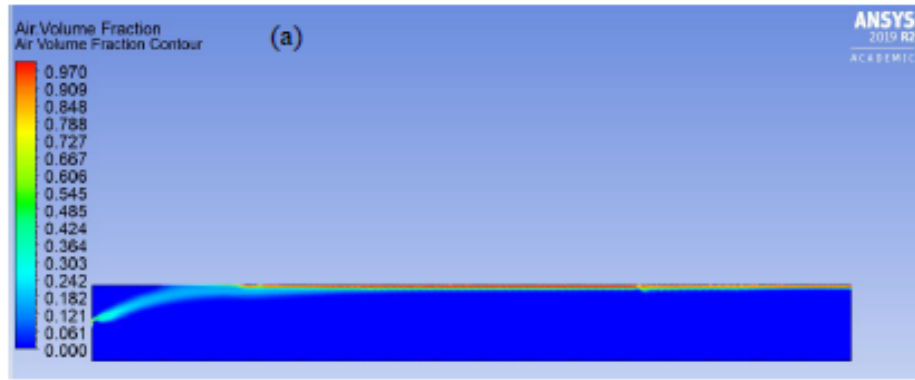
Figure 4.9 Air Volume Fraction Contour for AV/WV Ratio of (a) 1 (b) 10 (c) 100 (d) 1000

4.3.3 Air Volume Fraction Graphs for 2D Horizontal Pipe

Graphs of Y axis against air volume fraction for AV/WV ratios of 0.01, 0.05, 0.1, 1, 10, 100 and 1000 are displayed in Figure 4.10 to Figure 4.13. The graphs of Y axis against air volume fraction are plotted at X coordinates of -1 m, -0.5 m, 0 m, 0.5 m and 1 m. From Figure 4.10 to Figure 4.13, it can be observed that the volume fraction of air is 1 at the air inlet of the 2D horizontal pipe for all the different ratios of AV/WV. It is found that for AV/WV ratio smaller than 1, the air volume fraction is directly proportional to the AV/WV ratio. The air volume fraction increases when the AV/WV ratio increases until 1. Not only that, the air travels the furthest at the centre before migrating to the top wall of the 2D horizontal pipe when the ratio of AV/WV is 1. For AV/WV ratio larger than 1, the air migrates to the top wall in shorter time due to the larger buoyancy force.
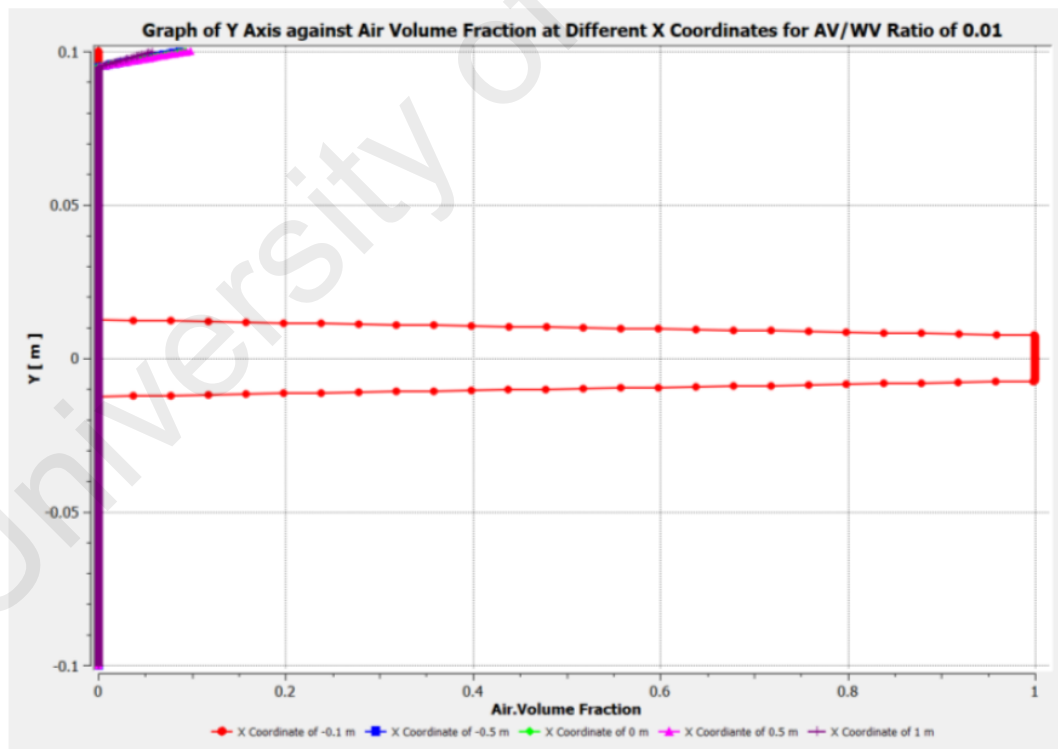
Figure 4.10 Graph of Y Axis against Air Volume Fraction for AV/WV Ratio of 0.01
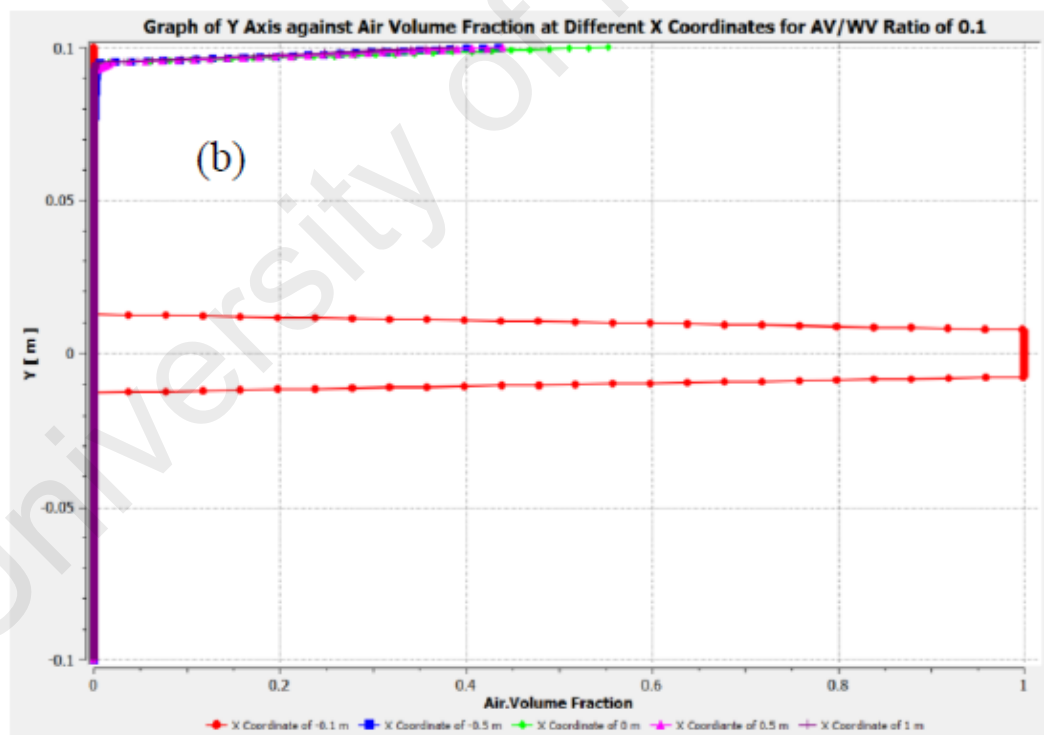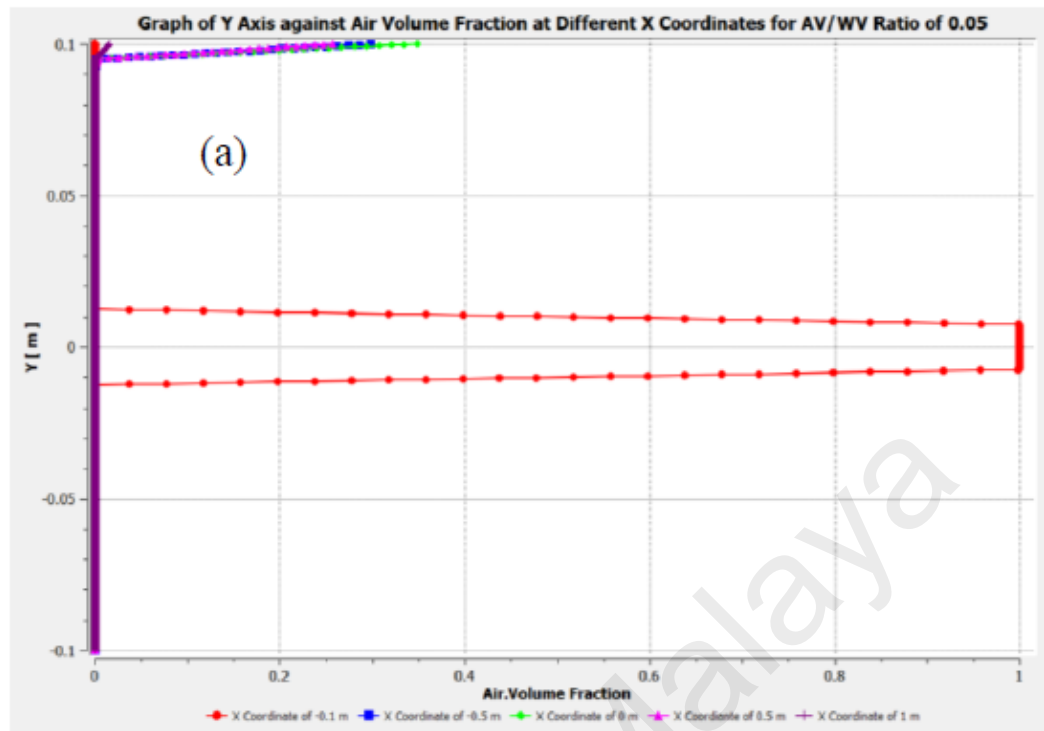
Figure 4.11 Graph of Y Axis against Air Volume Fraction for AV/WV Ratio of (a) 0.05 (b) 0.1
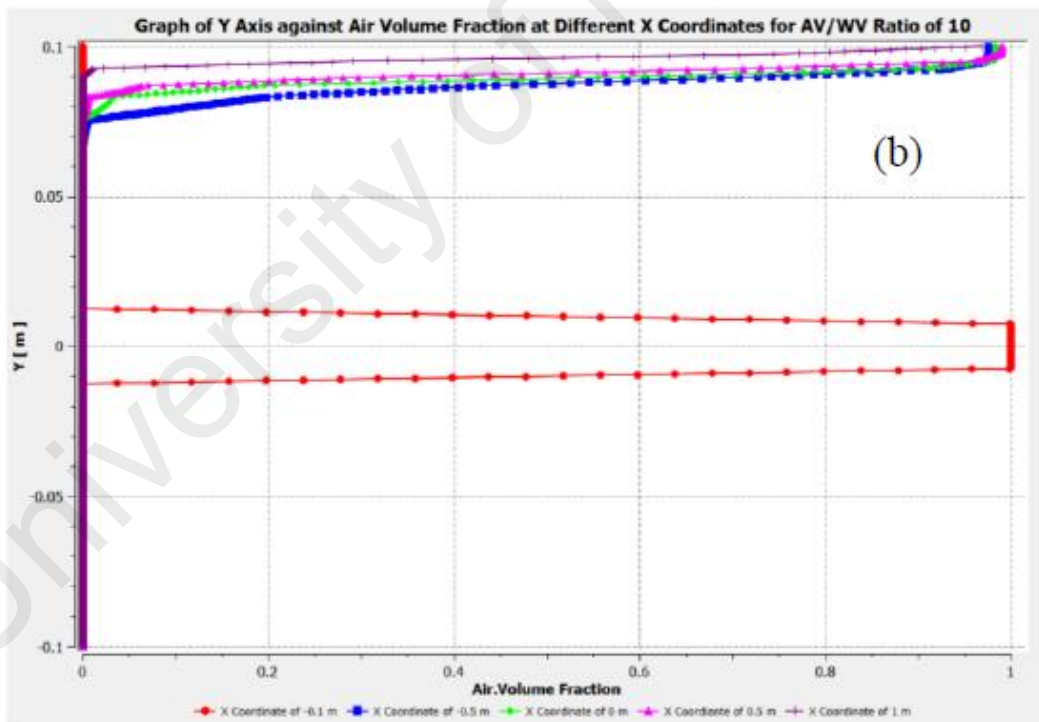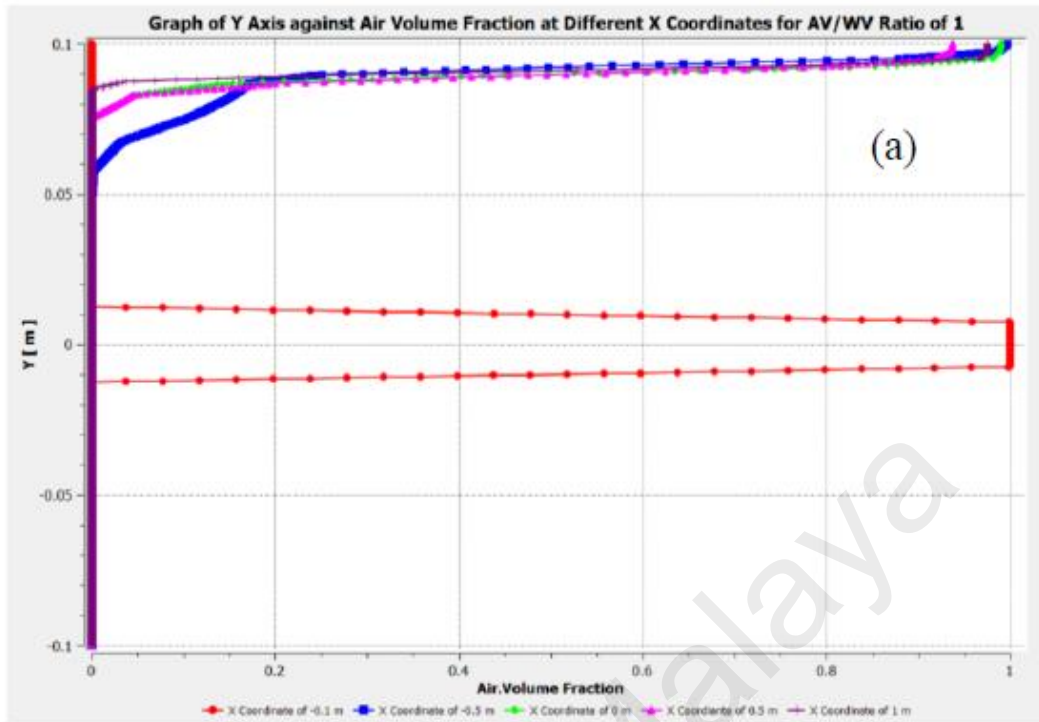
Figure 4.12 Graph of Y Axis against Air Volume Fraction for AV/WV Ratio of (a) 1 (b) 10
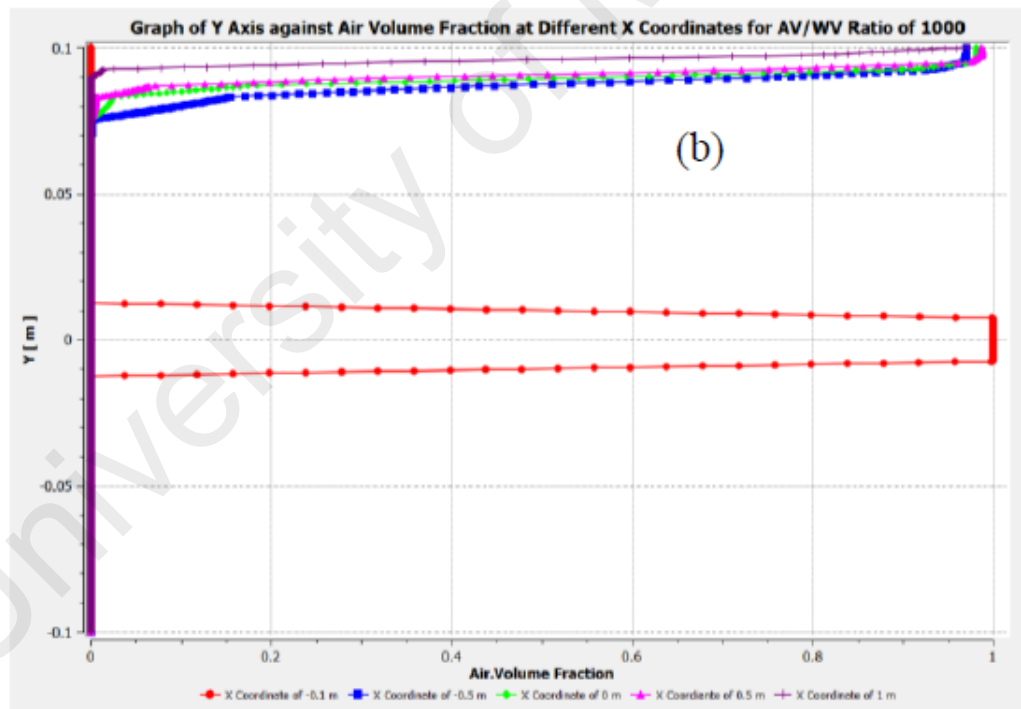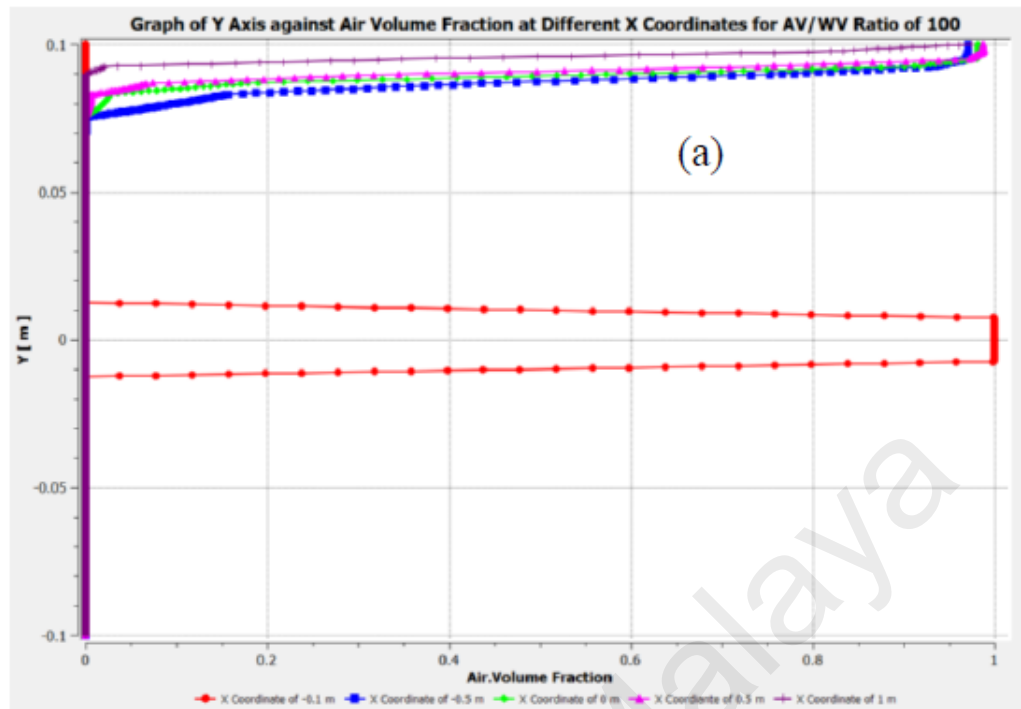
Figure 4.13 Graph of Y Axis against Air Volume Fraction for AV/WV Ratio of (a) 100 (b) 1000

4.3.4 Air Bin 0 Fraction Contours for 2D Horizontal Pipe

Air bin 0 fraction contours for AV/WV ratios of 0.01, 0.05 and 0.1 are displayed in Figure 4.14 whereas air bin 0 contours for AV/WV ratios of 1, 10, 100, and 1000 are displayed in Figure 4.15. From Figure 4.14 and Figure 4.15, it can be observed that the trend of the air bin 0 fraction contours is similar to the air volume fraction contours. The air bubbles migrate to the top wall of the 2D horizontal pipe due to the buoyancy force and density difference between air bubble and water when the air bubbles flow from the air inlet to the outlet in the +X direction. It is found that the air bubbles travel the furthest at the centre before migrating to the top wall of the 2D horizontal pipe when the ratio of AV/WV is 1. Not only that, it is also found that for AV/WV ratio smaller than 1, the distance the air bubbles travel at the centre before migrating to the top wall decreases when the AV/WV ratio decreases. Lastly, the air bubbles migrate to the top wall of the 2D horizontal pipe almost instantly due to the larger buoyancy force when the ratio of AV/WV larger than 1.
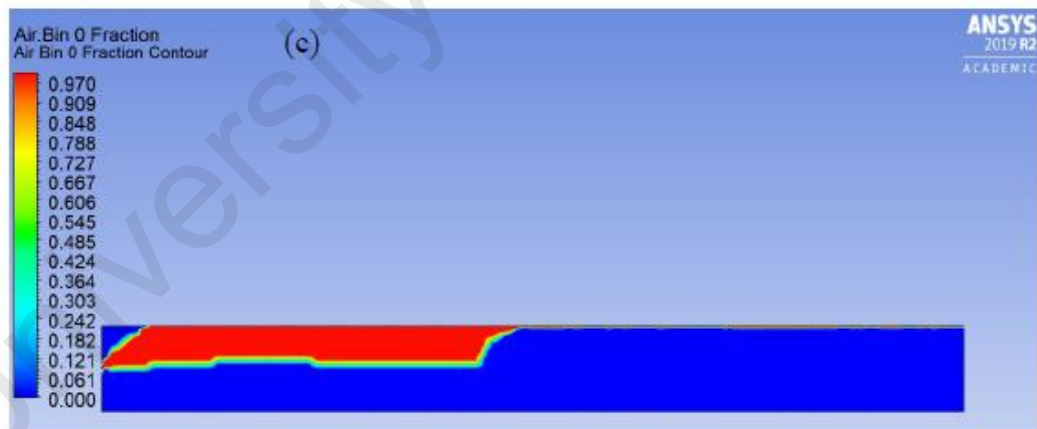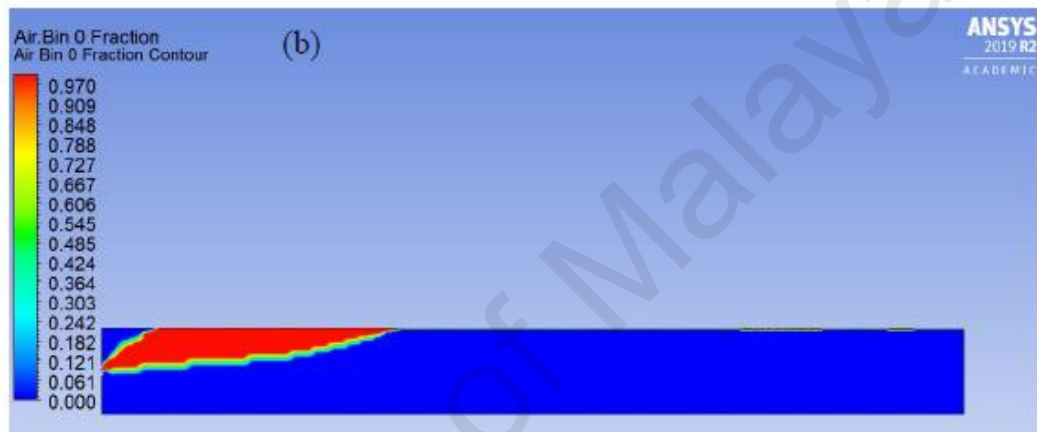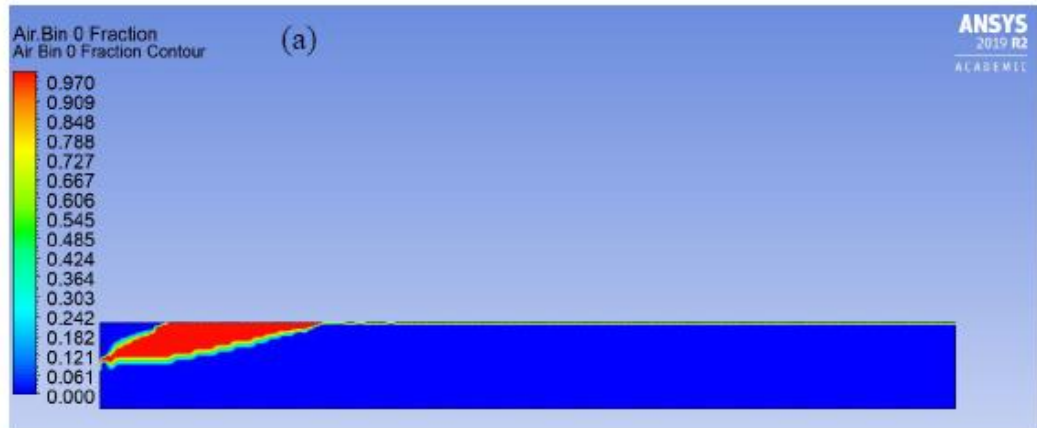
Figure 4.14 Air Bin 0 Fraction Contour for AV/WV Ratio of (a) 0.01 (b) 0.05 (c) 1
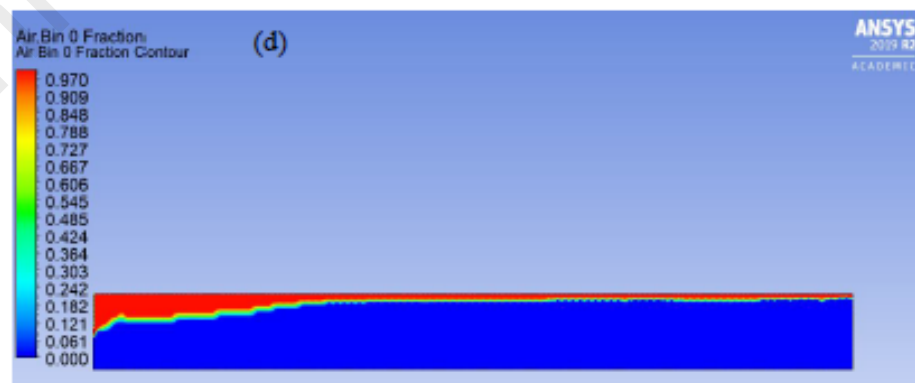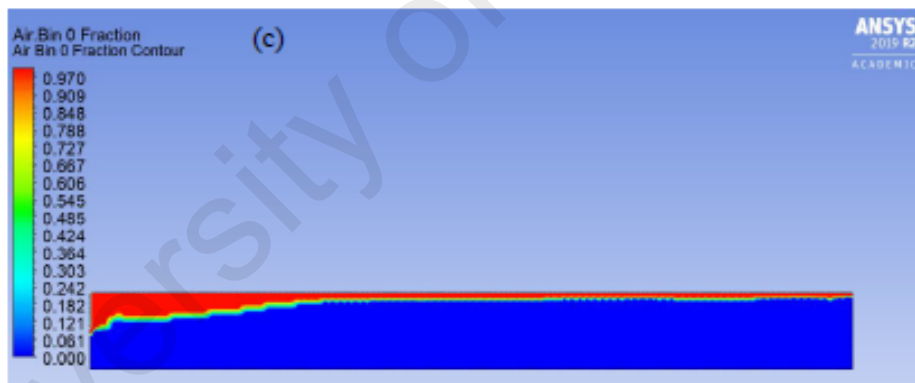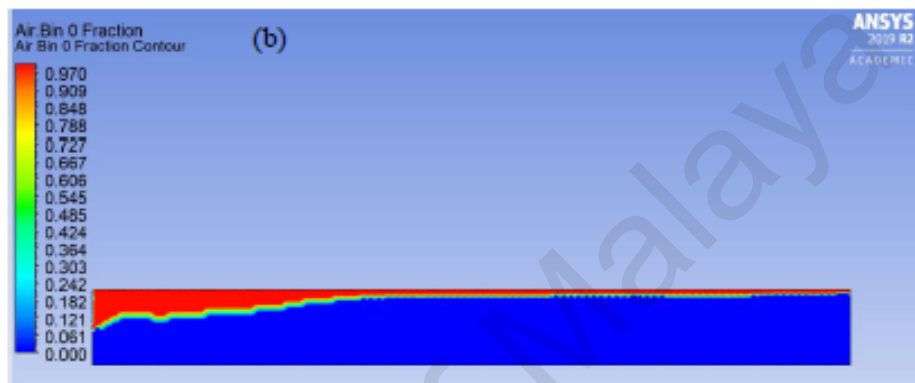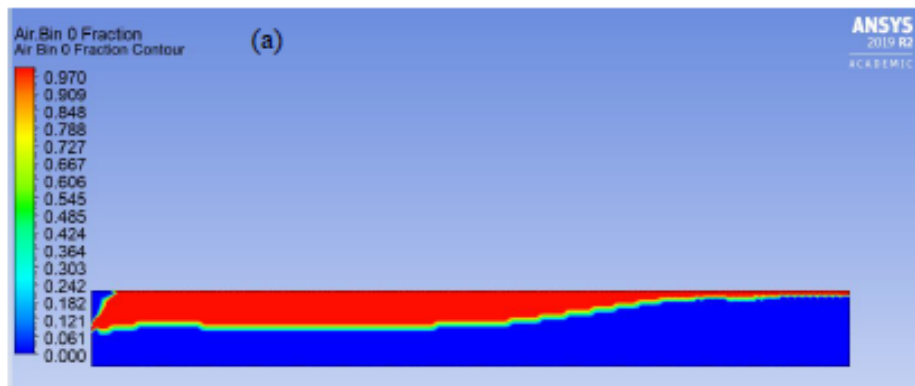
Figure 4.15 Air Bin 0 Fraction Contour for AV/WV Ratio of (a) 1 (b) 10 (c) 100 (d) 1000

4.3.5   Air Bin 0 Fraction Graphs for 2D Horizontal Pipe

Graphs of Y axis against air bin 0 fraction for AV/WV ratios of 0.01, 0.05, 0.1, 1, 10, 100 and 1000 are displayed in Figure 4.16 to Figure 4.19. The graphs of Y axis against air bin 0 fraction are plotted at X coordinates of -1 m, -0.5 m, 0 m, 0.5 m and 1 m. From Figure 4.16 to Figure 4.19, it can be observed that the trend of the graphs is almost similar to the graphs in Figure 4.10 and Figure 4.13. It is found that the air bin 0 fraction is 1 at the air inlet of the 2D horizontal pipe for all the different ratios of AV/WV. It is also found that the air bin 0 fraction will eventually reaches 1 at the top wall of the 2D horizontal pipe for all the different ratios of AV/WV. Not only that, the distance the air bubbles travel at the centre before migrating to the top wall decreases when the ratio of AV/WV decreases for AV/WV ratio smaller than 1. Lastly, the air bubbles migrate to the top wall of the 2D horizontal pipe almost instantly due to the larger buoyancy force when the AV/WV ratio is larger than 1.
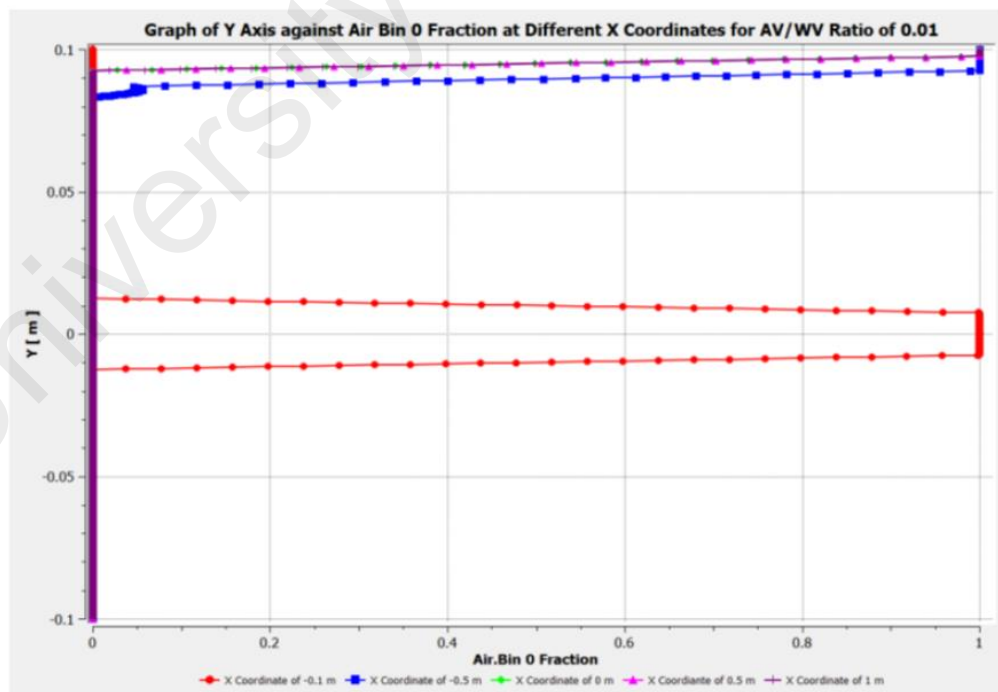
Figure 4.16 Graph of Y Axis against Air Bin 0 Fraction for AV/WV Ratio of 0.01
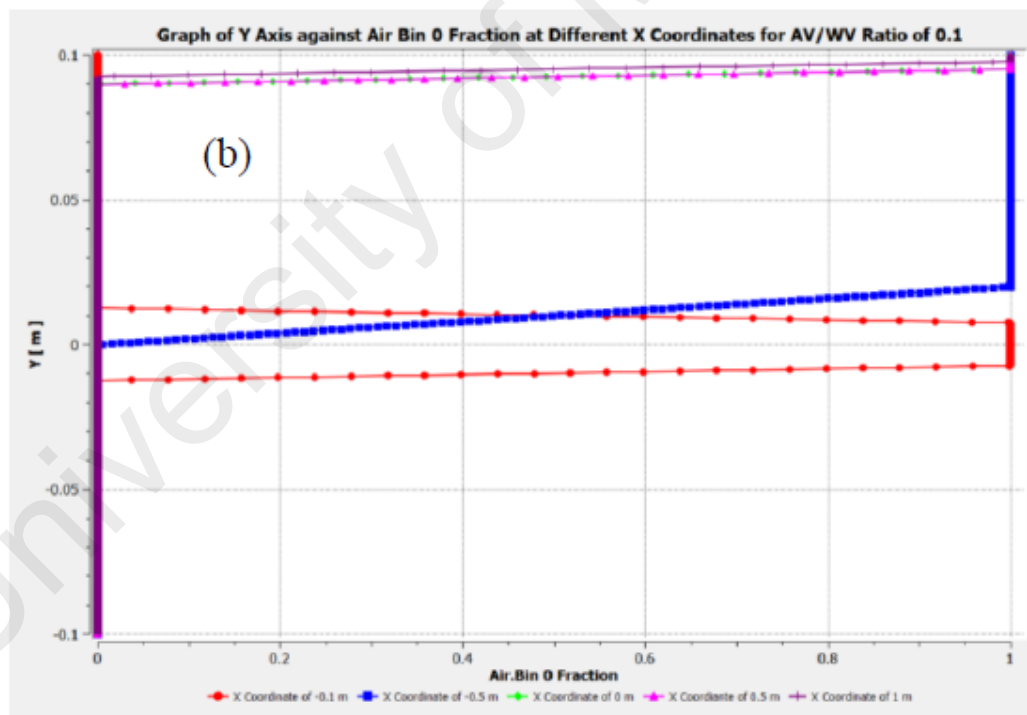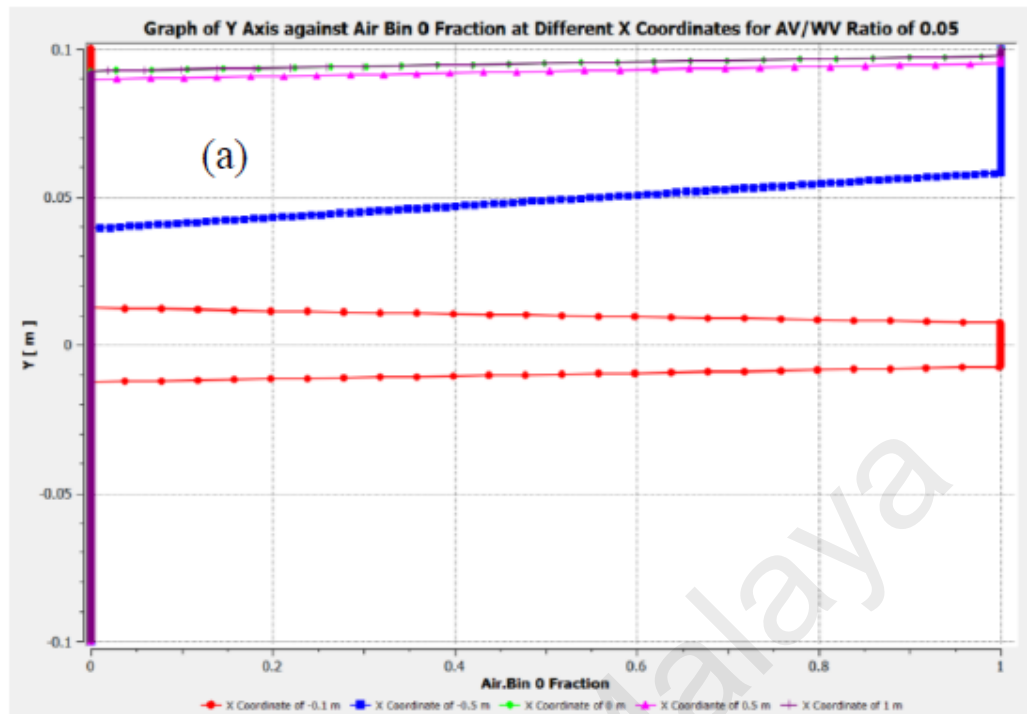
Figure 4.17 Graph of Y Axis against Air Bin 0 Fraction for AV/WV Ratio of (a) 0.05 (b) 0.1
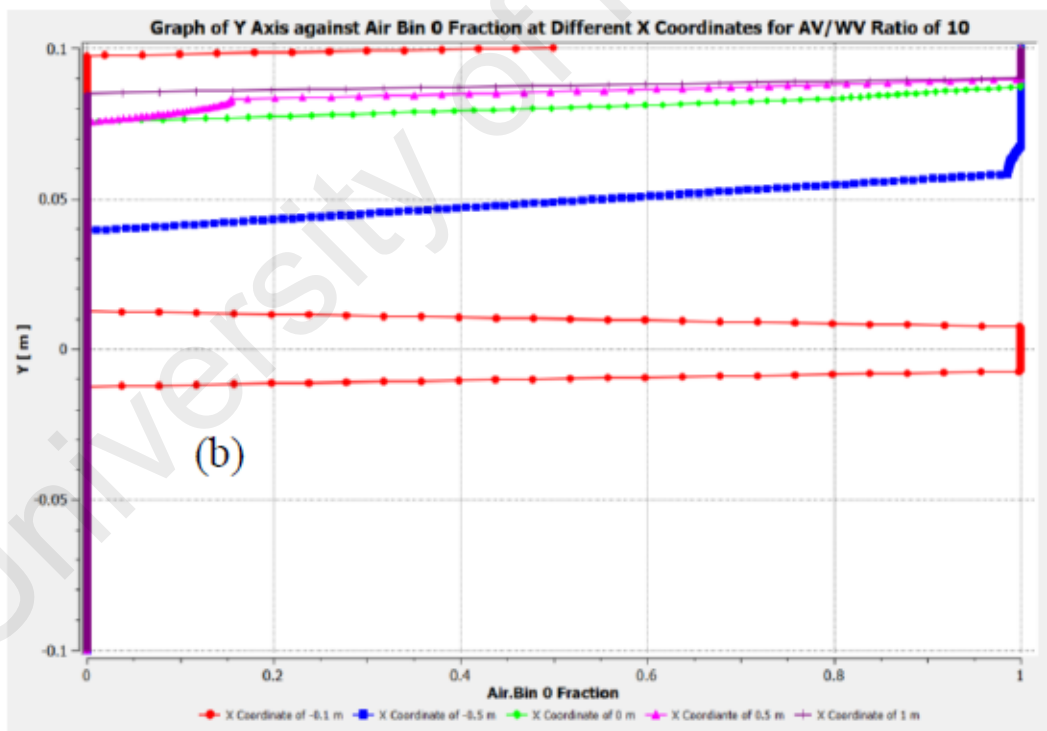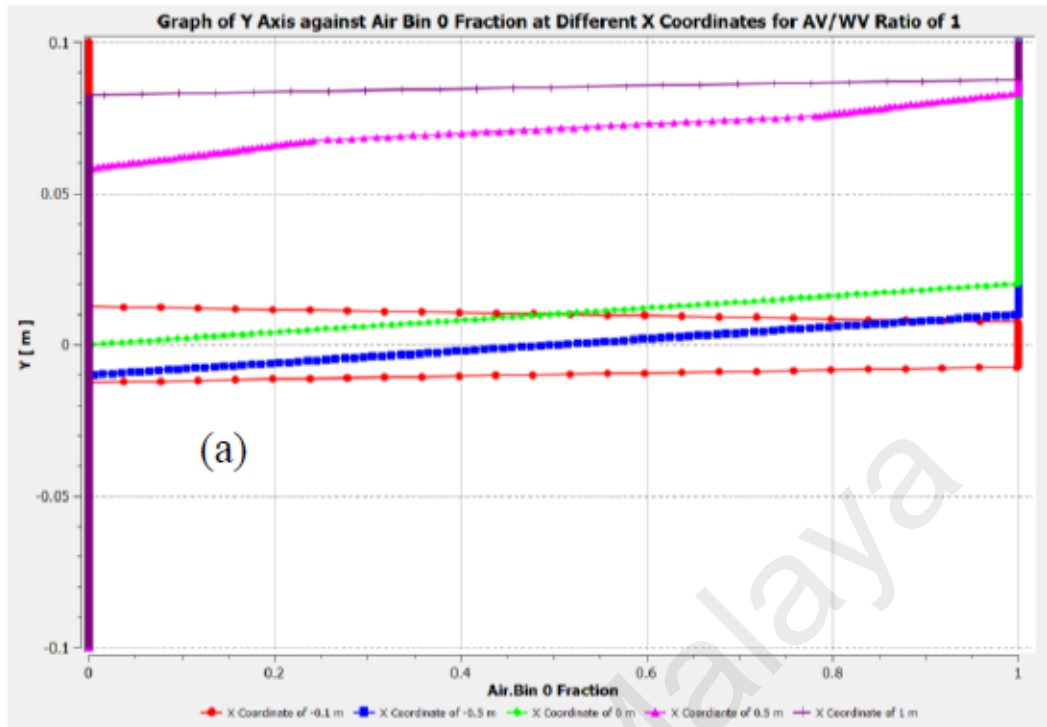
Figure 4.18 Graph of Y Axis against Air Bin 0 Fraction for AV/WV Ratio of (a) 1 (b) 10
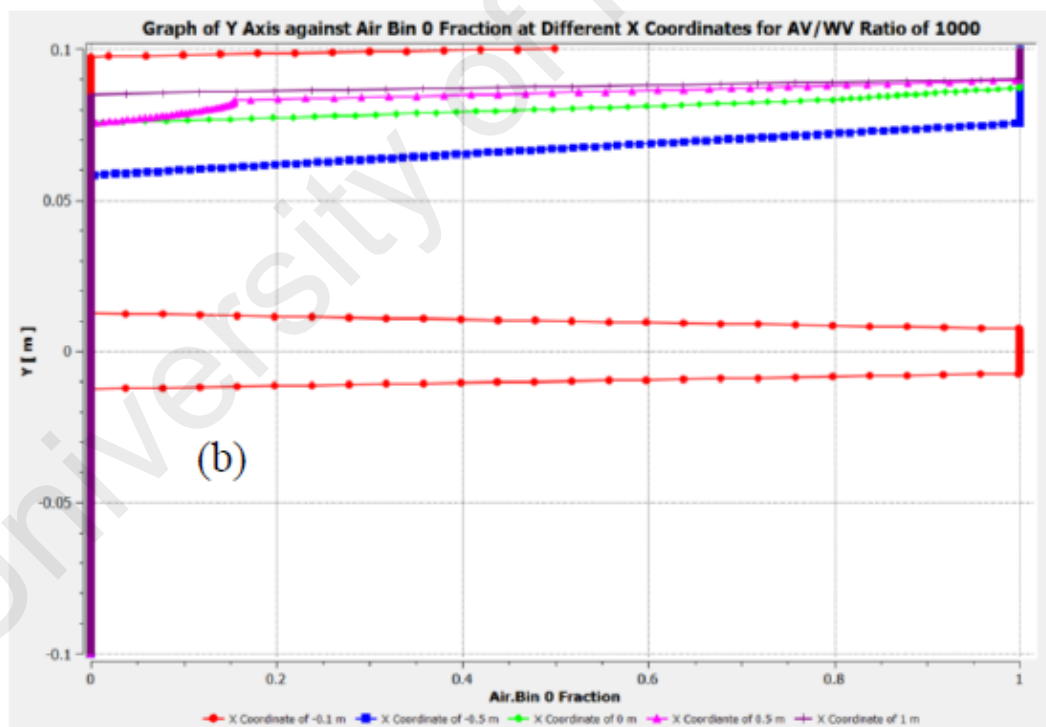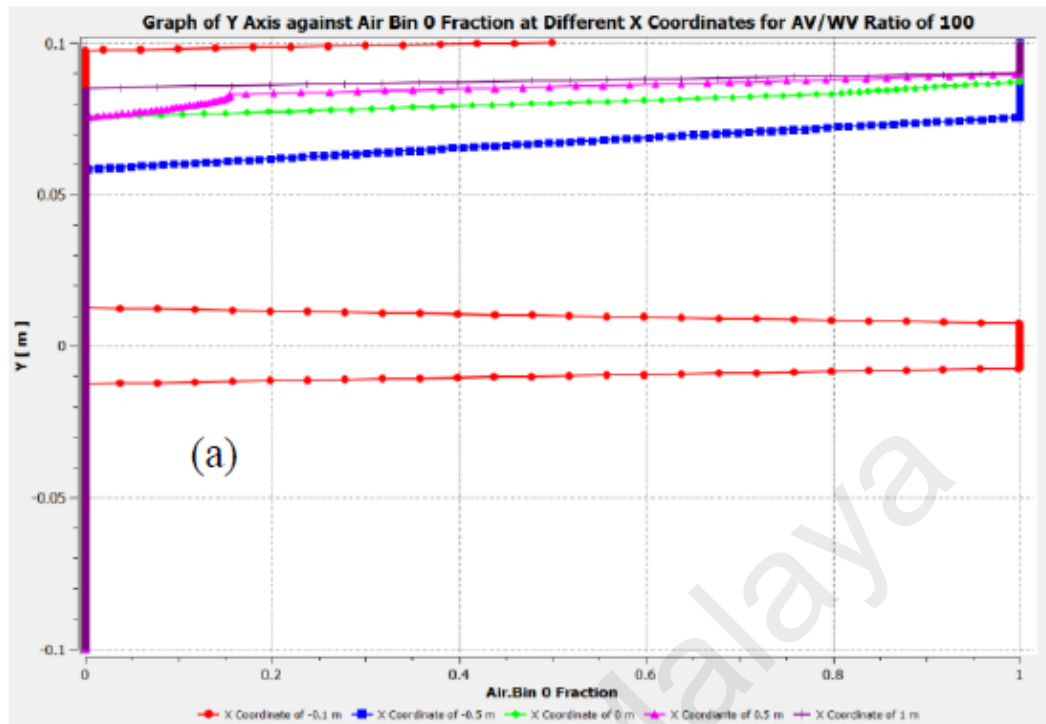
Figure 4.19 Graph of Y Axis against Air Bin 0 Fraction for AV/WV Ratio of (a) 100 (b) 1000

4.3.6   Outlet Boundary Condition

The boundary condition at the outlet of the 2D horizontal pipe used is outflow. Outflow boundary condition is suitable to be used only when the fluid flow is fully developed. Not only that, outflow boundary condition is not suitable to be used with the multiphase models in FLUENT, such as Eulerian model and VOF model (ANSYS, Inc., 2009). Using outflow boundary condition at the outlet of the 2D horizontal pipe will affect the accuracy of the simulation results. Therefore, it is recommended to change the boundary condition at the outlet of the 2D horizontal pipe from outflow to pressure-outlet to improve the accuracy of the simulation results in future studies.

4.4   CFD Simulation of Water-Air Multiphase Flow in 3D Kenics Static Mixer

4.4.1   Flux Reports for 3D Kenics Static Mixer

The flux reports of net mass flow rate of mixture, water and air in 3D Kenics static mixer for different inlet air volume fractions are tabulated in Table 4.3. From Table 4.3, it can be observed that the net mass flow rate of mixture, water and air in the 3D Kenics static mixer for different inlet air volume fractions are almost 0. This indicates that the mass of mixture, water and air in the 3D Kenics static mixer are conserved.

Table 4.3 Flux Reports for Different Inlet Air Volume Fractions for 3D Kenics Static Mixer

Inlet Air Volume Fractions	Mass Flow Rate (kg/s)		
	Mixture	Water	Air
0.1	-3.378755×10^{-7}	-3.382901×10^{-7}	4.145833×10^{-10}
0.2	-3.868393×10^{-6}	-3.873145×10^{-6}	4.752291×10^{-9}
0.3	-5.569506×10^{-6}	-5.576345×10^{-6}	6.838442×10^{-9}

4.4.2 Air Volume Fraction Contours for 3D Kenics Static Mixer

The air volume fraction contours in isometric view for inlet volume fractions of 0.1, 0.2 and 0.3 are displayed in Figure 4.20. The air volume fraction contours at the inlets, at the end of first Kenics element to the end of ninth Kenics element and at the outlets for inlet air volume fractions of 0.1, 0.2 and 0.3 are displayed in Figure 4.20 to Figure 4.31. From Figure 4.20 to Figure 4.31, it can be observed that the maximum air volume fractions in the 3D Kenics static mixer are around 0.1, 0.2 and 0.3 for inlet air volume fractions of 0.1, 0.2 and 0.3 respectively. It is found that the air volume fraction contours for the various inlet air volume fractions show almost similar mixing characteristics between air and water. The only main difference between them is the values of the air volume fraction. From Figure 4.20, it is observed that the maximum and minimum air volume fractions for different inlet air volume fractions occur near the air inlet and water inlet of the 3D Kenics static mixer respectively. This is because only water enters from the water inlet whereas air and water enter from the air inlet. The air volume fraction then gradually becomes more homogeneous as the mixture of water and air travels from the inlets to the outlets in the -Z direction. However, the air volume fraction at the top outlet is almost 0 due to the reversed flow of water. This is because the boundary conditions of the outlets used are pressure-outlets and the air backflow volume fractions are set as 1, which means the backflow only consists of water. The actual air backflow volume fraction must be determined experimentally.

From Figure 4.21, it can be observed that the air volume fractions at the air inlet are 0.1, 0.2 and 0.3 for inlet air volume fractions of 0.1, 0.2 and 0.3 respectively whereas the air volume fractions at the water outlet are 0 for all the various inlet air volume fractions. This is because only water enters from the water inlet whereas air and water enter from the air inlet. From Figure 4.22, it can be observed that the mixing between air and water

has just started at the end of first Kenics element for all the cases. Small amount of water enters the air-water mixture region whereas small amount of air-water mixture enters the water region. From Figure 4.23, it can be observed that large amount of water enters the air-water mixture region whereas large amount of air-water mixture enters the water region at the end of the second Kenics element for all the cases. However, the boundaries between regions of different volume fractions are still very distinct.

From Figure 4.24 to Figure 4.29, it can be observed that the homogeneity of the air-water mixture improves as the air-water mixture flows to the end of the eighth Kenics element in the -Z direction for all the cases. The air volume fractions are converging to a constant value. However, it is found that homogeneity of the air and water mixture is the highest for air inlet volume fraction of 0.1, follow by 0.2 and 0.3. The air volume fraction is the highest and the region of high air volume fraction is the largest for inlet air volume fraction of 0.3, followed by 0.2 and 0.1. This is because there is lesser amount of air when the inlet air volume fraction is lower. Lesser amount of air will certainly ease the mixing task between the air and water. Not only that, it is observed that the air volume fraction is higher at the top region of the Kenics elements for all the cases. This is because the air floats to the top region due to the buoyancy force and the density difference between air and water. The density of air set in FLUENT, which is 1.225 kg/m^3 is much lower than the density of water set in FLUENT, which is 998.2 kg/m^3.

From Figure 4.30, it is observed that the air volume fraction at the bottom region of the end of the ninth Kenics element suddenly decreases to almost 0 for inlet air volume fractions of 0.2 and 0.3. This indicates that the bottom region consists of mostly water for inlet air volume fractions of 0.2 and 0.3. The region of mostly water is higher for inlet air volume fraction of 0.3 compared to 0.2. This is due to the reversed flow of water at the

outlets. There is no indication of any reversed flow for inlet air volume fraction of 0.1. Instead, the homogeneity of the air and water improves compared to at the end of the eighth Kenics element. From Figure 4.31, it can be observed that reversed flow occurs especially at the top outlets for all the different inlet air volume fractions. This is because the boundary conditions of the outlets used are pressure-outlets and the air backflow volume fractions are set as 0, which means the backflow only consists of water. Besides, it is found that there is more reversed flow of water when the inlet volume fraction is higher. This is due to the larger amount of air affecting the flow of water exiting the outlets when the air volume fraction in the water-air mixture is larger which will then cause a larger amount of reversed flow of water. Another reason is the outlets are too close to the last Kenics element. The reversed flow of water issue can be solved by moving the outlet much further away from the last Kenics element, thus preventing the issue of reversed flow of water. Lastly, the homogeneity of the air-water mixture can be further improved by increasing the number of Kenics elements to improve the mixing performance between air and water by passing through more Kenics elements.
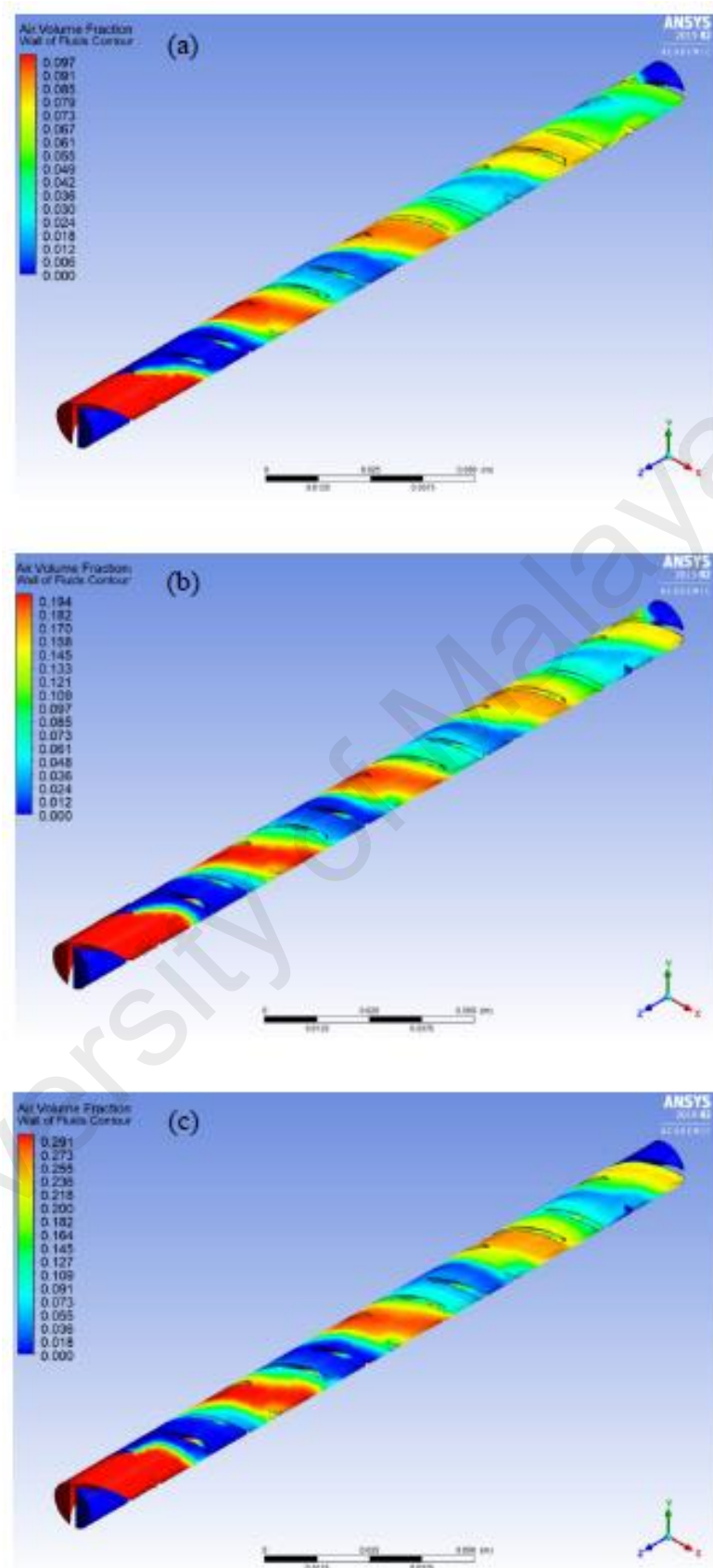
Figure 4.20 Air Volume Fraction Contour in Isometric View for Inlet Air Volume Fraction of (a) 0.1 (b) 0.2 (c) 0.3
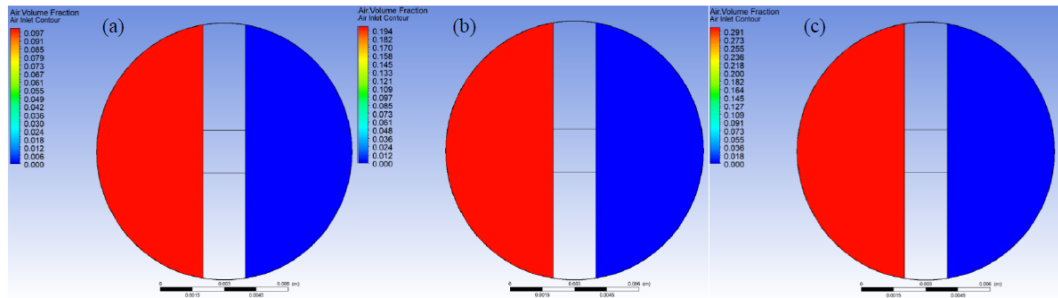
Figure 4.21 Air Volume Fraction Contour at the Inlets for Inlet Air Volume Fraction of (a) 0.1 (b) 0.2 (c) 0.3
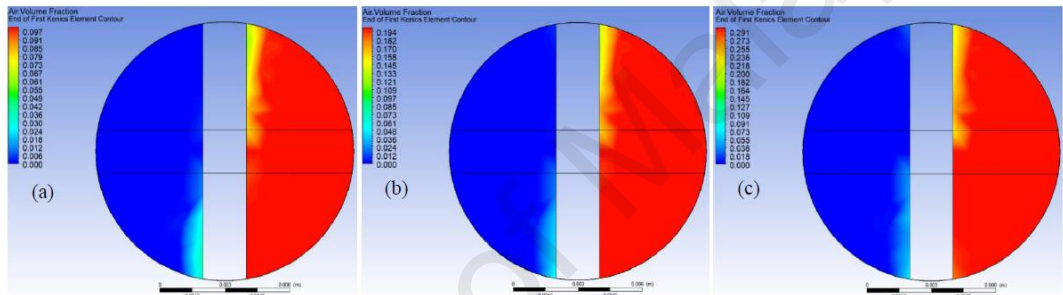
Figure 4.22 Air Volume Fraction Contour at the End of First Kenics Element for Inlet Air Volume Fraction of (a) 0.1 (b) 0.2 (c) 0.3
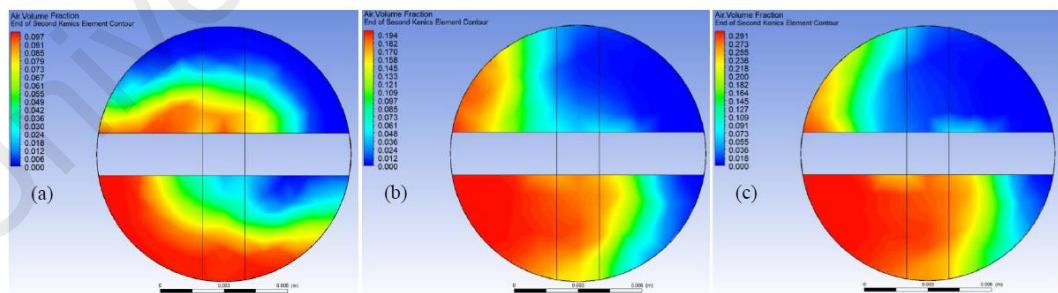
Figure 4.23 Air Volume Fraction Contour at the End of Second Kenics Element for Inlet Air Volume Fraction of (a) 0.1 (b) 0.2 (c) 0.3
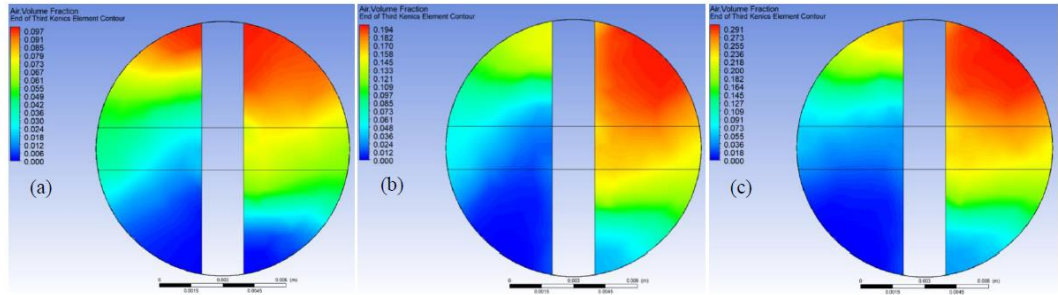
Figure 4.24 Air Volume Fraction Contour at the End of Third Kenics Element for Inlet Air Volume Fraction of (a) 0.1 (b) 0.2 (c) 0.3
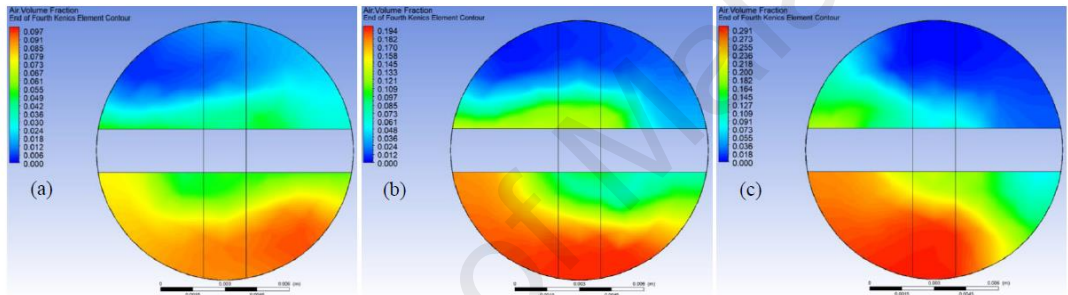
Figure 4.25 Air Volume Fraction Contour at the End of Fourth Kenics Element for Inlet Air Volume Fraction of (a) 0.1 (b) 0.2 (c) 0.3
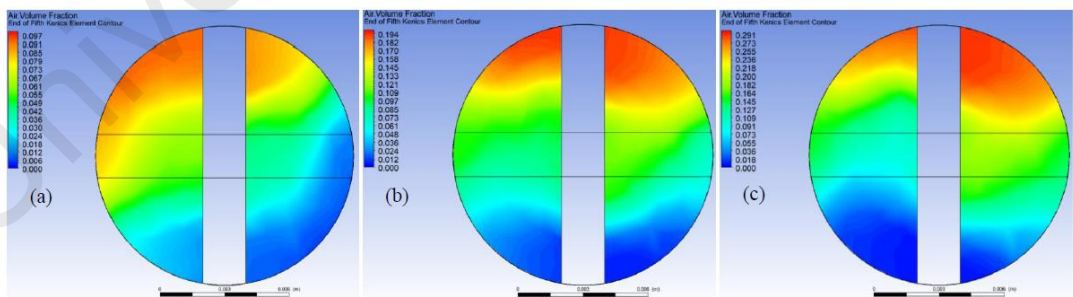
Figure 4.26 Air Volume Fraction Contour at the End of Fifth Kenics Element for Inlet Air Volume Fraction of (a) 0.1 (b) 0.2 (c) 0.3
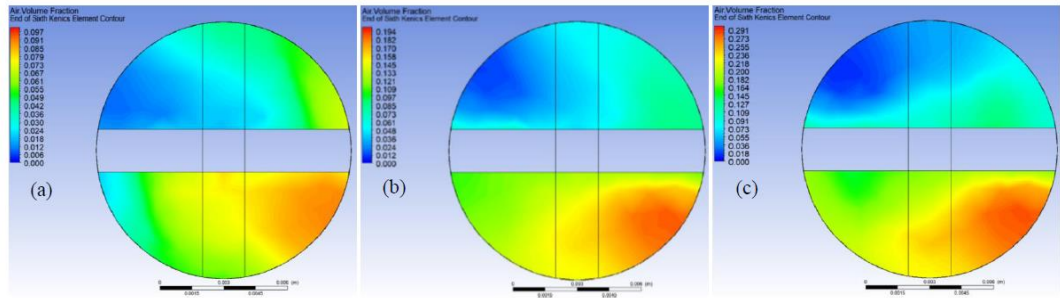
Figure 4.27 Air Volume Fraction Contour at the End of Sixth Kenics Element for Inlet Air Volume Fraction of (a) 0.1 (b) 0.2 (c) 0.3
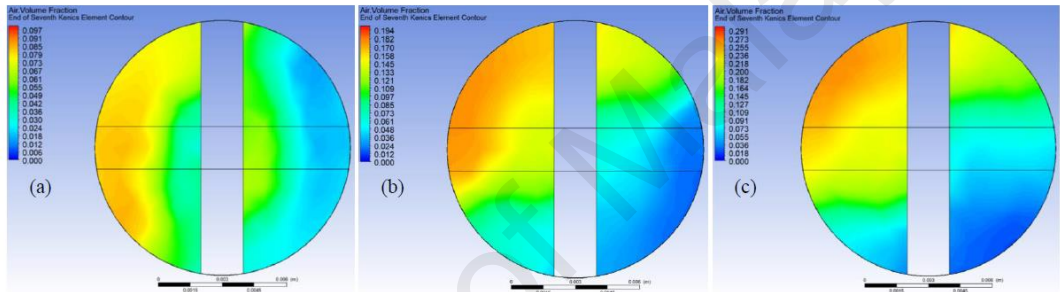
Figure 4.28 Air Volume Fraction Contour at the End of Seventh Kenics Element for Inlet Air Volume Fraction of (a) 0.1 (b) 0.2 (c) 0.3
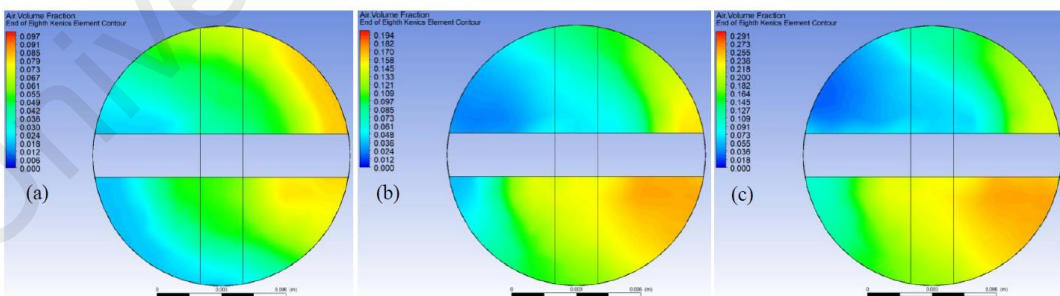
Figure 4.29 Air Volume Fraction Contour at the End of Eighth Kenics Element for Inlet Air Volume Fraction of (a) 0.1 (b) 0.2 (c) 0.3
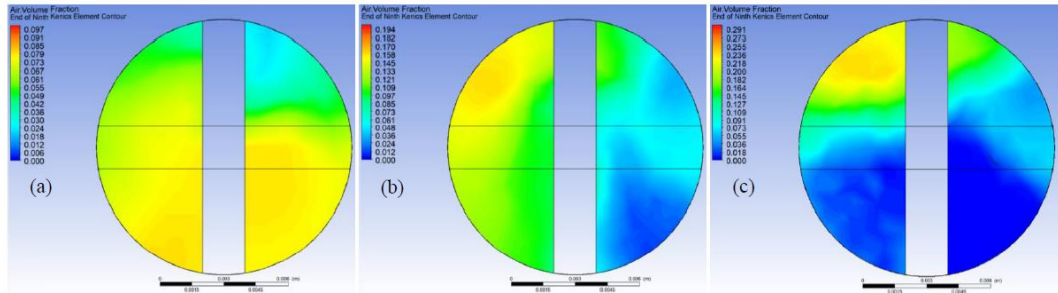
Figure 4.30 Air Volume Fraction Contour at the End of Ninth Kenics Element for Inlet Air Volume Fraction of (a) 0.1 (b) 0.2 (c) 0.3
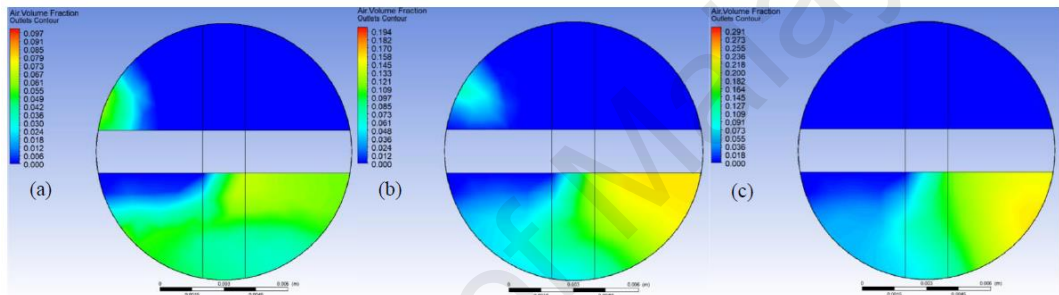
Figure 4.31 Air Volume Fraction Contour at the Outlets for Inlet Air Volume Fraction of (a) 0.1 (b) 0.2 (c) 0.3

.

CHAPTER 5: CONCLUSIONS

5.1   Conclusions

In a nutshell, the three main objectives of this research project are successfully achieved. For the first objective, CFD cases of bubbly flow in a 2D vertical bubble column reactor simulated using PBM and IAC model are studied and compared with an available case study from ANSYS. It is found that the results simulated using PBM compared to IAC model have higher similarity with the results from the case study. There are some differences between the results simulated using PBM and the results from the case study because there are some differences in the settings in FLUENT, such as the spatial discretization. For the spatial discretization, most of the equations are solved in second order for the results simulated using PBM whereas the equations are solved in first order for the case study. The results simulated using PBM should be more accurate than the results from the case study since most of the equations are solved in second order which includes a greater number of points than first order during discretization. It is also found that the main limitation of IAC model is unable to vary the size of air bubbles. User defined functions must be included into FLUENT in order to vary the size of the air bubbles. Therefore, PBM is chosen to simulate the results as required by the second objective.

For the second objective, bubbly flow in a 2D horizontal pipe is investigated by manipulating the ratio of AV/WV using PBM. It is found that the AV/WV ratio greatly affects several parameters of bubbly flow in a 2D horizontal pipe, such as the air volume fraction, air bin 0 fraction and the distance the air or air bubbles travel at the centre before migrating to the top wall of the 2D horizontal pipe. It is recommended to change the boundary condition at the outlet of the 2D horizontal pipe from outflow to pressure-outlet to improve the accuracy of simulation results.

Not only that, air-water multiphase flow in a 3D Kenics static mixer is also investigated by manipulating the inlet air volume fraction using VOF multiphase model for the third objective. It is found that the mixing characteristics of the 3D Kenics static mixer are almost similar for different inlet air volume fractions. It is also found that the homogeneity of air-water mixture improves after passing through each Kenics element in the 3D Kenics static mixer. Reversed flow of water is an issue and the issue can be solved by moving the outlet much further away from the last Kenics element.

Lastly, the accuracy of the simulation results obtained can be improved by reducing the mesh size. Reducing the mesh size indicates that the number of nodes and elements are increased. However, Courant number (CFL) is an important consideration. CFL is an important parameter that indicates the stability for the calculation of solution. CFL is recommended to be smaller than 1 in order to prevent solution divergence. For second order spatial discretization, CFL is defined as $dt/(dx^2)$, whereas dt is the time step size and dx is the smallest cell size. Dx will decrease if the mesh size is reduced. Hence, dt needs to be reduced until the CFL is smaller than 1 to ensure stability for calculation of solution. This will greatly increase the computational cost in terms of computational power and simulation time. Therefore, it is very important for engineers to balance between the accuracy of simulation results and the simulation time.

5.2   Recommendations for Future Work

There are several recommendations for future research that can be done in order to further investigate multiphase flows, especially bubbly flows in tubes. The first recommendation is to improve the scope of the second objective. The number of bins in PBM can be set to more than 1 to increase the number of air bubbles with different sizes in the 2D horizontal pipe. The aggregation kernel and breakage kernel in PBM can be enabled to allow the air bubbles to aggregate and break in order to form new air bubbles with different sizes. The flow physics of air bubbles in 2D horizontal pipe and the simulation results generated would be more accurate and more similar to practical applications with these settings in PBM. Not only that, the second recommendation is to include air bubbles in 3D Kenics static mixer for the third objective. Air bubbles can be introduced into the 3D Kenics static mixer using PBM. The settings in PBM would be almost similar to as mentioned in the first recommendation. The bubbly flow and flow physics of air bubbles in 3D Kenics static mixer can be investigated and studied. Besides, the third recommendation is to study the mixing characteristics of different geometries of static mixers. There are other different geometries of static mixers other than Kenics static mixers, such as SMX static mixers, KOMAX static mixers and many more. Air bubbles can be introduced into the different types of static mixers using PBM with settings that are almost similar to as mentioned in the first recommendation too. The mixing characteristics of the different types of static mixers can be investigated and compared. Flow characteristics of bubbly flow, such as flow physics of the air bubbles in the different types of static mixers can also be investigated and compared. Lastly, mesh dependency test should be done in order to ensure the accuracy and consistency of the simulation results.

REFERENCES

ANSYS, Inc. (12 January, 2009). *1. Introduction*. (ANSYS, Inc.) Retrieved 22 July, 2020, from ANSYS: https://www.afs.enea.it/project/neptunius/docs/fluent/html/popbal/node8.htm

ANSYS, Inc. (12 January, 2009). *1.1 The Discrete Method*. (ANSYS, Inc.) Retrieved 22 July, 2020, from ANSYS: https://www.afs.enea.it/project/neptunius/docs/fluent/html/popbal/node9.htm

ANSYS, Inc. (23 January, 2009). *16.4.9 Interfacial Area Concentration*. (ANSYS, Inc.) Retrieved 22 July, 2020, from ANSYS: https://www.afs.enea.it/project/neptunius/docs/fluent/html/th/node317.htm#:~:te xt=Interfacial%20Area%20Concentration- ,16.4.,phases%20per%20unit%20mixture%20volume.&text=The%20interfacial %20area%20concentration%20model,in%20liquid%20at%20this%20stage.

ANSYS, Inc. (23 January, 2009). *16.5.3 Conservation Equations*. (ANSYS, Inc.) Retrieved 22 July, 2020, from ANSYS: https://www.afs.enea.it/project/neptunius/docs/fluent/html/th/node322.htm

ANSYS, Inc. (23 January, 2009). *18.3.3 Evaluation of Gradients and Derivatives*. (ANSYS, Inc.) Retrieved 22 July, 2020, from ANSYS: https://www.afs.enea.it/project/neptunius/docs/fluent/html/th/node368.htm

ANSYS, Inc. (12 January, 2009). *2.2 The Population Balance Equation (PBE)*. (ANSYS, Inc.) Retrieved 22 July, 2020, from ANSYS: https://www.afs.enea.it/project/neptunius/docs/fluent/html/popbal/node14.htm

ANSYS, Inc. (12 January, 2009). *2.2.1 Particle Growth and Dissolution*. (ANSYS, Inc.) Retrieved 22 July, 2020, from ANSYS: https://www.afs.enea.it/project/neptunius/docs/fluent/html/popbal/node15.htm

ANSYS, Inc. (12 January, 2009). *2.2.2 Particle Birth and Death Due to Breakage and Aggregation*. (ANSYS, Inc.) Retrieved 22 July, 2020, from ANSYS: https://www.afs.enea.it/project/neptunius/docs/fluent/html/popbal/node16.htm

ANSYS, Inc. (29 January, 2009). *7.3.11 Outflow Boundary Conditions*. (ANSYS, Inc.) Retrieved 2 August, 2020, from ANSYS: https://www.afs.enea.it/project/neptunius/docs/fluent/html/ug/node247.htm

ANSYS, Inc. (7 March, 2012). *Tutorial: Modeling Bubble Breakup and Coalescence in a Bubble Column Reactor*. Retrieved 22 July, 2020, from mr-cfd: https://dl.mr-cfd.com/tutorials/ansys-fluent/03-bubble-break.pdf

ANSYS, Inc. (n.d.). *bubcol_new2.msh.gz*. (Chomikuj) Retrieved 22 July, 2020, from Chomikuj.pl: http://chomikuj.pl/arturb1985/Tutorials/Ansys/ANSYS+FLUENT/multiphase-fluent/tut-07-bubble-break/bubcol_new2.msh,1546039228.gz(archive)

Athulya, S. A., & Miji, R. C. (2015). CFD Modelling of Multiphase Flow through T Junction. *International Conference on Emerging Trends in Engineering, Science and Technology (ICETEST 2015). 24*, pp. 325-331. Trichur: ELSEVIER. Retrieved 22 July, 2020

Colombo, M., & Fairweather, M. (26 October, 2018). Influence of Multiphase Turbulence Modelling on Interfacial Momentum Transfer in Two-Fluid Eulerian-Eulerian CFD Models of Bubbly Flows. *Chemical Engineering Science, 195*(2019), 968-984. Retrieved 22 July, 2020

Ekambara, K., Sean Sanders, R., Nandakumar, K., & Masliyah, J. H. (14 January, 2012). CFD Modeling of Gas-Liquid Bubbly Flow in Horizontal Pipes: Influence of Bubble Coalescence and Breakup. *International Journal of Chemical Engineering, 2012*, 1-20. Retrieved 22 July, 2020

Encyclopedia.com. (14 August, 2020). *Mesh*. (Encyclopedia.com) Retrieved 22 July, 2020, from https://www.encyclopedia.com/science-and-technology/computers-and-electrical-engineering/computers-and-computing/mesh

Fang, J. Z., & Lee, D. J. (6 February, 2001). Micromixing Efficiency in Static Mixer. *Chemical Engineering Science, 56*(2001), 3797-3802. Retrieved 22 July, 2020

Fatchurrohman, N., & Chia, S. T. (2017). Performance of Hybrid Nano-Micro Reinforced MG Metal Matrix Composites Brake Calliper: Simulation Approach. *4th International Conference on Mechanical Engineering Research (ICMER2017). 257*, pp. 1-7. Pahang: IOP Publishing Ltd. Retrieved 22 July, 2020

Fetoui, I. (17 November, 2017). *Multiphase flow regimes*. (Production Technology) Retrieved 20 July, 2020, from PRODUCTION TECHNOLOGY: https://production-technology.org/multiphase-flow-regimes/

Fluent Inc. (28 November, 2001). *Chapter 20. General Multiphase Models.* Retrieved 22 July, 2020, from aew.dvi: https://www.afs.enea.it/fluent/Public/Fluent-Doc/PDF/chp20.pdf

Fraga, B., Stoesser, T., Lai, C. C., & Socolofsky, S. A. (10 November, 2015). A LES-Based Eulerian-Lagrangian Approach to Predict the Dynamics of Bubble Plumes. *Ocean Modelling, 97*(2016), 27-36. Retrieved 22 July, 2020

Ghanem, A., Lemenand, T., Valle, D. D., & Peerhossaini, H. (15 July, 2013). Static Mixers: Mechanisms, Applications and Characterization Methods - A Review. *Chemical Engineering Research and Design, 92*(2014), 205-228. Retrieved 22 July, 2020

Göbel, F., Golshan, S., Norouzi, H. R., Zarghami, R., & Mostoufi, N. (11 February, 2019). Simulation of Granular Mixing in a Static Mixer by the Discrete Element Method. *Power Technology, 346*(2019), 171-179. Retrieved 22 July, 2020

Habchi, C., Ghanem, A., Lemenand, T., Valle, D. D., & Peerhossaini, H. (21 December, 2018). Mixing Performance in Split-And-Recombine Milli-Static Mixers - A Numerical Analysis. *Chemical Engineering Research and Design, 142*(2019), 298-306. Retrieved 22 July, 2020

Haddadi, M. M., Hosseini, S. H., Rashtchian, D., & Ahmadi, G. (22 August, 2019). CFD Modeling of Immiscible Liquids Turbulent Dispersion in Kenics Static Mixers: Focusing on Droplet Behavior. *Chinese Journal of Chemical Engineering, 28*(2020), 348-361. Retrieved 22 July, 2020

Haddadi, M. M., Hosseini, S. H., Rashtchian, D., & Olazar, M. (15 October, 2019). Comparative Analysis of Different Static Mixers Performance by CFD Technique: An Innovative Mixer. *Chinese Journal of Chemical Engineering, 28*(2020), 672-684. Retrieved 22 July, 2020

Kashinsky, O. N., & Randin, V. V. (28 June, 1998). Downward Bubbly Gas-Liquid Flow in a Vertical Pipe. *International Journal of Multiphase Flow, 25*(1999), 109-138. Retrieved 22 July, 2020

Kataoka, Isao, Serizawa, & Akimi. (7 September, 2010). *Bubble Flow*. Retrieved 22 July, 2020, from THERMOPEDIA: http://www.thermopedia.com/content/8/#:~:text=Bubble%20flow%20is%20defined%20as,substances%20in%20a%20liquid%20continuum.

Khan, I., Wang, M., Zhang, Y., Tian, W., Su, G., & Qiu, S. (17 April, 2020). Two-Phase Bubbly Flow Simulation using CFD Method: A Review of Models by Interfacial Forces. *Progress in Nuclear Energy, 125*(2020), 1-17. Retrieved 22 July, 2020

Kumar, V., Shirke, V., & Nigam, K. (31 July, 2007). Performance of Kenics Static Mixer over A Wide Range of Reynolds number. *Chemical Engineering Journal, 139*(2008), 284-295. Retrieved 22 July, 2020

Kwon, B., Liebenberg, L., Jacobi, A. N., & King, W. P. (27 March, 2019). Heat Transfer Enhancement of Internal Laminar Flows using Additively Manufactured Static Mixers. *International Journal of Heat and Mass Transfer, 137*(2019), 292-300. Retrieved 22 July, 2020

Lisboa, P. F., Fernandes, J., Pedro, S., Mota, J. P., & Saatdjian, E. (12 August, 2010). Computational-fluid-dynamics study of a Kenics static mixer as a heat exchanger for a supercritical carbon dioxide. *The Journal of Supercritical Fluids, 55*(2010), 107-115. Retrieved 22 July, 2020

Meijer, H. E., Singh, M. K., & Anderson, P. D. (27 December, 2011). On the Performance of Static Mixers: A Quantitative Comparison. *Progress in Polymer Science, 37*(2012), 1333-1349. Retrieved 22 July, 2020

nanoScience Instruments. (n.d.). *Surface and Interfacial Tension*. (nanoScience Instruments) Retrieved 22 July, 2020, from nanoScience: https://www.nanoscience.com/techniques/tensiometry/surface-interfacial-tension/#:~:text=For%20example%2C%20the%20surface%20tension,C%20is%2072.0%20mN%2Fm.

Rabha, S., Schubert, M., Grugel, F., Banowski, M., & Hampel, U. (18 September, 2014). Visualization and Quantitative Analysis of Dispersive Mixing by a Helical Static Mixer in Upward Co-Current Gas-Liquid Flow. *Chemical Engineering Journal, 262*(2015), 527-540. Retrieved 22 July, 2020

Rafiee, M., Simmons, M. J., Ingram, A., & Stitt, E. H. (7 June, 2013). Development of Positron Emission Particle Tracking for Studying Laminar Mixing in Kenics Static Mixer. *Chemical Engineering Research and Design, 91*(2013), 2106-2113. Retrieved 22 July, 2020

Ramsay, J., Simmons, M., Ingram, A., & Stitt, E. (29 July, 2016). Mixing Performance of Viscoelastic Fluids in a Kenics KM In-Line Static Mixer. *Chemical Engineering Research and Design, 115*(2016), 310-324. Retrieved 22 July, 2020

Rauline, D., Le Blévec, J. -M., Bousquet, J., & Tanguy, P. A. (April, 2000). A Comparative Assessment of the Performance of the Kenics and SMX Static Mixers. *Trans IChemE, 78*(3), 389-396. Retrieved 22 July, 2020

Rzehak, R., & Kriebitzsch, S. (9 November, 2014). Multiphase CFD-Simulation of Bubbly Pipe Flow: A Code Comparison. *International Journal of Multiphase Flow, 68*(2015), 135-152. Retrieved 22 July, 2020

Soman, S. S., & Madhuranthakam, C. M. (16 October, 2017). Effects of Internal Geometry Modifications on the Dispersive and Distributive Mixing in Static Mixers. *Chemical Engineering & Processing: Process Intensification, 122*(2017), 31-43. Retrieved 22 July, 2020

Song, H.-S., & Han, S. P. (27 June, 2005). A General Correlation for Pressure Drop in a Kenics Static Mixer. *Chemical Engineering Science, 60*(2005), 5696-5704. Retrieved 22 July, 2020

Szalai, E. S., & Muzzio, F. J. (January, 2002). Validation of the ORCA CFD Software Using SMX and Kenics Static Mixer Elements. *Chemical and Biochemical Engineering Journal, 1*(2002), 1-8. Retrieved 22 July, 2020

Thakur, R. K., Vial, C., Nigam, K. D., Nauman, E. B., & Djelveh, G. (Aubière Cedex, New Delhi and New York August, 2003). Static Mixers in the Process Industries - A Review. *Trans IChemE, 81*(7), 787-824. Retrieved 22 July, 2020

van Wageningen, W. F., Kandhai, D., Mudde, R. F., & van den Akker, H. E. (August, 2004). Dynamic Flow in a Kenics Static Mixer: An Assessment of Various CFD Methods. *AIChE Journal, 50*(8), 1684-1696. Retrieved 22 July, 2020

Vikhansky, A. (11 February, 2020). CFD Modelling of Turbulent Liquid-Liquid Dispersion in a Static Mixer. *Chemical Engineering & Processing: Process Intensification, 149*(2020), 1-7. Retrieved 22 July, 2020

Wikipedia. (31 July, 2015). *Sauter mean diameter*. (Wikipedia) Retrieved 1 August, 2020, from WIKIPEDIA: https://en.wikipedia.org/wiki/Sauter_mean_diameter

Wikipedia. (26 June, 2020). *Multiphase flow*. (Wikipedia) Retrieved 22 July, 2020, from WIKIPEDIA: https://en.wikipedia.org/wiki/Multiphase_flow

Zhang, L., Dong, J., Jiang, B., Sun, Y., Zhang, F., & Hao, L. (10 December, 2014). A Study of Mixing Performance of Polyacrylamide Solutions in a New-Type Static Mixer Combination. *Chemical Engineering and Processing: Process Intensification, 88*(2015), 19-28. Retrieved 22 July, 2020

Zidouni, F., Krepper, E., Rzehak, R., Rabha, S., Schubert, M., & Hampel, U. (8 July, 2015). Simulation of gas-liquid flow in a helical static mixer. *Chemical Engineering Science, 137*(2015), 476-486. Retrieved 22 July, 2020

Zou , Y., Ye, S.-S., Wang, Y.-D., & Fei, W.-Y. (27 October, 2015). CFD Simulation and PIV Measurement of Liquid-Liquid Two-Phase Flow in Pump-Mix Mixer. *Journal of the Taiwan Institude of Chemical Engineers, 60*(2016), 15-25. Retrieved 22 July, 2020